1 2  9 0

UNIVERSIDADE D
COIMBRA

Daniela dos Santos Guedes

How old are you?
An attempt of estimating age at death through FTIR-ATR analysis of human bones and teeth

Dissertação no âmbito do Mestrado em Química Forense,
orientada pelo Professor Doutor Luís Alberto Batista de Carvalho
e pela Professora Doutora Maria Paula Marques, coorientada pelo Doutor David Gonçalves
e apresentada ao Departamento de Química da Faculdade de Ciências e Tecnologia
da Universidade de Coimbra.

Setembro de 2019

FACULDADE DE CIÊNCIAS E TECNOLOGIA DA UNIVERSIDADE DE COIMBRA

HOW OLD ARE YOU?

AN ATTEMPT OF ESTIMATING AGE AT DEATH THROUGH FTIR-ATR ANALYSIS OF HUMAN BONES AND TEETH

DANIELA DOS SANTOS GUEDES

Dissertação no âmbito do Mestrado em Química Forense, orientada pelo Professor Doutor Luís Alberto Batista de Carvalho e pela Professora Doutora Maria Paula Marques, e coorientada pelo Doutor David Gonçalves e apresentada ao Departamento de Química da Faculdade de Ciências e Tecnologia da Universidade de Coimbra.

SEPTEMBER 2019

1 2 9 0

UNIVERSIDADE D
COIMBRA

AGRADECIMENTOS

Aos orientadores desta dissertação, Professor Doutor Luís Batista de Carvalho e Professora Doutora Maria Paula Marques, agradeço pela oportunidade de realizar este projeto na Unidade de Química-Física Molecular, bem como pela orientação científica prestada, conhecimentos transmitidos, dedicação e constante simpatia. Ao meu coorientador, Doutor David Gonçalves, um agradecimento por todo o apoio e disponibilidade, análises críticas e sugestões ao longo desta investigação.

Ao Laboratório de Antropologia Forense da Universidade de Coimbra, agradeço pelo acesso concedido à Coleção de Esqueletos Identificados do século XXI e, pela confiança e simpatia durante os extensos meses de amostragem. Ao Calil, um agradecimento especial por toda a simpatia e pelos ensinamentos fundamentais em antropologia.

À Adriana, agradeço toda a motivação incondicional, conselhos, tempo e ensinamentos prestados. Estou grata por te ter conhecido. À Inês, a simpatia em pessoa, agradeço o tempo disponibilizado com a análise estatística. E ao restante grupo de investigação, por todos os conselhos, disponibilidade e momentos que partilharam comigo.

Às amigas que Coimbra me deu, Ana Beatriz, Rita, Mariana e Océane, obrigada por todas as palavras, risos e aventuras ao longo destes cinco anos. Ao grupo de forense, um obrigada pela amizade.

Ao meu Carlinhos, sempre com a razão na palavra e um enorme coração, obrigada por estares sempre presente, pela paciência e motivação essencial. Aos meus felinos, Óscar e Romã, fiéis companheiros de estudo.

Finalmente, dedico um agradecimento especial a toda a minha família, por tão bem me querer e, no fundo, à família que somos. E os últimos são os primeiros, aos meus pais e à minha irmã, resta a maior palavra de agradecimento, por tudo o que me proporcionaram até hoje.

A todos, o meu mais sincero obrigada.

TABLE OF CONTENTS

Index of Figures vii
Index of Tables xi
Abbreviations xiii
Abstract xv
Resumo xvii
1. Introduction 1
1.1. Age at Death Estimation in Anthropology 4
1.2. Bones and Teeth Composition 5
1.3. Bone Organization 7
1.4. Bone Remodelling Rate 8
1.5. Diagenesis 10
1.6. Methodology Review 11
1.6.1. Fourier Transform Infrared Spectroscopy 11
1.6.2. Spectroscopic Indices 15
1.7. Theoretical Foundations 17
1.8. Aims of the Study 18
2. Experimental 21
2.1. Sample Description 23
2.2. Sample Preparation 25
2.3. Fourier Transform Infrared Spectroscopy, in Attenuated Total Reflectance (ATR) mode 27
2.4. Spectra Analysis 27
2.5. Statistical Analysis 30
3. Results and Discussion 33
3.1. Spectral Analysis 35
3.2. Exploratory Statistical Analysis 38
3.2.1. Bones Analysis 38
3.2.2. Analysis by Age Cohorts 40
3.2.3. Analysis by Bone Types 42
3.2.3.1. Parietal *vs* Femur 43
3.2.3.2. Parietal *vs* Rib 44
3.2.3.3. Parietal *vs* Humerus 45
3.2.4. Teeth Analysis 47
3.3. Inferential Statistical Analysis 52
3.3.1. Bones Analysis 52

3.3.1.1. Prediction of Chronological Age through Chemometric Indices 62
3.3.1.2. The Effect of *Post-Mortem* Interval on Chemometric Indices 65
3.3.2. Teeth Analysis 65
3.3.2.1. Prediction of Chronological Age through Chemometric Indices 70
4. Conclusion 75
5. References 81
Appendix 97

INDEX OF FIGURES

Figure 1.1. Representation of chemical substitutions in bioapatite crystal lattice…..…….. 6
Figure 1.2. Representation of cortical and trabecular bone. Adapted from [64]..... 8
Figure 1.3. Schematic representation of the energy levels and vibrational transitions of IR absorption. Adapted from [99]……..……..…. 12
Figure 1.4. Schematic representation of Fourier Transform Infrared (FTIR) spectrometer in Attenuated Total Reflectance (ATR) mode……..……..…. 13
Figure 2.1. Sampling illustration on the posterior part of the mid-section of the femoral diaphysis of skeleton CEI_XXI_132……..……..…… 25
Figure 2.2. Sampling illustration on the posterior part of the mid-section of the humeral diaphysis of skeleton CEI_XXI_132……..……..…… 26
Figure 2.3. Sampling illustration on the parietal bone of skeleton CEI_XXI_132..……..… 26
Figure 2.4. Sampling illustration on the proximal rib of skeleton CEI_XXI_132……..…… 26
Figure 2.5. Sampling illustration on the first metatarsal of skeleton CEI_XXI_132……..… 26
Figure 2.6. Examples of mid-IR spectra of tooth and bone powder. The spectral bands used for indices calculation are highlighted……. 28
Figure 2.7. Display of band positions for CI (a), C/P (c,b), API (c,a), BPI (c,a), C/C (c), ν_4PO_4/Amide I (a,c) and ν_1PO_4/Amide I (b,c) calculation……..…. 29
Figure 3.1. FTIR-ATR spectra (430 to 1800 cm^{-1}) of the different human bone samples (powders): femur, humerus, metatarsal, rib and parietal of individual CEI_XXI_122……. 35
Figure 3.2. Representation of the variations caused by different operators in the collected IR data: (A) mean FTIR-ATR spectra of femur and humerus, for samples obtained by operators 1 (blue) and 2 (red); (B) PCA scores; (C) PCA loadings. PC1: 61.85%; PC2: 23.22%; PC3: 8.31%; PC4: 2.51%; PC5: 1.78%, exhibiting 97.67% of total variance……... 39
Figure 3.3. Representation of all bones correlation with age groups below 60 years old – younger group – and over 80 years old – older group: (A) mean FTIR-ATR spectra of younger and older group; (B) PCA scores; (C) PCA loadings. PC1: 61.07%; PC2: 18.96%; PC3: 11.88%; PC4: 2.62%; PC5: 1.80%, exhibiting 96.33% of total variance……... 41
Figure 3.4. Representation of all bone types correlation restricted to the 1350–1730 cm^{-1} region: (A) mean FTIR-ATR spectra of all bone types; (B) PCA scores; (C) PCA loadings. PC1: 69.88%; PC2: 12.53%; PC3: 8.27%; PC4: 4.82%; PC5: 2.34%, exhibiting 97.84% of total variance……..... 42

Figure 3.5. Representation of the correlation between parietal and femur restricted to the 1350–1730 cm^{-1} region: (A) mean FTIR-ATR spectra; (B) PCA scores; (C) PCA loadings. PC1: 73.84%; PC2: 12.86%; PC3: 5.57%; PC4: 3.65%; PC5: 2.05%, exhibiting 97.98% of total variance……..... 44

Figure 3.6. Representation of the correlation between parietal and rib restricted to the 1350–1730 cm^{-1} region: (A) mean FTIR-ATR spectra; (B) PCA scores; (C) PCA loadings. PC1: 68.67%; PC2: 17.60%; PC3: 6.04%; PC4: 2.98%; PC5: 2.78%, exhibiting 98.07% of total variance……..... 45

Figure 3.7. Representation of the correlation between parietal and femur restricted to the 1350–1730 cm^{-1} region: (A) mean FTIR-ATR spectra; (B) PCA scores; (C) PCA loadings. PC1: 68.35%; PC2: 15.71%; PC3: 7.78%; PC4: 4.38%; PC5: 1.68%, exhibiting 97.90% of total variance…….. 46

Figure 3.8. Representation of teeth with age groups below 40 years old – younger group – and over 60 years old – older group: (A) mean FTIR-ATR spectra of younger and older group; (B) PCA scores; (C) PCA loadings. PC1: 65.79%; PC2: 17.45%; PC3: 6.40%; PC4: 4.36%; PC5: 1.77%, exhibiting 95.76% of total variance…….. 48

Figure 3.9. Representation of teeth correlation with age groups below 40 years old – younger group – and over 60 years old – older group – restricted to the 430–1370 cm^{-1} region: (A) mean FTIR-ATR spectra of younger and older group; (B) PCA scores; (C) PCA loadings. PC1: 79.87%; PC2: 9.42%; PC3: 4.45%; PC4: 2.25%; PC5: 1.79%, exhibiting 97.79% of total variance……..... 49

Figure 3.10. Representation of teeth correlation with age groups below 40 years old – younger group – and over 60 years old – older group – restricted to the ν_1,ν_3(PO_4^{3-}) domain: (A) mean FTIR-ATR spectra of younger and older group; (B) PCA scores; (C) PCA loadings. PC1: 89.29%; PC2: 6.07%; PC3: 2.62%; PC4: 0.86%; PC5: 0.46%, exhibiting 99.9% of total variance……..…. 50

Figure 3.11. Graphic representation of chronological age correlation to crystallinity index……... 71

Figure A1. Representation of teeth with age groups below 50 years old – younger group – and over 50 years old – older group: (A) mean FTIR-ATR spectra of younger and older group; (B) PCA scores; (C) PCA loadings. PC1: 65.98%; PC2: 16.61%; PC3: 6.83%; PC4: 4.35%; PC5: 1.73%, exhibiting 95.50% of total variance…….. 99

Figure A2. Representation of teeth with age groups below 40 years old – younger group – and over 40 years old – older group: (A) mean FTIR-ATR spectra of younger

and older group; (B) PCA scores; (C) PCA loadings. PC1: 65.98%; PC2: 16.61%; PC3: 6.83%; PC4: 4.35%; PC5: 1.73%, exhibiting 95.50% of total variance…… 100

INDEX OF TABLES

Table 1.1. Description of anthropological methods available to age at death estimation and interval age ranges…… 5

Table 1.2. Infrared vibration wavenumber observed for human teeth and bone samples…15

Table 2.1. Number of bone samples to each type of bone according to age at death group and sex, for the individuals of the CEI_XXI collection…….. 24

Table 2.2. Number of teeth samples according to each age group and sex…… 24

Table 2.3. Description of the indices used to evaluate the chemical composition of each sample……..... 27

Table 3.1. Presence and absence of discrimination between bone types……..... 46

Table 3.2. Descriptive statistics and results of one-way ANOVA tests for the CI, C/C and C/P indices and Kruskal-Wallis tests for the API, BPI, ν_4PO_4/Amide I and ν_1PO_4/Amide I indices, according to bone type…… 53

Table 3.3. Descriptive statistics according to each sex and results of t-student tests for the CI, C/C and C/P indices and Mann-Whitney tests for the API, BPI, ν_4PO_4/Amide I and ν_1PO_4/Amide I indices…… 56

Table 3.4. Descriptive statistics to each age group and results of one-way ANOVA tests for the CI and C/P indices and Mann-Whitney tests for the API, BPI, C/C, ν_4PO_4/Amide I and ν_1PO_4/Amide I indices…… 57

Table 3.5. Coefficients for the linear regression of age group from the C/C according to bone type……..... 61

Table 3.6. Descriptives for the performance of regression models to age group according to bone types…… 61

Table 3.7. Descriptive statistics to Spearman correlation between age and indices, according to bone type models……..... 63

Table 3.8. Summary of results of linear regression to the variables C/C and C/P to predict the age at death, according to bone type…….. 64

Table 3.9. Descriptives for the performance of regression models for individual age estimation, according to bones with diaphysis…… 64

Table 3.10. Descriptive statistics to Spearman correlation between *post-mortem* interval and indices…… 65

Table 3.11. Descriptive statistics according to each sex and results of t-student tests for the CI, C/P, API, BPI, C/P, ν_4PO_4/Amide I and ν_1PO_4/Amide I indices……..... 67

Table 3.12. Descriptive statistics to each age group and results of Kruskal-Wallis tests for the CI, C/P, API, BPI, C/P, ν_4PO_4/Amide I and ν_1PO_4/Amide I indices …… 67
Table 3.13. Results of Mann-Whitney test for pairwise comparison between age groups to CI index…….…… 69
Table 3.14. Summary of linear regression of age groups correlation to CI……..…. 69
Table 3.15. Descriptives for the performance of regression models based on the CI for age groups…… 69
Table 3.16. Descriptive statistics to Spearman correlation between age and indices…… 70
Table 3.17. Summary of linear regression of age correlation with CI, C/C and ν_1PO_4/Amide I……..…... 70
Table 3.18. Descriptives for the performance of regression models for chronological age……... 71

ABBREVIATIONS

ANOVA	Analysis of Variance
API	Type A Carbonate Amount
BPI	Type B Carbonate Amount
BMD	Bone Mineral Density
BMT	Bone Mineral Turnover
CEI-XXI	Collection of Identified Skeletons from Century XXI, from Portuguese Coleção de Esqueletos Identificados do Século XXI
CI	Crystallinity Index
CV	Coefficient of Variation
FTIR-ATR	Fourier Transform Infrared spectroscopy in Attenuated Total Reflection
HAp	Hydroxyapatite
IR	Infrared
MAE	Mean Absolute Error
PCA	Principal Component Analysis
PC1	First Principal Component
PC2	Second Principal Component
PC3	Third Principal Component
PC4	Fourth Principal Component
PC5	Fifth Principal Component
PMI	*Post-Mortem* Interval
RMSE	Root Mean Square Error
VIF	Variance Inflation Factor
vs	*Versus*

ABSTRACT

In forensic contexts, the estimation of the biological profile of skeletal human remains is of extreme importance from the ethical, legal and criminal perspective. The prediction of chronological age at death in adults is considered one of the biggest struggles of Forensic Anthropology, since anthropological macroscopic methods usually have large estimation intervals.

The human skeleton from distinct individuals presents idiosyncrasies at the atomic and molecular level, induced by intrinsic and extrinsic factors, such as the tissue composition and organization, remodelling rate, collagen degradation and diagenetic pathways, which promote different features affecting the skeleton differently.

Femur, humerus, metatarsal, ribs, parietal and teeth samples were analyzed through Fourier Transform Infrared spectroscopy in Attenuated Total Reflectance mode. An exploration of chemometrics as a potential indicator of chronological age in adults was carried out. This was performed by skeletal structural characterization and searching for patterns in order to determine the most representative regions of the spectra and the potential statistical differences among indices *per* bone types, sex, age cohorts and age. To achieve this, an exploratory and inferential statistical analysis was implemented. The chemometric indices investigated in this study were the CI, C/P, API, BPI, C/P, ν_4PO_4/Amide I and ν_1PO_4/Amide I.

The combination of this exploratory and inferential analysis enabled to obtain distinct spectral information. Through the exploratory statistical analysis, achieved through principal components analysis, differences among bone types were observed relative to spectral variations – namely in the intensity of the $\nu_3(CO_3)_B$, amide I and amide II bands. Only for teeth discrimination among age cohorts was revealed, through the $\nu_1,\nu_3(PO_4^{3-})$ domain. Whereas *via* inferential statistical analysis, poor ability was found for age determination. Reasonable results regarding the prediction of age cohorts or chronological age from both bones and teeth were only obtained by using the CI and C/C spectral indices. High mean absolute errors were obtained for age cohorts (0.25–1.84 for long bones; 0.26–1.85 for ribs; and 0.93–1.06 for teeth) and for chronological age (4.45–25.86 for long bones and 23.57–24.45 for teeth).

RESUMO

Em contextos forenses, a estimativa do perfil biológico em restos humanos esqueletizados é de extrema importância numa perspetiva ética, legal e criminal. A previsão da idade cronológica à morte em adultos é considerada uma das maiores lacunas em Antropologia Forense, tendo em conta que os métodos antropológicos macroscópicos costumam apresentar grandes intervalos nas suas estimativas.

Os esqueletos humanos de indivíduos distintos apresentam idiossincrasias a nível atómico-molecular, induzidas por fatores intrínsecos e extrínsecos, tais como a composição e organização dos tecidos, a taxa de remodelação, a degradação do colagénio e processos diagenéticos. Estes fatores promovem diferentes características e, consequentemente, afetam o esqueleto de maneira diferente.

Recorrendo à espetroscopia de Infravermelho em Refletância Total Atenuada foram analisadas amostras humanas de fémur, úmero, metatarso, costela, parietal e dentes. Foi levada a cabo uma exploração quimiométrica para avaliar o seu potencial como indicador da idade cronológica em adultos. Tal foi realizado através da caracterização estrutural dos esqueletos e pela procura de padrões, com o objetivo de determinar as regiões mais representativas do espetro e as potenciais diferenças estatísticas entre índices para tipos de osso, sexo, classes etárias e idade. Deste modo, uma análise estatística exploratória e inferencial foi implementada. Os índices quimiométricos investigados neste estudo foram os seguintes: CI, C/P, API, BPI, C/P, ν_4PO_4/Amida I e ν_1PO_4/Amida I.

A combinação destas análises exploratória e inferencial permitiu obter informações espetrais distintas. Através da análise estatística exploratória, realizada através da análise de componentes principais, foram observadas diferenças entre tipos de osso relativamente a variações espetrais – nomeadamente na intensidade das bandas $\nu_3(CO_3^{2-})_B$, amida I e amida II. Apenas para as amostras de dentes foram encontradas discriminações entre faixas etárias, através da banda $\nu_1,\nu_3(PO_4^{3-})$. A análise estatística inferencial, por seu lado, para além da diferenciação por tipos de osso foram detetadas diferenças estatisticamente significativas para as classes etárias e idade cronológica, tanto para ossos como para dentes, de acordo com os índices espetrais IC e C/C. Os valores dos erros médios absolutos foram elevados tanto para as faixas etárias (0.25–1.84 para os ossos longos; 0.26–1.85 para as costelas; e 0.93–10.6 para os dentes) como para a idade cronológica (4.45–25.86 para ossos longos e 23.57–24.45 para os dentes).

CHAPTER 1

INTRODUCTION

1. INTRODUCTION

Forensic sciences have a vital role in the criminal Justice system by providing scientific information from various disciplines, including: chemistry, toxicology, biology, genetics, ballistics, psychology and anthropology. Forensic anthropology consists in the applications of methods from physical anthropology to forensic settings, and consequently the application of scientific knowledge to law practices [1].

In any fatality incident, victim positive identification is of primary importance and, when successful, is of crucial significance from the ethical, legal and criminal perspective [2, 3]. Disasters resulting in mass facilities commonly present a range of differentially preserved remains that may include bodies and/or body parts that are: intact, fairly intact, decomposed, fragmentary, commingles, burned or a combination of several of these states of preservation thus complicating the positive identification process [3, 4]. In any forensic case involving human skeletal remains or partially skeletonized human remains, forensic anthropologists are fundamental to obtain information from bones and teeth in order to achieve a biological profile and to reconstruct the circumstances of death.

The analysis of forensic anthropologists involves ten questions: “is it bone?”, “is it human?”, “when did the individual die?”, “what bones are present?”, “how many individuals are present?”, “age at death?”, “sex?”, “race?”, “stature?” and “factors of individualization?” [5]. The first three questions are of extreme importance to define if forensic anthropologists should be brought into the investigation. If it is not bone or if it is not human, the forensic anthropologist is no longer needed. Relatively to the third question, the case can either be considered forensic or archaeological, according to the time since individual died. The number of years a homicide takes to expire is established by the law of the country where the remains are found. In Portugal, according to the articles 122º and 131º from Código Penal Português [6], this term is 15 years to determine if the prison sentence can be applied or if have already prescribed. The last five questions – “age at death, “sex?”, “race?”, “stature?” and “factors of individualization?” – represent the basis to the estimation of the victim’s biological profile [4, 5].

One of the biggest struggles of anthropology is to estimate the age at death which is paramount to achieve positive identification. Age at death estimation can be based on several skeletal features, namely osteometry, dental features, skeletal union and fusion and skeletal metamorphosis and degeneration [7–10].

1.1. AGE AT DEATH ESTIMATION IN ANTHROPOLOGY

In anthropology, up to now, multiple methods are described allowing an age at death estimation in adults. However, several errors are associated due to the low precision of these methods, and the estimation interval is often too large to be helpful [11].

Over the course of a lifetime, elements of the skeleton undergo sequential chronological changes which can thus be used to estimate age at death. However, one must bear in mind that only physiological age can be estimated which might be quite different from chronological age because individuals of the same chronological age can show different degrees of development [10]. Also, the older the person is, the larger is the discrepancy between physiological and chronological age.

Age estimation is less precise in adults than in subadults because skeletal and dental development, the most reliable features used for that purpose, occur only until the third decade of life [10]. Age estimation in adults depend on the more highly variable degeneration in skeletal and teeth structures, and individualistic factor *e.g.* lifestyle, health and nutrition, can influence skeletal remodeling life, introducing an additional source of bias into the final assessment. Different parts of the skeleton can lead to different age rates, both between and within individuals [9]. Therefore, the older the person is, the less precise the methods are, taking into account the increasing estimate error [11].

Tooth development is more closely associated with chronological age than is the development of most of the other skeletal parts [10]. Age estimation methods apply various forms of tooth modification, including wear [12, 13], root dentine transparency [14–17], tooth cementum annulation [18, 19], racemization of aspartic acid [20, 21] and apposition of secondary dentine [22–24].

Some of the most used anthropological methods to estimate adult age are based on the: pubic symphyseal surface [25–27]; auricular surface of the ilium [28–30]; acetabulum [31]; and sternal rib end [32–36]. The interval age ranges to predict the age at death to the pubic symphyseal surface by Suchey and Brooks, auricular surface of the ilium by Buckberry and Chamberlain and acetabulum by Rougé-Maillart methods, according to the respective phases, are described in Table 1.1.

Table 1.1. Description of anthropological methods available to age at death estimation and interval age ranges.

ANTHROPOLOGICAL METHODS	CATEGORY						
	I	II	III	IV	V	VI	VII
Suchey and Brooks [27]	15–23	19–35	22–43	23–59	29–79	36–87	--
Buckberry and Chamberlain [29]	16–19	21–38	16–65	28–81	29–88	39–91	53–92
Rougé-Maillart [31]	16–28	19–39	30–68	23–67	28–83	48–95	62–94

The extensive age interval to each category illustrates the poor reliability to the age at death estimation of the different anthropological methods applied to different anatomical regions.

Hence, the exploration of other potentially useful indicators is crucial, such as chemometrics, to develop a new method based at the chemical characteristics of human bones and teeth, contributing to the establishment of human remains in forensic and archaeologic contexts.

1.2. BONES AND TEETH COMPOSITION

Bone is a complex tissue that consists predominantly in an inorganic fraction (about 60%), an organic fraction (about 25%) and water (approximately 10%) [37–40].

The organic phase is mainly composed of lipids and proteins, largely of type I collagen, which accounts for approximately 90%, and the remainder being composed of varied cellular constituents, such as non-collagenous proteins [38, 40–42]. Type I collagen is a large fibrous protein with a highly repetitive amino acid sequence, allowing three polypeptide chains to fold into a unique triple helical structure, consisting of three domains [43–45].

The inorganic phase mostly comprises carbonated-substituted apatite. This apatite, named bioapatite, is similar in composition and structure to hydroxyapatite and can be summarized as the following formula: $Ca_{10}(PO_4^{3-})_{6-x}(OH^-)_{2-y}(CO_3^{2-})_{x+y}$, exhibiting plate-like crystals with 20 to 80 nm in length and 2 to 5 nm thick [40, 46].

Concerning the incorporation of carbonate ions into the apatite lattice, as represented in Figure 1.1, replacement of carbonates (CO_3^{2-}) occurs for the phosphate groups (PO_4^{3-}), designed by type B substitution, or for the hydroxyl groups (OH^-), leading to type A substitution much less common [47, 48]. Presenting different properties, carbonates have a different geometry and charge than phosphates, and are much higher than hydroxyl groups. Consequently, these substitutions creates distortions in the crystal lattice promoting a reduction of crystallinity in bioapatite compared to hydroxyapatite [49–53]. The

particularity of nonstoichiometry of the bone mineral, leads to an incorporation of varying amounts of water and other ions such as calcium (Ca^{2+}), sodium (Na^{+}), magnesium (Mg^{2+}), strontium (Sr^{2+}), potassium (K^{+}), fluorine (F^{-}) or chlorine (Cl^{-}) into the crystal lattice [42, 51, 54–56].

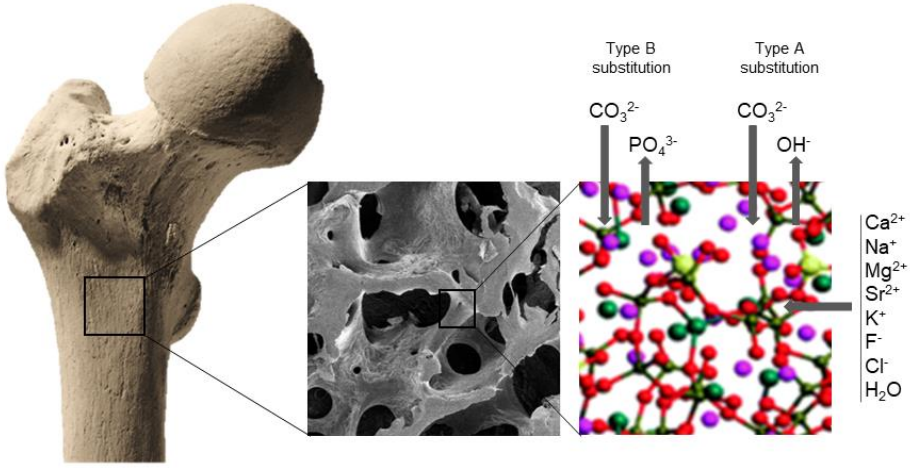

Figure 1.1. Representation of chemical substitutions in bioapatite crystal lattice.

The relative proportions of these constituents, as well as its geometric and spatial arrangement, may vary as a result of factors of development, depend on the bone type – cortical or trabecular –, pathologies, age at death, *post-mortem* period and environmental factors that could be in contact with the remains [44, 57].

Chemical properties of bioapatite crystals are affected by several intrinsic and extrinsic factors including collagen properties and the distribution of non-collagenous proteins, which represent an important role to the mineralization and growth of crystals, cell viability and bone turnover [41, 58]. The less crystalline mineral is more favourable to the incorporation of water in lattice, and the water of hydration presence will facilitate further substitutions in bone and so change properties. Thus, as bioapatite has a lower crystallinity than hydroxyapatite derived by his high carbonate substitution degree, is directly responsible for small sized crystals, with a high structural strain, a high surface area and increased solubility in water [58–60]. These features promotes bone to *post mortem* alterations, accompanied by loss of the organic phase, caused by environmental factors [61, 62].

The inorganic fraction of bone is intimately associated with the organic matrix and they are responsible for the functional characteristics of bone matrix, contributing to the mineral homeostasis of the organism. Collagen molecules intertwine to form flexible and slightly elastic fibres in bone, and mineral components provide bone with rigidity and

hardness, remaining these characteristics unaltered after death, in contrast to flexibility [40, 42, 63, 64].

Relatively to the teeth composition, teeth are divided into two main parts, crown and root, and contain four dental tissues: pulp, enamel, dentine and cementum. With the exception of pulp, the other tissues are mineralised. Whilst the crown is covered by enamel the root is covered by cementum. Interiorly, the tooth is composed of dentine [65, 66].

The chemical composition of tooth is similar to the bone and also possesses a molecular structure comprising organic and inorganic compounds. Inorganic matter represents the major part of the constitution, almost 70% for dentine and cementum, and 95% for enamel [62]. The mineralised tissues contain trace amounts of collagen, and non-collagenous proteins [40].

Histologically, cementum is partially cellular, has a structure equivalent to bone, and his layer thickness generally increases with age of individual [66–68]. Enamel is the hardest, densest and least porous of the mineralised tissues due to the high percentage of mineral compounds consequently, it is the most durable of human tissues [41, 68, 69].

1.3. BONE ORGANIZATION

Bone organization in the adult skeleton has two basic structural components, depending on the structure type of bone tissue: cortical or compact bone and trabecular or spongy bone, as represented in Figure 1.2 [41, 64]. They differ according to their organization: cortical bone is found in the walls of bone shafts and on external surfaces and presents a solid and dense appearance; trabecular bone has a more spongy, porous, lightweight structure, and could be found under protuberances where tendons attach – in the vertebra bodies, in the ends of long bones, in short bones, and sandwiched within flat bones [64].

The molecular and cellular compositions of compact and trabecular bone tissue are similar, only possess difference in porosity that permits separate these gross anatomical bone types [64].

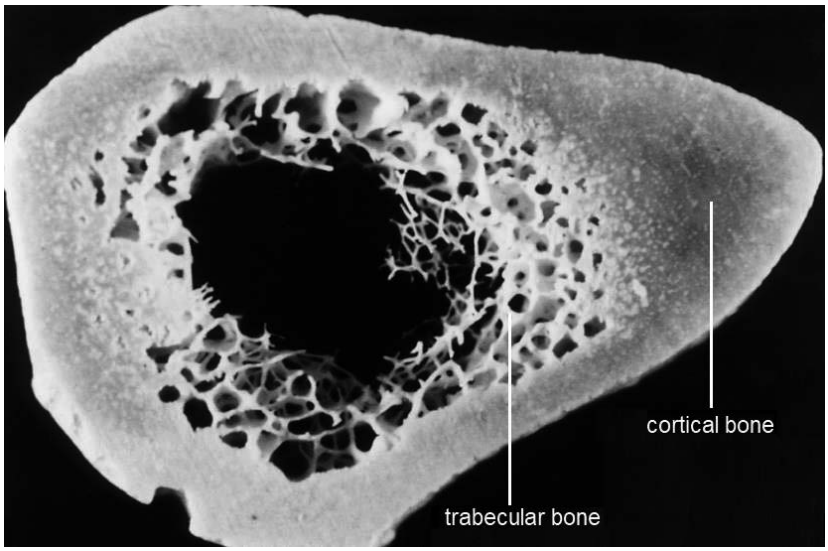

Figure 1.2. Representation of cortical and trabecular bone. Adapted from [64].

In vivo, bone is a live tissue and the composition along the same bone varies as a consequence of the constant bone resorption/regeneration metabolic processes [38–40, 70]. Cummaudo *et al.* [71] pointed the existence of variability in histomorphology between different bones of the same individual, in different portion of the same bone and in different part of the same section. Long bones present a higher variability, whilst flat and irregular bones appeared to be described by a greater uniformity.

1.4. BONE REMODELLING RATE

During life, bone undergoes modelling and remodelling. Bone modelling commences in utero and continues until the early teenage years, and characterize the process by which bone change shape and size in response to physiologic influences or mechanical forces that are encountered by the skeleton [72, 73].

Bone remodelling is conducted by osteoclasts and osteoblasts and involves the removal of old bone, and the replacement of this by newly formed bone matrix which then undergoes mineralisation to form new bone [72]. Bone remodelling is essential to the ability of bone repair damage tissue and successfully adapt to variable loading conditions. Therefore, this process occurs throughout the whole human lifespan until death to prevent the accumulation of microdamage in the skeleton, and to bone may maintain its strength and mineral homeostasis [43, 74].

Bone resorption and bone formation are tightly coupled in bone remodelling, and an imbalance of these two processes lead to bone mineral diseases such as osteoporosis

when there is excess of bone loss and osteopetrosis when there is excess of bone formation [72]. A gradual deterioration of the mechanical properties in bone collagen occurs with age and has a tendency to increase with age, also there is an age-related reduction of collagen that may contribute to changes occurred in whole bone strength and toughness, increasing fracture risk, in older men and women [75, 76]. Zioupos *et al.* [77] assumed that aging is accompanied by increased remodelling and replacing of bone material, so a bone of an individual of a certain chronological age presents microstructural elements of various tissue ages, consequently an older bone shows a heterogeneous composition. Molecular changes in either inorganic and organic fractions of the matrix, the rate of bone turnover or the degree of mineralisation can also be related to changes in the mechanical properties of bone [76].

Osteoporosis possess an incidence rate considerably elevated in women, when compared to men. Most white women under age 50 have normal density, but with advancing age, the tendency to have osteoporosis increases drastically [78]. Although osteoporosis primarily affects older persons, predisposition to the condition is established in young adulthood, bone tissue undergoes a continuous remodelling process consisting of periods of bone resorption and formation, followed by relatively stable bone mineral density until the menopause transition. The risk of fracture in early postmenopausal women is, in large part related to the bone mineral density (BMD). Elevated levels of bone turnover markers (BTM) are associated with lower bone mineral density at various skeletal sites and, consequently, directly correlated to the rate of bone loss. Levels are weaker in older men who have only slightly elevated levels and relatively slow bone loss. Thus, high bone turnover induces multitudinous alterations in bone: decrease in bone mineral density, deterioration of bone microarchitecture, decreased collagen-linking and bone tissue mineralisation [74, 79].

The estimated rate of remodelling varies according to biological sex, health, age, mechanical load and genetic predisposition. Considering the surface to volume ratio differences in bone shape and size, the rate depends on the specific kind of bone and part of the skeleton involved [73, 80–82].

In general, throughout life of an adult, cortical bone turnover presents a rate of 2% to 3% per year, remodelling over a period of decades, while bones with abundant trabecular tissue, such as ribs, can remodel entirely over a few years, 3 to 10 times faster [72, 80, 82, 83]. The rate of cortical bone turnover, which is due to rapid growth, modelling and remodelling reaches values about 50% per year in mid-shift of the femur during the first 2 years of life and eventually decreases to a rate of 2% to 5% per year in the elderly people [43]. The rate of trabecular bone is higher, indicating that trabecular bone turnover is more important for mineral metabolism.

The predicted collagen turnover rate during adolescent growth, for both sexes, is much higher than in later life (10% to 30% per year at age 10–15), although this value is

probably rather dependent on the geometrical growth pattern of the bone. During adolescence, male collagen turnover rate is much greater than the female rate [84]. Collagen turnover rate of females decreases, on average, from 4% to 3% per year from 20 to 80 years old, whilst male collagen turnover rate changes on average from 3% to 1,5% per year. So, in opposite to the pattern during adolescence, males have lower turnover rate than females when older [84].

1.5. DIAGENESIS

In vivo, the mineralised tissues experience an environment that is strictly controlled by the body's cellular and metabolic processes that remodel and repair the skeleton, maintain calcium homeostasis, and limit the action of microorganisms [41]. After death, once skeletonization has begun, the skeleton is exposed to an open system, and a diagenetic process begin.

Diagenesis is a highly complex phenomenon involving the physical, chemical, histological and mechanical alterations to bones and teeth that occur at different time scales from the time of death and depend on the local geochemical conditions [85, 86]. The diagenetic pathway affecting bone preservation are influenced by different factors related to microbial activity, temperature, humidity, hydrology, pH and conditions of the burial environment may rapidly lead to a particular or complete degradation of organic matter [85, 87]. Thus, bone undergoes several modifications in molecular structure, bone crystallites will spontaneously recrystallize and increase in size. The recrystallization process appears to be associated with collagen decomposition, carbonate loss and uptake of exogenous chemical elements (*e.g.* fluorine) [61, 84, 85, 88].

In opposite, dental tissues remains unaltered after deposition and the remodelling rate throughout life is minimal [80, 82].

Considering a possible association through the described features – composition and organization, remodelling rate and diagenesis –, a chemical evaluation based on the premises that macroscopic changes observed may interfere in other microscopic variations, eventually can confer some potential to the age at death estimation, through bone composition, in particular throughout crystallinity.

1.6. METHODOLOGY REVIEW

Bone and teeth evaluation required for specific tools to allow an interpretation of microstructure and possible chemical alterations caused by factors related to the advancing age and diagenetic pathways. An extensive range of techniques are described in literature to proceed bone and teeth analysis with forensic purposes, and the selection of the techniques takes into account the specific goal to be attained, since each one gives different information. Considering the vibrational spectrum a unique physical property and characteristic of a molecule, vibrational spectroscopy techniques contribute efficiently due to the spectral information obtained through organic and inorganic components, and the possibility to determine the influence of internal and external variables across human bones and teeth that may interfere with their intrinsic parameters. Namely, Fourier Transform Infrared (FTIR) spectroscopy, the most commonly applied vibrational spectroscopic technique for bone and teeth analysis, has been valuating bone crystallinity, as well as carbonate and organic contents [50, 54, 61, 89–93]. The fact that variations across elemental structure of these skeletal elements are clearly reflected in its vibrational fingerprint fully justifies the use of vibrational spectroscopy [94].

1.6.1. FOURIER TRANSFORM INFRARED SPECTROSCOPY

Infrared (IR) spectroscopy consists on the absorption of electromagnetic radiation at frequencies corresponding to the vibrational modes of the molecule, *i.e.,* the incident light with the same energy of a specific vibrational transition is absorbed, reproduced in a spectral band [95–98]. The atoms in molecules are in constant movement, oscillating around their equilibrium positions, changing bond lengths and angles, describing the vibrations modes as stretching and bendings, respectively [95]. The fundamental requirement to a molecule exhibit absorption on the IR range, a molecular electric dipole must change during the movement [95, 99].

A vibrational spectrum results from transitions – schematically represented in Figure 1.3 – between quantised vibrational energy states, each fundamental vibration mode, *i*, that involves nearly harmonic displacements of the atoms, corresponding to a characteristic frequency, v_i [96, 99]. The functional groups possess characteristic frequencies. The nature of the neighbourhood of these functional groups affect their vibrational modes' frequency, *i.e.* the same group in different atomic environments will vibrate slightly different, resulting in additional information about structural alterations [43, 96].

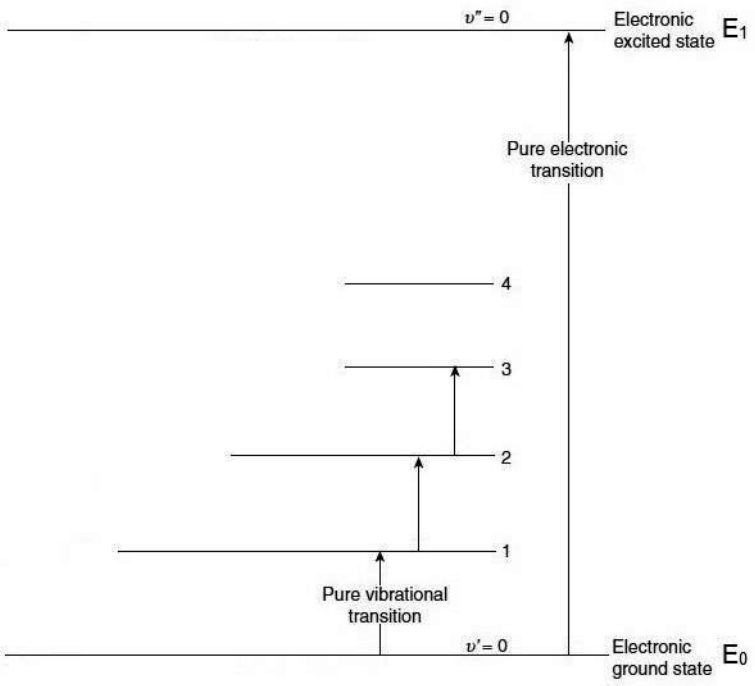

Figure 1.3. Schematic representation of the energy levels and vibrational transitions of IR absorption. Adapted from [99].

Each molecule has its own unique vibrational characteristics, so the observation of spectral features in a certain region of the spectrum is indicative of a specific chemical functional group in the molecule [96]. The intensity of an absorption band assigned to a functional group increases proportionally with the number of times that the functional group occurs within the molecule [97]. Therefore, each spectrum acts as a chemical fingerprint and can be analysed for unique information about bone composition, the absorbance bands can be ascribed to the internal vibrations of particular molecular groups, such as carbonate and phosphate.

The IR spectral region comprise the far-IR (< 200 cm^{-1}), mid-IR (200–4000 cm^{-1}) and near-IR (4000–13000 cm^{-1}). Generality, most of the fundamental vibrations occur among 400 and 4000 cm^{-1}, corresponding to the mid-IR region, considering the most useful spectral region. In turn, far-IR region is rarely used for structural elucidation, but contains useful information of the molecular skeleton through specific vibrations: torsions, crystal lattice modes, H-band-associated stretching, and oscillations involving heavy metals – especially for inorganic components [95, 96, 100]. The near-IR interval comprises overtones – multiples of fundamental vibration frequencies – and combinations of fundamental modes [95].

Interaction of IR radiation with a sample may occur in transmission, reflectance or transflection. The transmission mode is based upon the absorption of IR radiation as it

passes through a sample, which is contained within a pellet of an IR transparent support, usually KBr [95, 101]. This process comprises grinding in a mortar and applying pressure to form a homogeneous pellet. Despite the amount needs are very small, requires some time for sample preparation and the sample is not recoverable. Thompson *et al.* [102] and Surovell and Stiner [103] demonstrated experimentally that the methodology of FTIR-KBr analysis introduces alterations in bone crystallinity, influenced by sample preparation, the type and extension of grinding.

Relatively to the reflectance mode, Attenuated Total Reflectance (ATR), utilizes the phenomenon of total internal reflection. The radiation beams enters a crystal, with a high reflection index, and is internally reflected if the incidence angle in the sample crystal interface is greater than the critical angle [95, 98, 101], as demonstrated in Figure 1.4. Interaction between the radiation and the sample occurs on this surface and depends according to the sample characteristics and environment surrounding. The beam penetrates beyond the reflecting surface and when a material that selectively absorbs radiation is in close contact with the reflecting surface, the beam loses energy at the wavelength were the material absorbs [95, 98, 101].

In a FTIR spectrometer, the radiation emerging from the source passed through an interferometer before interact with the sample and reaching the detector. A mathematical algorithm, the Fourier transformation, is used to convert the interferogram – in the time domain – that are collected by a detector into the spectrum – in the wavenumber domain [95].

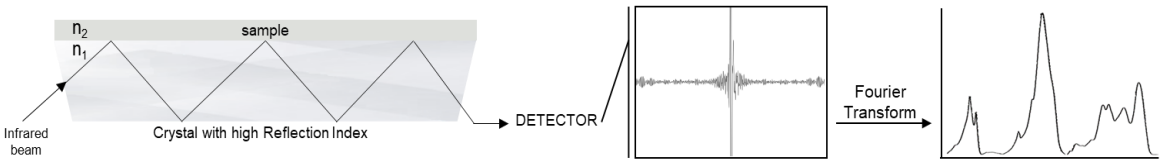

Figure 1.4. Schematic representation of Fourier Transform Infrared (FTIR) spectrometer in Attenuated Total Reflectance (ATR) mode.

FTIR-ATR is one of the most versatile technique for powder analysis, considering the data acquisition time, non-destructive analysis, reduced samples amount needed, minimal sample preparation and simple data analysis [102, 104]. The only requirement consists on the intimate contact of the sample with the crystal, which is achieved by pressing the solid into the crystal with a high pressure clamp.

Beasley *et al.* [85] reported that FTIR-ATR appears to be a reliable and quite appropriate technique for bone analysis with sufficient spectral resolution. Previous studies have concluded that is ideal for obtaining the spectra from powder samples because it

minimizes distortions due to optical saturation and dispersion, and are free of potential chemical alterations such as water adsorption and ion exchange [85, 86]. In comparison to FTIR-KBr, that is susceptible to the referred alterations possible produced during KBr pellet preparation.

Despite the fact that all IR techniques identify the same chemical information about the sample, differences in resolution of the spectra may occur, as reported by Beasley *et al.* [85], when comparing spectroscopic techniques, not allowing a direct comparison between spectroscopic indices obtained from these different techniques, indicating that the different techniques are not directly comparable.

In addition, ATR spectra present distortions of the relative peak intensities in comparison to those acquires in transmission mode, since depth of penetration by the incident radiation is dependent on its wavelength, the higher the wavelength the larger the band intensity. The depth of penetration is given by the following formula:

$$d_p = \frac{\lambda}{2\pi n_1 \sqrt{sin^2\theta - (n_2/n_1)^2}} \quad (1.1)$$

Where d_p is the penetration depth, λ is the wavelength of the incident radiation, and n_1 represents the refractive indices of the crystal and n_2 the angle of incident radiation [95, 101, 104]. Moreover, an effect of anomalous dispersion leads to peaks shifting, because the refraction index of the sample undergoes quick changes nearby an absorption peak [104]. Therefore, to remove the referred effects from the spectra, an ATR correction function should be applied.

An interference of the H_2O and CO_2 signals override relevant spectral information in the 1500–4000 cm^{-1} range, constituting an obstacle to the IR spectroscopic analysis. However, using a purged FTIR apparatus this problem is solved.

Considering the spectral region, from 400 to 4000 cm^{-1}, the main infrared vibrational wavenumbers observed for human teeth and bones samples described in literature are displayed in Table 1.2.

Table 1.2. Infrared vibration wavenumber observed for human bones and teeth samples.

WAVENUMBER (CM^{-1})	ASSIGNMENT	REFERENCE
3573	$\nu(OH^-)$ (HAp)	[37, 47]
3300	$\nu(OH^-)$ (water)	[47]
2960–2850	ν(CH) (lipids)	[47]
1640–1660	Amide I (collagen)	[47]
1650	$\delta(HOH)_{water}$	[47]
1540–1580	Amide II (collagen)	[47, 55]
1540	$\nu_3(CO_3^{2-})_A$	[92]
1460	$\delta(CH_2)_{lipids}$	[47, 89, 105]
1450	$\nu_3(CO_3^{2-})_{A+B}$	[51]
1415	$\nu_3(CO_3^{2-})_B$	[105]
1242 *w*	Amide III (collagen)	[47]
1090 *sh*	$\nu_3(PO_4^{3-})$ (presence of fluorapatite)	[106]
1035	$\nu_3(PO_4^{2-})$	[60, 107]
960	$\nu_1(PO_4^{3-})$	[60, 89]
878	$\nu_2(CO_3^{2-})_A$	[90, 108]
872	$\nu_2(CO_3^{2-})_B$	[90, 108]
700 *w*	$\nu_4(CO_3^{2-})$	[60]
710	$CO(CaCO_3)$	[107]
630	$OH_{libration}$ (HAp)	[47, 60, 109]
565, 603	$\nu_4(PO_4^{3-})$	[55, 89]
470	$\nu_2(PO_4^{3-})$	[60, 89]

**sh* – shoulder; *w* – weak; δ – in plane deformation; ν – stretching; $(CO_3^{2-})_A$ – A type carbonate; $(CO_3^{2-})_B$ – B type carbonate.

1.6.2. SPECTROSCOPIC INDICES

Considering the potential information of bone constituents at molecular level, several relationships were developed and displayed in literature to attempt to explore bone and teeth properties, relative to mineral and organic content, crystallinity, carbonate substitution into the apatite lattice and collagen crosslinking. The characteristics of bioapatite crystals are highly correlated and dependent on carbonate concentrations: causing changes in crystallinity as it is inversely related to crystal growth [53, 110].

The CI, Crystallinity Index, is considered an reliable index and one of the most widely used parameters to access bone and teeth properties and chemical alterations induced by multiple factors [50, 93, 111]. The crystallinity provides an indication of the combination among the relative sizes of crystals and the atomic order within lattice [88, 105, 107, 108, 112], especially with respect to relative positions of phosphate ions.

The mathematical calculation based on spectral data, suggested by Weiner and Bar-Yosef [112], based on the work by Termine and Posner [109], measures the heights at

the absorption bands at 565 and 605 cm^{-1} and the height of the minimum through between the split peaks. The Abs565 and Abs605 cm^{-1} describes the maxima of the bands assigned to the phosphate antisymmetric stretching mode, $\nu_4(PO_4^{3-})$, that is triple degenerate and appears split into two well-defined features – due to the anisotropic electric field of the crystalline apatite –, and Abs595 cm^{-1} represents the minima between these signals [49, 108].

Consequently, as CI represents the degree of order within the crystal matrix of the mineral component of bone: in fresh, unaltered bone, contain small size crystals with an irregular lattice structure, and as a consequence has a greater strain, resulting in a low CI value; whilst altered bone, subjected to chemical alterations, indicate large crystals size and a more regularly organized lattice, which therefore results in high values of CI [85, 103]. Because of its low crystallinity, bone apatite is highly reactive, and *post-mortem* processes tends to increase due to diagenesis, and bioapatite becomes less reactive [49, 51, 88, 93, 105].

Relatively to the carbonate content of bone mineral, the type and extent of the substitution influences the crystals' solubility, size and shape.

Carbonate to phosphate ratio (C/P), calculated throughout Abs1415 and Abs1035 cm^{-1} [54, 92, 107], measures the diagenesis reflecting the carbonate to phosphate content [85]. Thus, indicating the level of carbonate substitution, this parameter is considered a good indicator of the bone turnover and remodeling activity [113]. The signal at 1035 cm^{-1}, assigned to $\nu_3(PO_4^{3-})$, is a good reference for the total component of phosphate, since it is not affected by any splitting nor overlapped by any other relevant signal, in contrast to the intensity of the 1415 cm^{-1} band, which is solely assigned to type B carbonates, $\nu_3(CO_3^{2-})_B$ [49].

The amount of type A and type B carbonates relative to phosphate are represented by the API and BPI indices, respectively [51, 105]. The amount of type A carbonates within the bone matrix, API, is calculated through Abs1540 cm^1/Abs603 cm^{-1}. The vibrational band at 1540 cm^{-1} accounts for overlapping peaks, due to contribution from the amide II mode, at 1540–1550 cm^{-1}. Thus, care must be taken regarding API values, conveys such a large error, so it is not a reliable index. Type B carbonate to phosphate ratio, BPI, determined by dividing the intensity of the band at 1415 cm^{-1} by the band at 603 cm^{-1}, represents the amount of type B carbonates [51, 105]. Both the C/P and BPI ratios are inversely proportional to CI, the higher these values the higher is the amount of type B carbonates.

The C/C ratio is described by the division of the band height at *ca.* 1450 cm^{-1} and *ca.* 1415 cm^{-1}, and may be ascribed to a combination of the total content of type A and B carbonates (A+B) and the B type carbonates [51, 102]. However, the assignment of the

vibrational feature centered at 1450 cm^{-1} corresponds to both carbonate (A+B) and CH_2 deformation from the lipid components of bone.

Attending to the fact that the degradation of organic matter is higher than the bioapatite in most burial conditions, the bands related to structural features of collagen could be particularly informative about collagen preservation. The spectral relationship [114] among the relative proportion of mineral to the collagen fraction, is described by the quotient of the band heights at 960 cm^{-1}, attributed to phosphate stretching in bone mineral $\nu_1(PO_4^{3-})$, and at *ca.* 1640 cm^{-1}, assigned to amide I stretching that inform about the peptide backbone of collagen [115].

1.7. THEORETICAL FOUNDATIONS

Vibrational spectroscopy is considered an ideal platform for investigation of human bone and teeth tissues, essentially taking advantage through chemometric methods in order to reveal a more detailed spectral information. It has huge potentiality for discriminating between fossilised, archaeological and modern bones [51, 106, 116] or for *post-mortem* interval estimation in forensic cases [63, 117–120].

Focusing on the purpose of this study, alterations in bone microstructure due to aging has also been mentioned in literature. Nevertheless, bone tissue suffers a multivariable process of degradation that commences immediately following death, depending on environmental conditions, promoting variations of the chemical nature of the tissues and the degree of alteration of both mineral and organic phases, consequently causing alterations in spectroscopic indices. Besides the external induced factors, crystallinity is not uniform throughout the skeleton, and it varies between the different mineralized tissues of the human body [121].

Termine and Posner [109], through a quantitative analysis of whole femurs from male rats, demonstrated that the amount of amorphous calcium phosphate decreases in whole bone while the crystalline bone apatite increases during early stages of bone formation. Bartsiokas and Middleton [122] evidenced a potential in relating crystallinity or crystal size to age, with the older the bone the higher is its crystallinity. Paschalis *et al.* [123] proved the relation between bone age and crystallinity/maturity, meaning that younger normal bone is less mature/crystalline than older. Thus, mineral quality changes in monotonic fashion with bone age: the older the mineral, the more mature and crystalline it becomes. Matsushima and Hikichi [124] showed that significant changes in structure and composition occur with age and maturation. The increase in the crystallinity with age is

attributed to an increase in crystallite size, a decrease in lattice imperfections, or a combination of both effects.

In healthy bone, the average carbonate content is about 6%, although it is known to vary according to the age of the individual – increases with increasing bone age – as well as anatomical compartment [125, 126].

An examination of chicken bones of different ages stages has revealed that it is the unstable carbonate fraction that increases with age, while the ratio of A type to B type carbonate remains constant. Yet, the age distribution of crystals in bone will contain a certain proportion of the very youngest crystals and a certain proportion of the very oldest crystals, as well as a distribution of crystals of all other ages, depending on the age, the rates of bone formation, and the rates and location of bone resorption [125].

Relatively to the organic fraction of bone, Very *et al.* [127] discovered that bone aging cause small positional and intensity shifts in bands associated with the amide I and amide II vibrations, possibly due to conformational changes in the proteins that make up the organic matrix. Thus, a quantitative change in the entire organic part of bone tissue is consistent with the effect of aging.

The physicochemical properties of bone tissue suffer alterations: the orderliness of the mineral crystal lattice improved, the collagen matrix became more mineralized and there were more carbonate ions occupying the stoichiometric phosphate locations. Related with that, an increase of mineral crystallinity, mineral/matrix ratio and B type carbonate substitution were correlated with the deterioration of structural and tissue-level mechanical properties of aging compact bone. Deducing, the age-related degradation in tissue and organ-level mechanical properties of rat femoral cortical bone was significantly correlated with age-related changes in the physicochemical status of mineral crystals of bone tissue [128].

In contrast to the described state-of-the-art of age estimation, some studies have found little or no correlation between CI and the age of a bone sample [108, 129, 130].

1.8. AIMS OF THE STUDY

Human bones and teeth are often found in both archaeological and forensic contexts, and their importance for the study of past populations or for victim identification in forensic investigation is unquestionable. The age at death estimation, consisting in one of the parameters to achieve positive identification or to complete a biological profile, is crucial to complete the skeleton individualization. Nevertheless, being considered one of the biggest struggles in forensic anthropology, due to the errors associated to the osteometric

methods, the chemical evaluation of bone and teeth components possibly can reflect individualizing characteristics according to the properties associated to the individual age.

The present investigation focuses in the use of chemometrics through vibrational spectroscopy as a potential indicator of chemical alterations occurring at the microscopic level in human bone and teeth according to different age cohorts. The several associated parameters of these anatomical skeletal remains influence the internal characteristics, consequently altering the chemical composition which possibly causes changes taking place at specific wavenumbers.

CHAPTER 2

EXPERIMENTAL

2. EXPERIMENTAL

2.1. SAMPLE DESCRIPTION

The bone samples were obtained from 21st century identified skeletal collection (CEI_XXI) [131] housed at the Laboratory of Forensic Anthropology of the University of Coimbra, Portugal. The teeth samples were provided by different dental clinics after informed consent (Ref. 108-CE-2014) obtained under the scope of previous work [132, 133].

The bone samples were obtained on five different elements: skull – samples collected from the parietal –, first metatarsal, one of the third to ninth ribs and the mid-section of the diaphysis of femur and humerus. Different bones were selected due to the heterogeneity of bone composition and bone remodelling, as described in sub-chapter 1.4.

The right antimeres of the skeleton were selected to proceed with the chemical analysis in order to maintain the integrity of left bones which are conventionally used for anthropological studies. However, in cases where the right bones were absent, the left ones were used instead.

Additionally, some of the bones were interdicted for use such as, autopsied skulls – preventing the collection of the samples from the parietal bone –, extremely fragile/degraded bones and bones with evidence for pathologies and/or disease. As a consequence, the number of samples collected from each type of bone is different.

The skeletons were grouped in five different age groups: from 28 to 59 years old, 60 to 69 years old, 70 to 79 years old, 80 to 89 years old and 90 to 99 years old, each group being composed by at least, thirty individuals –as represented in Table 2.1. The first group includes a wide range of ages because the skeleton collection has few younger individuals. The numbers of males and females in each group were kept as similar as possible in order to identify possible sex-related chemical differences observable in the spectra.

Since the goal of the present study is the estimation of age at death, this information for each individual was obtained as well as the *post-mortem interval* (PMI) which may have an effect on diagenesis. The age at death and sex distribution of the individuals from the CEI_XXI collection, can be found in Table 2.1.

Table 2.1. Number of bone samples to each type of bone according to age at death group and sex, for the individuals of the CEI_XXI collection.

AGE GROUP (YEARS)	NUMBER OF BONE SAMPLES	NUMBER OF MALES	NUMBER OF FEMALES
AGE <60			
Femur	15	71	8	7
Humerus	15			
MT1	15			
Rib	15			
Parietal	11			
AGE 60-69			
Femur	27	132	14	13
Humerus	27			
MT1	27			
Rib	26			
Parietal	25			
AGE 70-79			
Femur	30	148	15	15
Humerus	29			
MT1	30			
Rib	29			
Parietal	30			
AGE 80-89			
Femur	30	150	15	15
Humerus	30			
MT1	30			
Rib	30			
Parietal	30			
AGE 90-99			
Femur	22	109	9	13
Humerus	22			
MT1	22			
Rib	22			
Parietal	21			
BONE TYPE			
Femur	124		
Humerus	123		
Metatarsal	124		
Rib	122		
Parietal	117		
TOTAL	**610**	**61**	**63**

Regarding the teeth samples, age and sex was known – comprising individuals aged between 18 to 82 years old – Table 2.2. These samples are from all teeth types and quadrants and unlike bone samples, they mainly belonged to young individuals.

Table 2.2. Number of teeth samples according to each age group and sex.

AGE GROUP	NUMBER OF TEETH SAMPLES	MALE	FEMALE
AGE 18-29	29	15	14
AGE 30-39	16	5	11
AGE 40-59	20	11	9
AGE 60-69	20	13	7
AGE 70-82	20	14	6
TOTAL	**105**	**58**	**47**

In total, 715 samples were collected: 610 bone samples from 124 skeletons, 61 males and 63 females, and 105 teeth, from 58 males and 47 females.

2.2. SAMPLE PREPARATION

For samples collection, a scalpel was used. First the superficial layer of bone was carefully removed, after a thin bone powder was collected by scraping, and stored in Eppendorf tubes identified with the individual and bone origin. Between samples collection, the scalpel was cleaned with tissue paper in order to avoid contamination. The teeth samples were collected from the root, using the same procedure. The mineralized tissue in these teeth samples is cementum, comprising 70% of inorganic matter and trace amounts of collagenous and non-collagenous proteins.

The femora and humeri from the skeletons CEI_XXI_1 to CEI_XXI_85 – excluding the CEI_XXI_17, CEI_XXI_24, CEI_XXI_26, CEI_XXI_32, CEI_XXI_48, CEI_XXI_64 and CEI_XXI_77 – were sampled by a different operator.

The sampling site was specific for each type of bone, as demonstrated in Figures 2.1 to 2.5. According to Thompson *et al.* [93] and Gonçalves *et al.* [111], the selection of osteological sites to the long bones – from the periosteal surface at the mid-point of the diaphysis – is crucial, since interferences based on the chemical composition of bone are local specific, demonstrated by heterogeneity at intrabone, intraskeleton and interskeleton level. Areas that are traditionally susceptible to intensive reorganization, *e.g.* areas of entheseal attachments, or presenting pathologies or traumas, should be avoided. Hence, this selection will reduce the effect of some influencing variables, considering the impact of certain pathological conditions [134].

Figure 2.1. Sampling illustration on the posterior part of the mid-section of the femoral diaphysis of skeleton CEI_XXI_132.

Figure 2.2. Sampling illustration on the anterior part of the mid-section of the humeral diaphysis of skeleton CEI_XXI_132.

Figure 2.3. Sampling illustration on the parietal bone of skeleton CEI_XXI_132.

Figure 2.4. Sampling illustration on the proximal rib of skeleton CEI_XXI_132.

Figure 2.5. Sampling illustration on the first metatarsal of skeleton CEI_XXI_132.

2.3. FOURIER TRANSFORM INFRARED SPECTROSCOPY, IN ATTENUATED TOTAL REFLECTANCE (ATR) MODE

A Bruker Optics Vertex 70 FTIR spectrometer, purged by CO_2-free dry air, with a Platinum ATR single reflection diamond accessory, with a KBr beam splitter, was used to record the spectrum of powder bone and teeth in the mid-IR range, 400 cm^{-1} to 4000 cm^{-1}. A spectral resolution of 2 cm^{-1} and 128 scans was used. The detector, Mercury Cadmium Telluride (MCT), was cooled with liquid nitrogen.

Using the *Opus 8.1 spectroscopy* software, atmospheric compensation was applied and the spectra were corrected for the frequency dependence of the penetration deep of the electric field in ATR, considering the mean reflection index of sample 1.25. Under these conditions, the wavenumber accuracy is better than 1 cm^{-1}.

2.4. SPECTRA ANALYSIS

The spectra were baseline corrected and normalized to [0,1] relative to the most intense phosphate band at *ca.* 1035 cm^{-1}. In order to evaluate the chemical composition of the samples several indices, summarized in Table 2.3, were calculated.

Table 2.3. Description of the indices used to evaluate the chemical composition of each sample.

INDEX	CALCULATION	REFERENCES
Crystallinity Index (CI)	$\frac{\mathrm{Abs}(605\ \mathrm{cm^{-1}}) + \mathrm{Abs}(565\ \mathrm{cm^{-1}})}{\mathrm{Abs}(595\ \mathrm{cm^{-1}})}$	Weiner and Bar-Yosef, 1990
Carbonate to Phosphate (C/P)	$\frac{\mathrm{Abs}(1415\ \mathrm{cm^{-1}})}{\mathrm{Abs}(1035\ \mathrm{cm^{-1}})}$	Thompson *et al.*, 2013
Type A Carbonates (API)	$\frac{\mathrm{Abs}(1450\ \mathrm{cm^{-1}})}{\mathrm{Abs}(603\ \mathrm{cm^{-1}})}$	Snoeck *et al.*, 2014 Sponheimer and Lee-Thorp, 1999
Type B Carbonates (BPI)	$\frac{\mathrm{Abs}(1415\ \mathrm{cm^{-1}})}{\mathrm{Abs}(603\ \mathrm{cm^{-1}})}$	Snoeck *et al.*, 2014 Lee Thorp and Sponheimer, 1999
Carbonates A + Carbonates B to Carbonates B (C/C)	$\frac{\mathrm{Abs}(1450\ \mathrm{cm^{-1}})}{\mathrm{Abs}(1415\ \mathrm{cm^{-1}})}$	Snoeck *et al.*, 2014
$\boldsymbol{\nu}_4$ Phosphate to Amide I ($\boldsymbol{\nu}_4PO_4$/Amide I)	$\frac{\mathrm{Abs}(565\ \mathrm{cm^{-1}})}{\mathrm{Abs}(1640\ \mathrm{cm^{-1}})}$	This study
$\boldsymbol{\nu}_1$ Phosphate to Amide I ($\boldsymbol{\nu}_1PO_4$/Amide I)	$\frac{\mathrm{Abs}(960\ \mathrm{cm^{-1}})}{\mathrm{Abs}(1640\ \mathrm{cm^{-1}})}$	France *et al.,* 2014

A correlation among *post-mortem* interval (PMI), *i.e.* the period of time ranging from the inhumation until the date of spectra acquisition, and the several indices, is important to perform to verify if this period have some effect on the results.

Overlap spectrum of tooth and bone powder is demonstrated in Figure 2.6, the fingerprint region of bioapatite is selected, and the followed figures indicate the several bands used to calculate the spectral relationships – Figure 2.7.

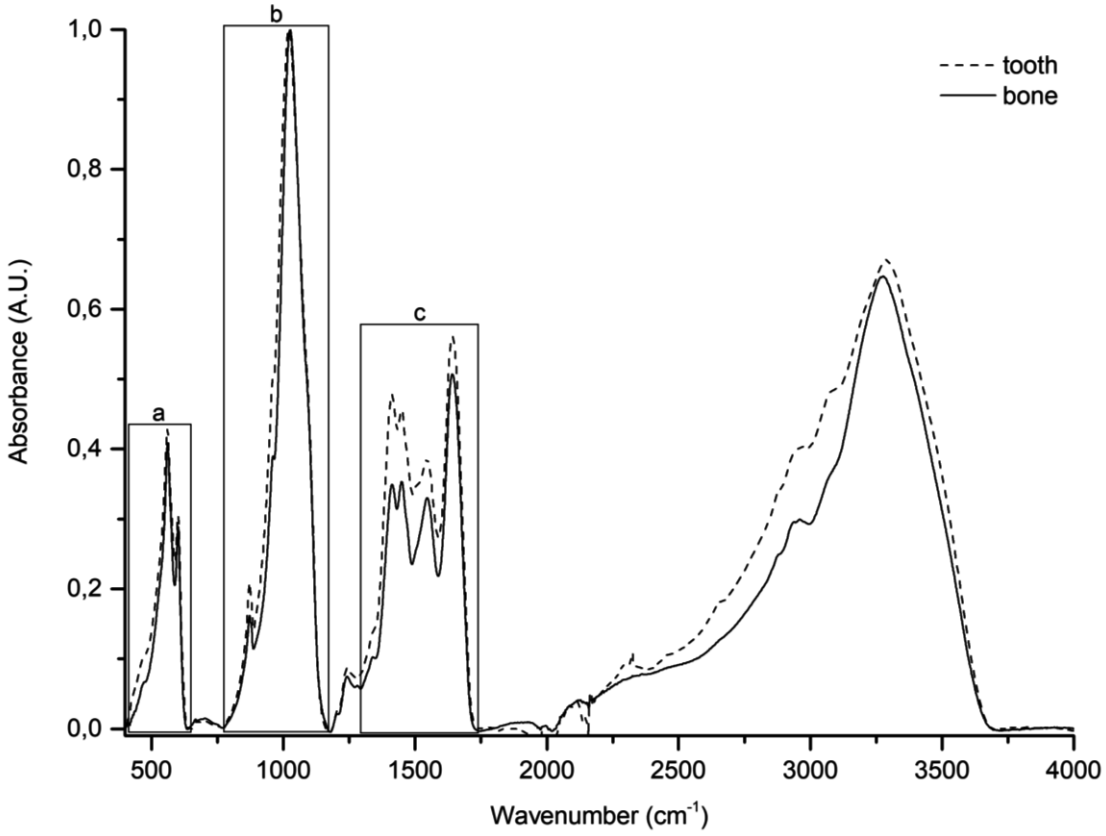

Figure 2.6. Examples of mid-IR spectra of tooth and bone powder. The spectral bands used for indices calculation are highlighted.

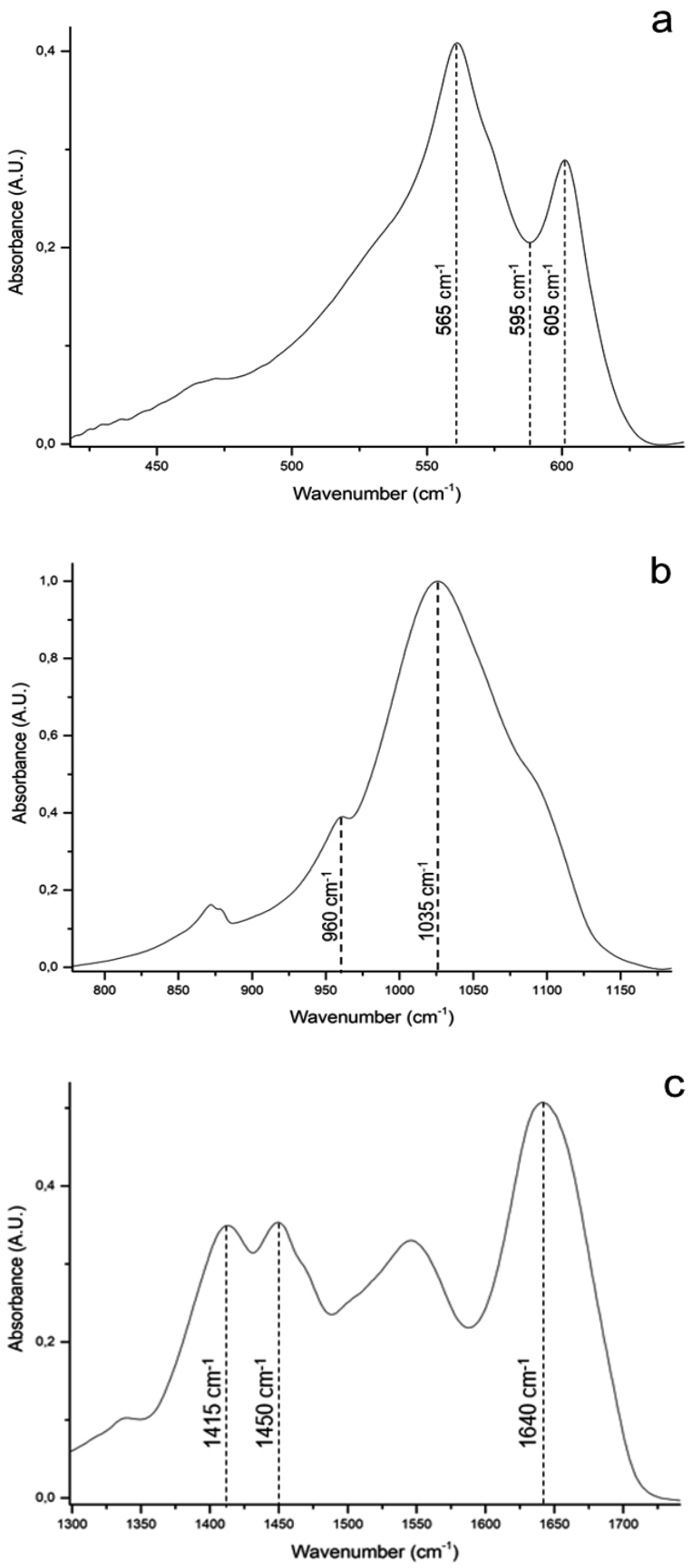

Figure 2.7. Display of band positions for CI (a), C/P (c,b), API (c,a), BPI (c,a), C/C (c), ν_4PO_4/Amide I (a,c) and ν_1PO_4/Amide I (b,c) calculation.

2.5. STATISTICAL ANALYSIS

In order to determine the most representative regions of the spectra, the variance across the spectral dataset was examined. Principal Components Analysis (PCA) is an unsupervised multivariate analysis method that enables data dimensionality reduction and, therefore, the analysis of large spectral datasets.

In this thesis, PCA was used to verify if the groups are inter-related and which region of the spectrum contains the most significant spectral variations that lead to differentiation in the bone and teeth data. This method allows to correlate different data according to the desired group, such as age range, sex, bone type and a possible relationship between them. As a result, to highlight the variability within the spectral dataset, scores and loadings were analyzed: score plots evaluate the possibility to discriminate between different classes, while loading plots represent the spectral data according to the wavenumbers of the variations which might differentiate and characterize the data ranges [135]. The order of the principal components denotes their importance to the dataset. PC1 describes the highest amount of variation, PC2 the second highest and so forth, until all the information included in the dataset has been explained. Generally, the first three PCs represent most of the variance in the experimental datasets and should be enough to yield a good visualization of the differentiation. This study aims to understand the information contained in the first five PCs. The software used for all computations was *Matlab R2018b* (Mathworks Inc., Natick, MA).

IBM SPSS statistic software (version 23.0) was also used, which permits verifying the potential statistical differences among indices *per* sex, age cohorts, age and bone types [136].

Results lower than an alpha of 0.01 were considered to be statistically significant. Parametric tests, namely students' t-test and ANOVA one-way were implemented for the comparison of independent samples according to sex groups and bone type groups whenever parametric assumptions were met. Otherwise, Mann-Whitney, Kruskal-Wallis and Spearman correlation tests were applied instead. Bonferroni adjustment of the alpha level was fulfilled whenever multiple comparisons were implemented. A linear regression model was built to assess the prediction power of indices significant correlations with age ranges (categorical variable) and age as a continuous variable.

CHAPTER 3

RESULTS AND DISCUSSION

3. RESULTS AND DISCUSSION

3.1. SPECTRAL ANALYSIS

The vibrational study was performed in human bone tissue using FTIR in ATR mode, and Figure 3.1 presents the spectra in the 430 to 1800 cm^{-1} range according to bone type – femur, humerus, metatarsal, rib and parietal – for individual CEI_XXI_122, showing the kind of intra-skeleton variation observed in this research.

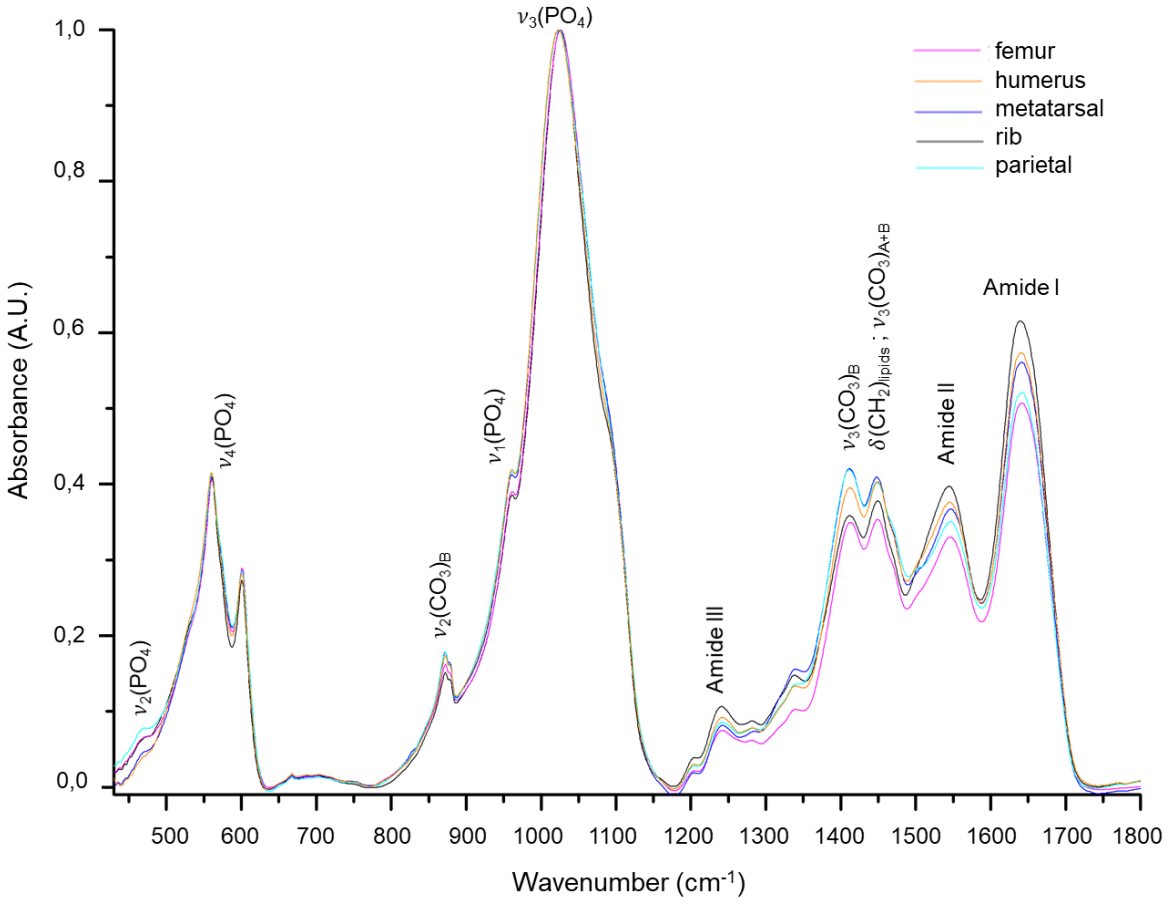

Figure 3.1. FTIR-ATR spectra (430 to 1800 cm^{-1}) of the different human bone samples (powders): femur, humerus, metatarsal, rib and parietal of individual CEI_XXI_122.

Empirically, the main spectral differences among bone type were detected, particularly in the organic components' region, from 1200 to 1800 cm^{-1}. The intensity differences were clearly evident in the 1200 to 1800 cm^{-1}, comprising the bands characteristic of collagen – amide I (C=O stretching mode), amide II (C–N stretching and N–H bending modes) and amide III (C–N stretching and N–H bending modes), at *ca.* 1640, 1544 and 1240 cm^{-1}, respectively. The feature at *ca.* 1410 cm^{-1} in turn, corresponds to the

carbonates' asymmetric stretching ($\nu_3(CO_3^{2-})_B$), and at wavenumbers comprised from 1440 to 1460 cm^{-1}, correspond to an overlapping of types A and B carbonates' asymmetric stretching ($\nu_3(CO_3^{2-})_{A+B}$), and to the deformations of methylene groups from lipids and protein ($\delta(CH_2)$). The observed intensity differences among the organic components to the different bone types can be associated to the intrinsic characteristics of an individual, promoted by an anisotropy of collagen distribution throughout the skeleton and, in turn, through the selected bone types. Furthermore, the influence of diagenetic factors, taking into account that the post-depositional processes can affect the bones differentially.

Regarding the inorganic content of some samples, differences were noted only in the phosphate symmetric stretching mode $\nu_1(PO_4^{3-})$, at 962 cm^{-1}, that has a considerably lower intensity in the ribs and femora. This signal seemed to be directly related to the degree of organization of the mineral lattice atomic arrangement [137]. The principal domain corresponding to the bands assigned to the phosphate antisymmetric stretching modes $\nu_4(PO_4^{3-})$ and $\nu_3(PO_4^{3-})$, at *ca.* 561 and 1024 cm^{-1}, respectively, were similar for all bone types. The $\nu_1,\nu_3(PO_4^{3-})$ domain has been reported to contain information about apatite stoichiometry. A band at *ca.* 1020 cm^{-1} is indicative of non-stoichiometric apatites (containing HPO_4^{2-} and/or CO_3^{2-}), while a band at 1030 cm^{-1} suggests stoichiometric apatites, $Ca_{10}(PO_4)_6(OH)_2$ [138, 139].

A meticulous analysis of amide I and II bands from protein evidences a higher intensity for the rib samples, followed by humerus, metatarsal, parietal and femur. The choice of different bone types in this study was related to inter-bone differences already described in section 1.4. Since not all the skeleton is submitted to the same activity or strength, and since bone organization also differs, these may possibly lead to different chemical alterations. Such chemical alterations have been proposed by Paschalis *et al.* [123], Cummaudo *et al.* [71] and Gonçalves *et al.* [111].

The discrepancy of the organic bands, 1200 to 1800 cm^{-1}, IR intensities may be related to bone remodelling. Fahy *et al.* [73] described that ribs and humerus had the highest rate of bone remodelling. Essentially, ribs are never at rest due to the load promoted by respiratory movements, and the surface area to volume ratio allows a relatively fast cortical turnover rate, which is approximately 4% per year after the age of 50 [140]. Moreover, the dense cortical bone of the femoral diaphysis is thought to have a slow turnover rate relative to rib bone, indicating the lowest relative intensity shown on the spectrum [84, 140]. Chemical alterations, prompted by diagenesis, also induce differences in bone composition. It is recognized that elements with high proportions of spongy bone are more susceptible to the diagenetic process [141, 142]. In summary, the rib, despite its higher uniformity, is subject to different and significant factors that induce an alteration in bone when compared to the other types of bones. That seems to be reflected by this study, since ribs possess the

most relative intense band, especially to amide I, confirms the highest turnover rate to which is subject and consequent collagen degradation [143], as well as the vulnerability to diagenetic process.

Therefore, the contribution of the mineral and organic components to the overall spectrum could be analyzed independently. Furthermore, the distinction *per* bone type presents a suggestive correlation with the organic fraction and could be associated with bone composition, anatomical compartment – cortical or trabecular – and bone remodelling rate.

Thus, as the organic content of bone is represented mainly by the amide bands – from protein –, particularly by the most intense amide I band, a relationship between the relative proportion of organic to the mineral fraction may be disguised: a spectroscopic correlation dividing $\nu_4(PO_4^{3-})$ to amide I. With the same purpose, was proposed by France *et al.* [114] the ratio between $\nu_1(PO_4^{3-})$ and amide I. This enables understanding, for instance, if there is a directly correlation between the organic content and the degree of bone remodelling rate, considering that the rate of bone turnover is directly associated with collagen degradation. So, it is expected to find a trend upon these indices and the representation of increase/decrease of collagen, in each bone according to age range.

An evaluation of CI and C/P values obtained from the infrared data permits recognizing the extension of diagenetic alterations induced to the bones. For crystallinity index, one of the most useful indices since it, represents a proxy for crystal order, strain and organization, the reference value described in the literature varies between 2.5 and 3.25 for modern fresh bones [85, 87, 102], and is anticipated to increase as crystal structure becomes more ordered. Changes in bone porosity resulting from diagenetic pathways have also been associated with variation in CI, as has the degree of organic content within the bone [61, 102, 144]. In this work, the range values found for bone samples were 2.87 to 3.69, whilst the values obtained for teeth samples were within the expected range, 2.82 to 3.24. For the carbonate-phosphate ratio, values of 0.34 ± 0.01 were reported in fresh bones [145], and the range values now obtained varies from 0.25 to 0.58. Indicating that bones with lower values suffered a diagenetic loss of carbonate fraction in bioapatite, whilst bones with higher values have had a net gain of carbonate from the burial environment. High values of API, BPI and C/C were also obtained for bone samples, when compared to the reference values from Snoeck *et al.* [51]. The CI and B type carbonate tend to be inversely correlated, which was here detected as well: incorporation of B types carbonate into the crystal lattice promotes crystal distortion and, consequently, lower CI values and higher C/P and BPI values.

A significant increase in the CI value in bones associated with increasing *post-mortem* interval was detected – statistical analysis presented in section 3.3.1.2. The

extension of diagenetic changes is dependent on the amount of the inhumation period, on the type of soil in contact with the remains and on environmental factors, such as water and flora [87]. Although this is not linear, major alterations should be somewhat correlated to increasing periods. This seems to be the case for the results in this study since teeth weren't inhumed and provide values more in accordance with the literature.

3.2. EXPLORATORY STATISTICAL ANALYSIS

3.2.1. BONES ANALYSIS

Analyzing the whole spectrum by different bone types allowed to reveal a considerable variation in femur and humerus, with a high percentage of differentiation – 61.85% for PC1. Nevertheless, as shown in Figure 3.2.(A) comparison of the mean spectrum of femur and humerus evidences a slight shift to higher wavenumbers across the whole spectrum, predominantly at the main phosphate band, $\nu_3(PO_4^{3-})$. This band is more susceptible to be affected by substitution of heavier and lighter ions than phosphate in the crystal lattice, according to diagenetic studies [146, 147]. Changes are based primarily on distortion of the crystal lattice upon substitution, causing an increase/decrease in size of the unit cell and promoting alterations to the characteristic wavenumber [142, 146]. A shift of $\nu_3(PO_4^{3-})$ to higher wavenumbers indicates the presence of substituting ions (*e.g.* Ca^{2+}, Cd^{2+}, Pb^{2+} and Sr^{2+}) within the lattice that reduce the size of the unit cell [142]. However, since this discrepancy only appears in the femur and humerus samples – the metatarsal, rib and parietal bones being unaffected –, it is unlikely that it is due to diagenetic factors.

As some samples of femur and humerus were collected by another operator, it is hypothesized that this effect may be associated to an operator artifact, as mentioned in chapter 2.2. Operator 2 measured 158 samples, and all of them display the $\nu_3(PO_4^{3-})$ band at *ca.* 1028 cm^{-1}, while for the samples from operator 1 this band occurs at *ca.* 1022 cm^{-1}. There are also some differences in intensity, which is slightly higher for operator 2 regarding the inorganic part – particularly in the $\nu_1,\nu_3(PO_4^{3-})$ domain –, and lower than operator 1 regarding the organic part – amide I, amide II, $\nu_3(CO_3^{2-})_B$, $\nu_3(CO_3^{2-})_{A+B}$ and $\delta(CH_2)_{lipids/protein}$.

In an attempt to understand the contrasting score plots, Figure 3.2.(B) shows that the data is clearly discriminated according to PC1, which explains a variation according to the operator – either 1 or 2. The corresponding loadings exhibit a main variance across the spectral region 1020 to 1030 cm^{-1}, apart from other less significant contributions – Figure 3.2.(C).

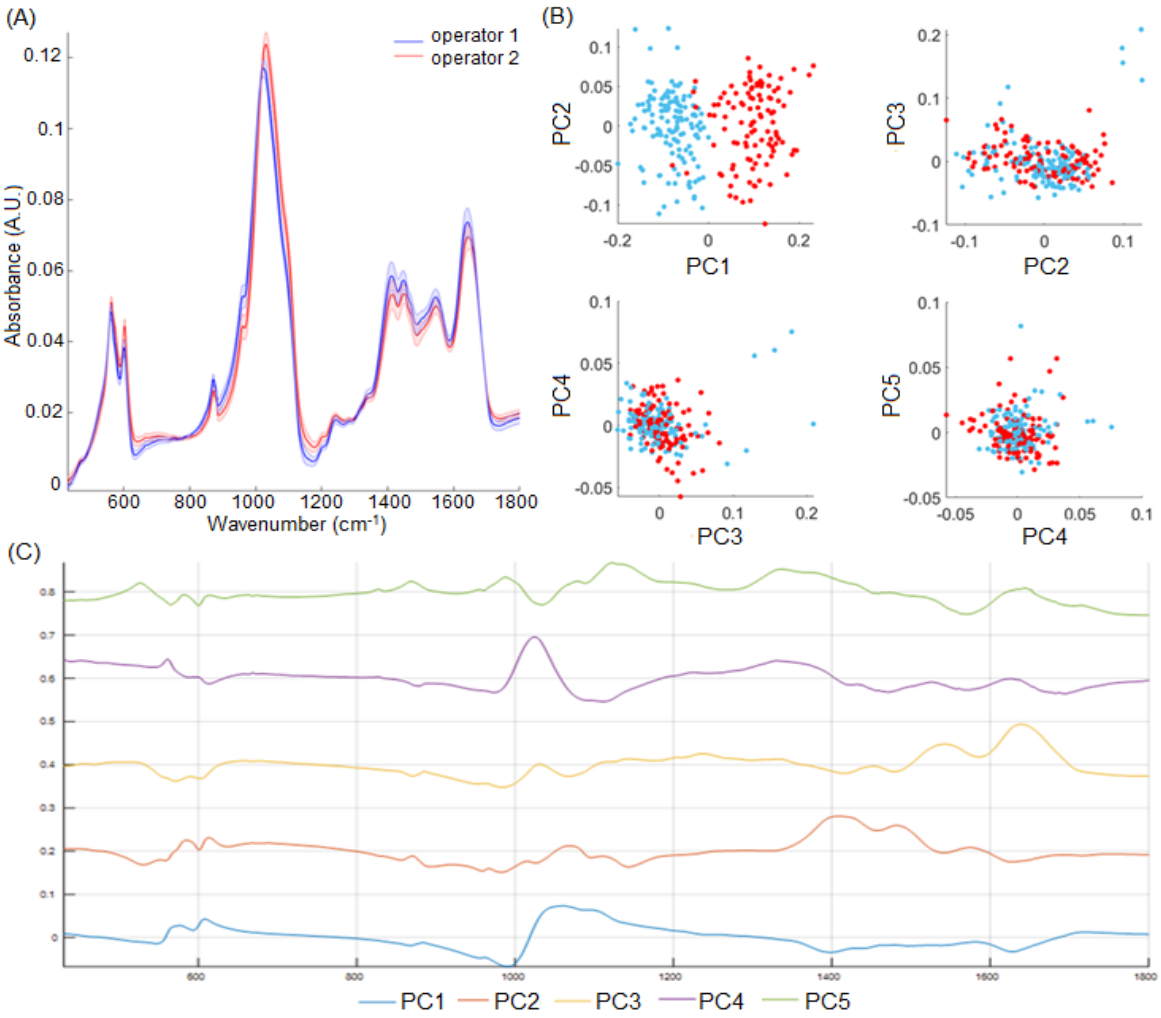

Figure 3.2. Representation of the variations caused by different operators in the collected IR data: (A) mean FTIR-ATR spectra of femur and humerus, for samples obtained by operators 1 (blue) and 2 (red); (B) PCA scores; (C) PCA loadings. PC1: 61.85%; PC2: 23.22%; PC3: 8.31%; PC4: 2.51%; PC5: 1.78%, exhibiting 97.67% of total variance.

An explanation for the occurrence of the shift at $\nu_1,\nu_3(PO_4^{3-})$ is still unclear, some hypotheses having been considered. The sampling method may induce the observable differences through three possible factors: (1) the applied force to scrap, (2) the effect of scalpel cleaning or (3) the particle size of the bone powder. Regarding the first possible cause, it was hypothesized that during scraping an excessive force could heat the sample, possibly promoting a change that may be reflected in an infrared frequency shift. Secondly, a methodological difference was identified between the two operators: operator 2 cleaned the scalpel with ethanol, and a residual contamination could be transmitted to the sample promoting a signal overlapping of bioapatite with ethanol, leading to a band shift. Finally, differences in particle size between the two operators due to differences in the scraping method could be responsible for the observed differences between the spectra. The particle size effect has been referred to in the literature, the IR intensity being higher and narrower

when the particle size decreases [148–151]. This could be simply assumed to be due to a better contact between the sample and the prism, and therefore to a larger penetration depth of the infrared radiation into the crystals. Kristova *et al.* [152] attributed this effect to the better packing and higher surface area of samples with smaller particles. Yet, the samples from operator 1 show a lower intensity of the inorganic bands – at 561, 600, 872, 960 and 1024 cm^{-1} – and have a reduced particle size, in contrast to the previously mentioned effect. Moreover, sampling scraping varies according to the toughness of the bones, a higher rigidity promoting an increased difficulty in obtaining small particles of bone powder. Different levels of toughness thus lead to a different particle sizes of the bone particles.

Despite the previous explanations regarding the shift detected for ν_1,ν_3(PO_4^{3-}), the overall spectrum variation cannot, at present, be explained. Thus, it is extremely important to develop a standard sampling method for bone powder preparation, allowing to improve data accuracy, precision, comparability and reproducibility.

In view of the added errors to the statistical analysis, it was decided to exclude the 158 samples from operator 2 from the remaining study.

3.2.2. ANALYSIS BY AGE COHORTS

Regarding the analysis of the data by age cohorts, a few considerations should be taken beforehand. The age distribution of the skeletons is notably biased towards older age groups, since only a reduced number of skeletons from the age group 28 to 59 years old were available for this study – as explained in section 2.1. Moreover, it was not expectable to observe differences between 50 to 60 years old, due to the proximity of these classes. Most often, not even anthropological macroscopic methods can reliably discriminate individuals of 50 years old from individuals with 60 years of age [31].

No discernible variation among age groups was observed. Comparing the extremes, the younger – 28 to 59 years old – with the older group – 80 to 99 years old –, and considering all bone types, the spectra are rather similar and only small variations could be detected, which does not allow an age-range discrimination – Figure 3.3.(A). Observing the score plots depicted in Figure 3.3.(B), no separation among groups is shown. Even though, the main difference, observed through the PC1 loading, corresponds to the band at *ca.* 1020 cm^{-1} and to the organic part of the spectra – Figure 3.3.(C).

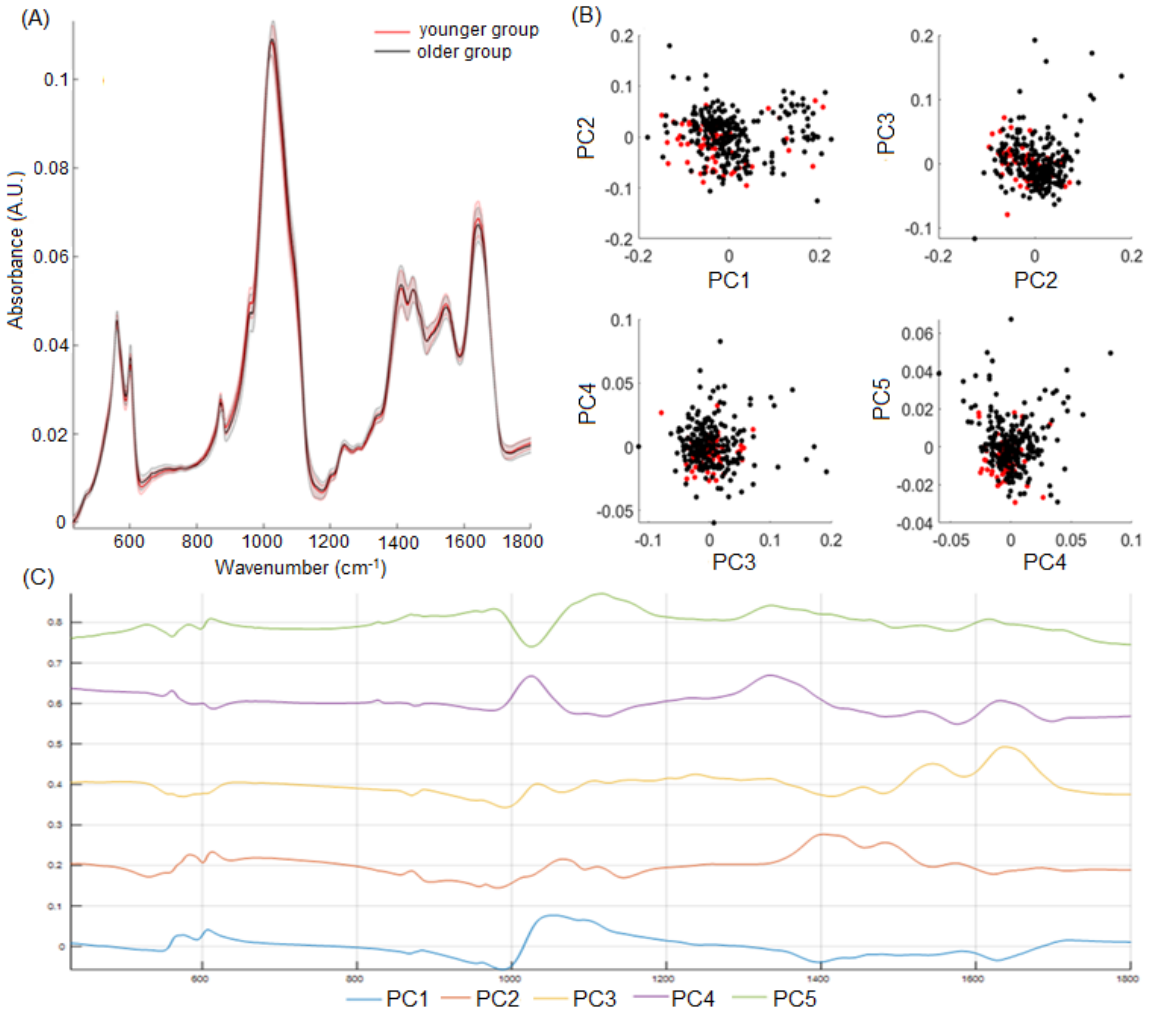

Figure 3.3. Representation of all bones correlation with age groups below 60 years old – younger group – and over 80 years old – older group: (A) mean FTIR-ATR spectra of younger and older group; (B) PCA scores; (C) PCA loadings. PC1: 61.07%; PC2: 18.96%; PC3: 11.88%; PC4: 2.62%; PC5: 1.80%, exhibiting 96.33% of total variance.

According to the results gathered from this spectral analysis, the most representative age-related region across all types of bones was the one corresponding to the organic components. Therefore, taking into account that no useful results were obtained from the whole spectra, an additional PCA was implemented by limiting the analysis to the wavenumber range between 1350 and 1730 cm^{-1}. It was perceptible that the intense signals from the inorganic constituents hinder the analysis of the organic components, thus leading to an apparent small contribution from the latter. Expectantly, by selecting only the organic region a possible differentiation through bone types was attempted – presented below.

In a nutshell, no visible differences were found between female and male samples, either considering the whole spectral range or solely the organic part. Not even between women older than 50 years against men of all age groups. This attempted correlation

according to sex was tried due to the clinical evidence that women are more susceptible to suffer osteoporosis, especially after the fifth decade of life [78].

3.2.3. ANALYSIS BY BONE TYPES

Comparing the mean spectrum of all bone types, represented in Figure 3.4.(A), it was possible to note that rib possessed the most intense band of amide I. And despite the minimal differences among distinct types of bones, the PC loadings displayed some variance in all peaks of the represented region – Figure 3.4.(C). PC1 described 69.88% of total variance, PC2 12.53%, PC3 8.27%, PC4 4.82% and PC5 2.34% – for a total variance of 97.84%. The scores plot, shown in Figure 3.4.(B), pooled all bone types but each one was condensed in somewhat circumscribed areas, thus reflecting a possible discrimination among bone types.

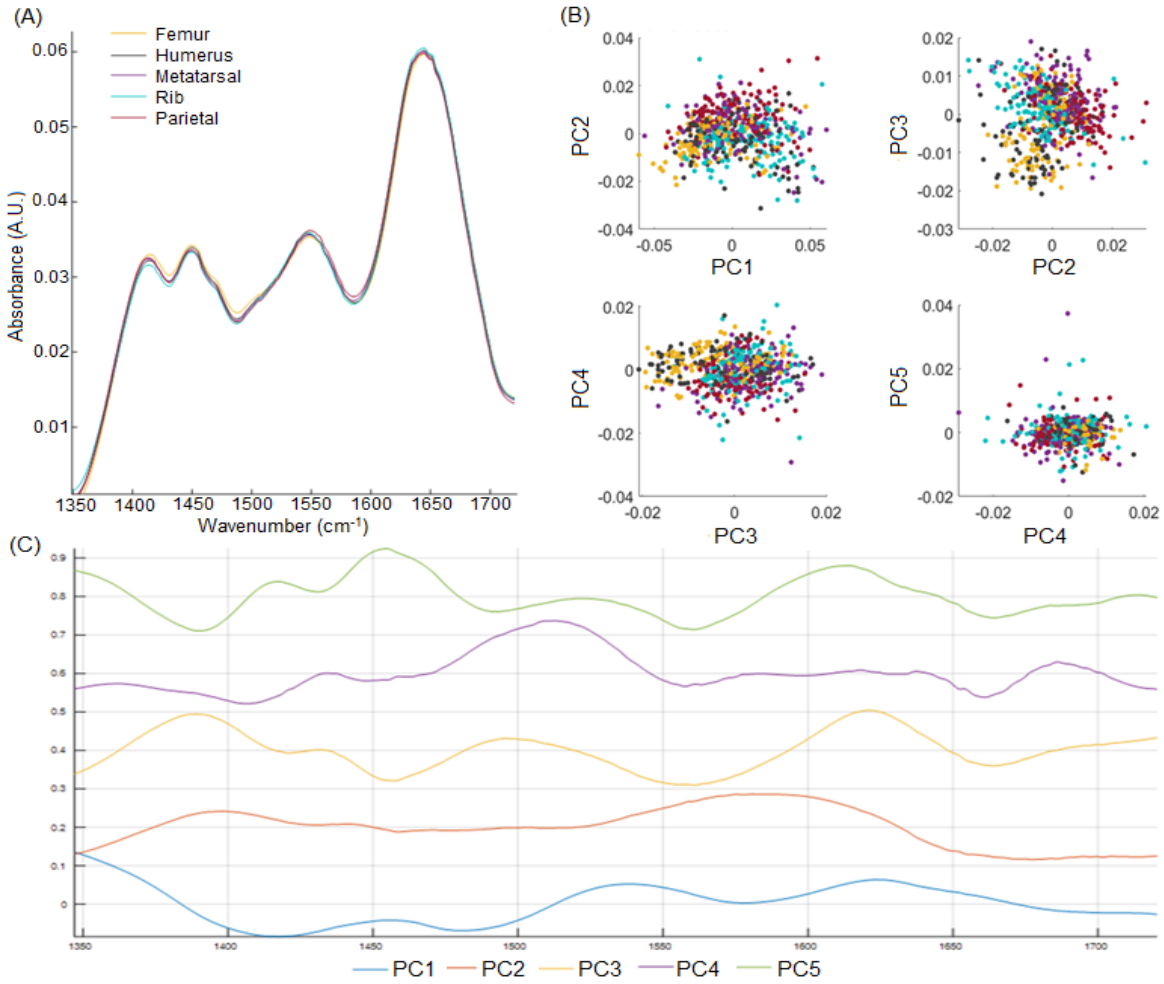

Figure 3.4. Representation of all bone types correlation restricted to the 1350–1730 cm^{-1} region: (A) mean FTIR-ATR spectra of all bone types; (B) PCA scores; (C) PCA loadings. PC1: 69.88%; PC2: 12.53%; PC3: 8.27%; PC4: 4.82%; PC5: 2.34%, exhibiting 97.84% of total variance.

Given the previous result, the analysis was then performed for bone *vs* bone for several pairs, and the following data were the ones demonstrating the most important variance.

3.2.3.1. PARIETAL vs FEMUR

By restricting the data analysis to a correlation between parietal and femur samples, the two different types of bone were relatively well discriminated. In Figure 3.5.(B), representing the PC scores, the data was perfectly separated along PC2 and the respective PC loading attributed the variance to the peaks at *ca.* 1410 cm^{-1} ($\nu_3(CO_3^{2-})_B$) and from 1500 to 1650 cm^{-1} – amide I and amide II. PC4 also discriminated these classes, the main variance occurring at *ca.* 1540 cm^{-1}, assigned to amide II. The loading plots are displayed in Figure 3.5.(C), in which PC1 accounts for 73.84% of the total variance, discriminating between parietal and femur according to the organic components, whereas PC2, PC3, PC4 and PC5 account for 12.86%, 5.57%, 3.65% and 2.05% of the variance, respectively.

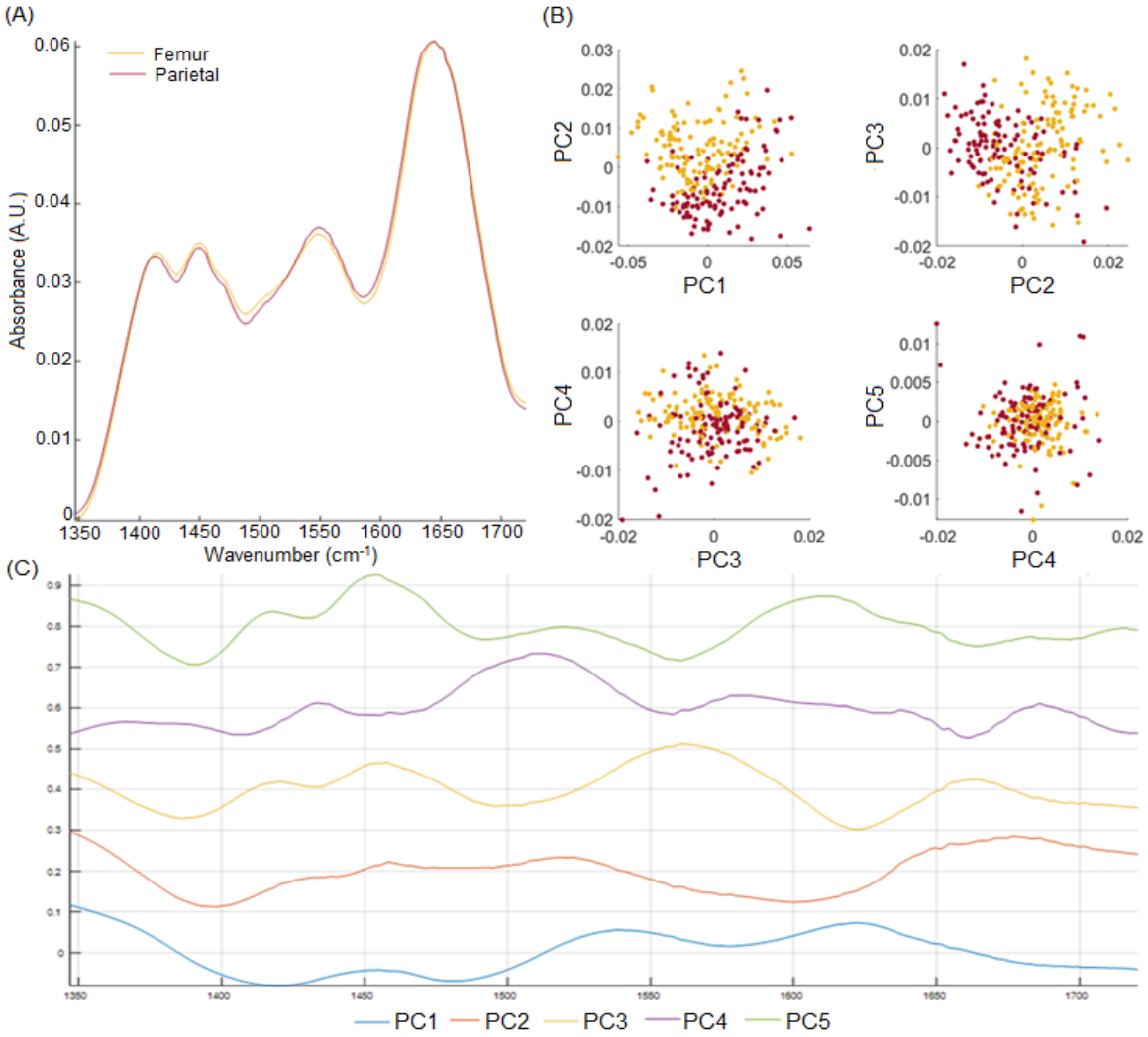

Figure 3.5. Representation of the correlation between parietal and femur restricted to the 1350–1730 cm^{-1} region: (A) mean FTIR-ATR spectra; (B) PCA scores; (C) PCA loadings. PC1: 73.84%; PC2: 12.86%; PC3: 5.57%; PC4: 3.65%; PC5: 2.05%, exhibiting 97.98% of total variance.

3.2.3.2. PARIETAL vs RIB

A similar relationship emerged between parietal and rib samples. PC1 describes 68.87% of the total variance, but PC2 was the principal component that best discriminated the groups, a scenario depicted in Figure 3.6.(B) with a variance of 17.60%. The PC2 loading and PC3, with a variance of 6.04%, presents the main variance at wavenumbers region 1540 to 1560 cm^{-1} assigned to amide II.

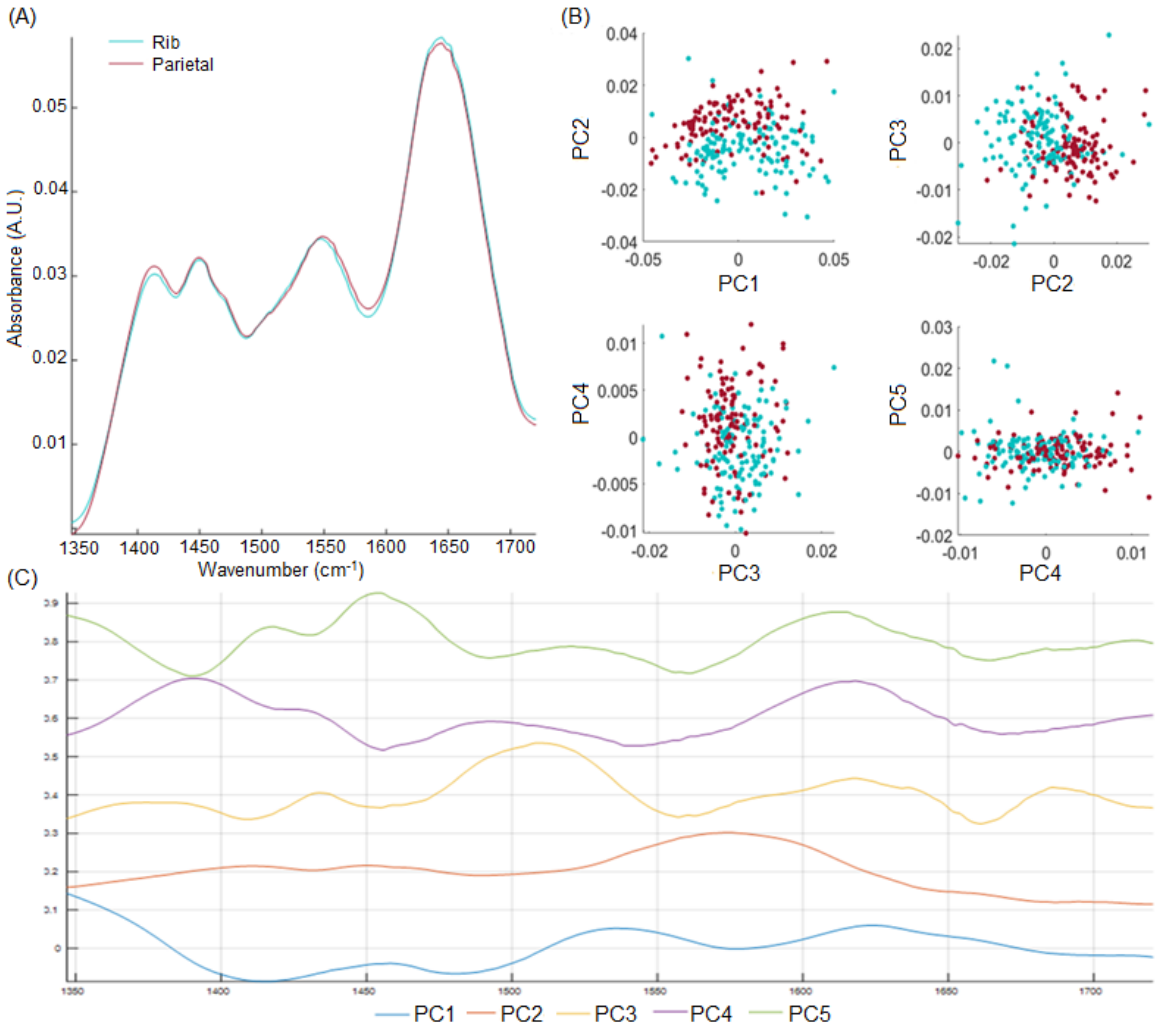

Figure 3.6. Representation of the correlation between parietal and rib restricted to the 1350–1730 cm^{-1} region: (A) mean FTIR-ATR spectra; (B) PCA scores; (C) PCA loadings. PC1: 68.67%; PC2: 17.60%; PC3: 6.04%; PC4: 2.98%; PC5: 2.78%, exhibiting 98.07% of total variance.

3.2.3.3. PARIETAL vs HUMERUS

Analysis of the score plots for the parietal and humerus samples – Figure 3.7.(B) – allows to conclude that differentiation between the two types of bone takes place mainly according to PC2 – introducing a variance of 15.71%. The most representative spectral information, evidenced in the loading plots, occurs at 1400 cm^{-1}, assigned to $\nu_3(CO_3^{2-})_B$, and at 1640–1660 cm^{-1} due to amide I – Figure 3.7.(C). PC1 has a total variance of 68.35%.

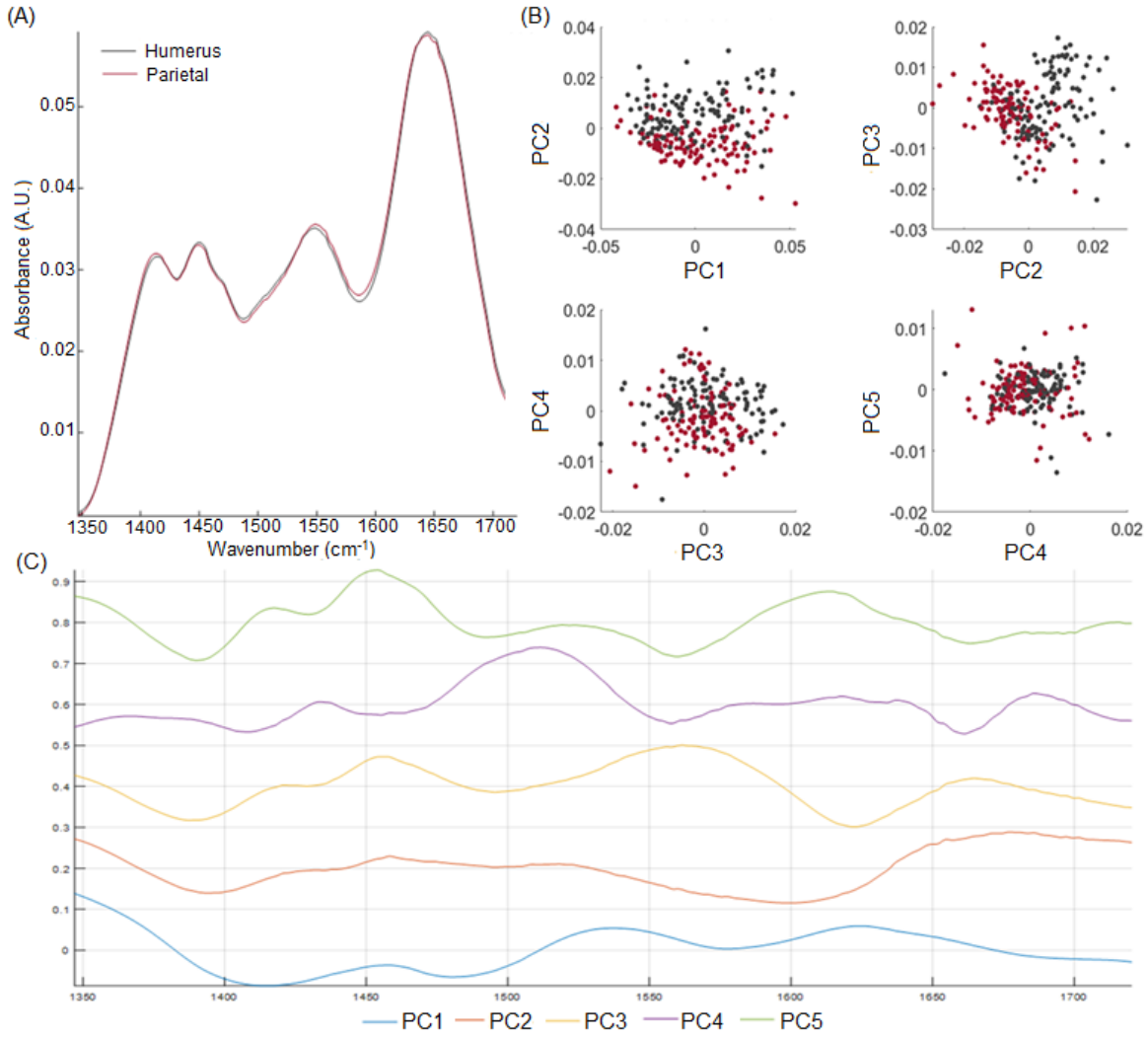

Figure 3.7. Representation of the correlation between parietal and femur restricted to the 1350–1730 cm^{-1} region: (A) mean FTIR-ATR spectra; (B) PCA scores; (C) PCA loadings. PC1: 68.35%; PC2: 15.71%; PC3: 7.78%; PC4: 4.38%; PC5: 1.68%, exhibiting 97.90% of total variance.

According to the experimental data presently described, the main differences were found between bone types (Table 3.1) clearly indicating a distinction among some bone types, in particular: parietal *vs* femur, parietal *vs* rib and parietal *vs* humerus. No significant differences were found between: metatarsal *vs* parietal, metatarsal *vs* femur or femur *vs* humerus.

Table 3.1. Presence and absence of discrimination between bone types.

	FEMUR	HUMERUS	RIB	METATARSAL	PARIETAL
FEMUR	---	x	x	x	**
HUMERUS	---	---	x	x	**
RIB	---	---	---	x	**
METATARSAL	---	---	---	---	x
PARIETAL	---	---	---	---	---

** bone types discrimination; x absence of discrimination; --- nothing to state.

In summary, no significant spectral variations occurs in the whole spectral IR range, which does not allow an accurate discrimination between age cohorts, sex or types of bone. Nonetheless, in an attempt to determine the most representative regions of the spectra, the analysis was restricted to the organic constituents – from 1350 to 1730 cm^{-1}.

Throughout this circumscribed analysis, differences in the chemical composition of distinct bone types were detected, relative to spectral variations at the intensity of organic bands: $\nu_3(CO_3^{2-})_B$, amide I and amide II. An association of the results with the chemical nature of bone tissues is evident, in which the degree of alteration or organic phases may vary according to anatomical compartment, bone remodeling rate, anisotropy of collagen distribution or different environmental conditions.

The bone remodelling rate varies according to the specific anatomical compartment or the section of the skeleton involved, and the discrimination occurs among the types of bone with the highest and lowest remodelling rate – parietal *vs* femur, parietal *vs* rib and parietal *vs* humerus – with similar percentages of total variance. Thus, the results indicated that parietal is the bone which permits an individualization, allowing a clear distinction among types of bones.

Apart from these factors, the collagen distribution throughout the skeleton influences each bone differently and could be reflected through the different intensities of collagen bands. Paschalis *et al*. [138] referred the existence of differences in the distribution of the different components in the same bone and even a variability in the same osteon.

Regarding the spectral analysis, the present results are in agreement, indicating the main variance across bone types is representative through the organic constituents of bone – possibly representing the quantity of collagen present.

3.2.4. TEETH ANALYSIS

Since teeth types were not considered for this study and were instead pooled together, the analysis was simplified only into age groups and possible sex differences.

Analyzing the several hypotheses of age groups, it was perceptible that when comparing teeth from individuals below and over 40 years, as well as below and over 50 years, despite the minimal variance observable the values of total variance of each PC contribute equally – see Appendix, and Figures A1 and A2. Hence, this suggests the need to discard the intermediate age cohort, from 50 to 60 years old, and verify if differences occurred between the age groups at the lower and upper ends, *i.e.* younger adults – below 40 years – and older adults – over 60 years. It is important to emphasize the homogeneity of the number of samples from these two groups which is 45 and 40, respectively.

The mean spectra of the younger and older group – Figure 3.8.(A) – indicated an important variation reflected in the $\nu_1,\nu_3(PO_4^{3-})$ domain as well as in the whole organic region, from 1400 to 1800 cm^{-1}. Regarding the corresponding PC loadings – Figure 3.8.(C) – PC1, PC2 and PC3 exhibited the main variance attributed to $\nu_1(PO_4^{3-})$ and $\nu_3(PO_4^{3-})$. PC1 described 65.79% of the total variance, PC2 added a variance of 17.45%, and PC3 represents 6.40%. Through the score plots, PC2 allowed a group separation into younger and older adults – Figure 3.8.(B).

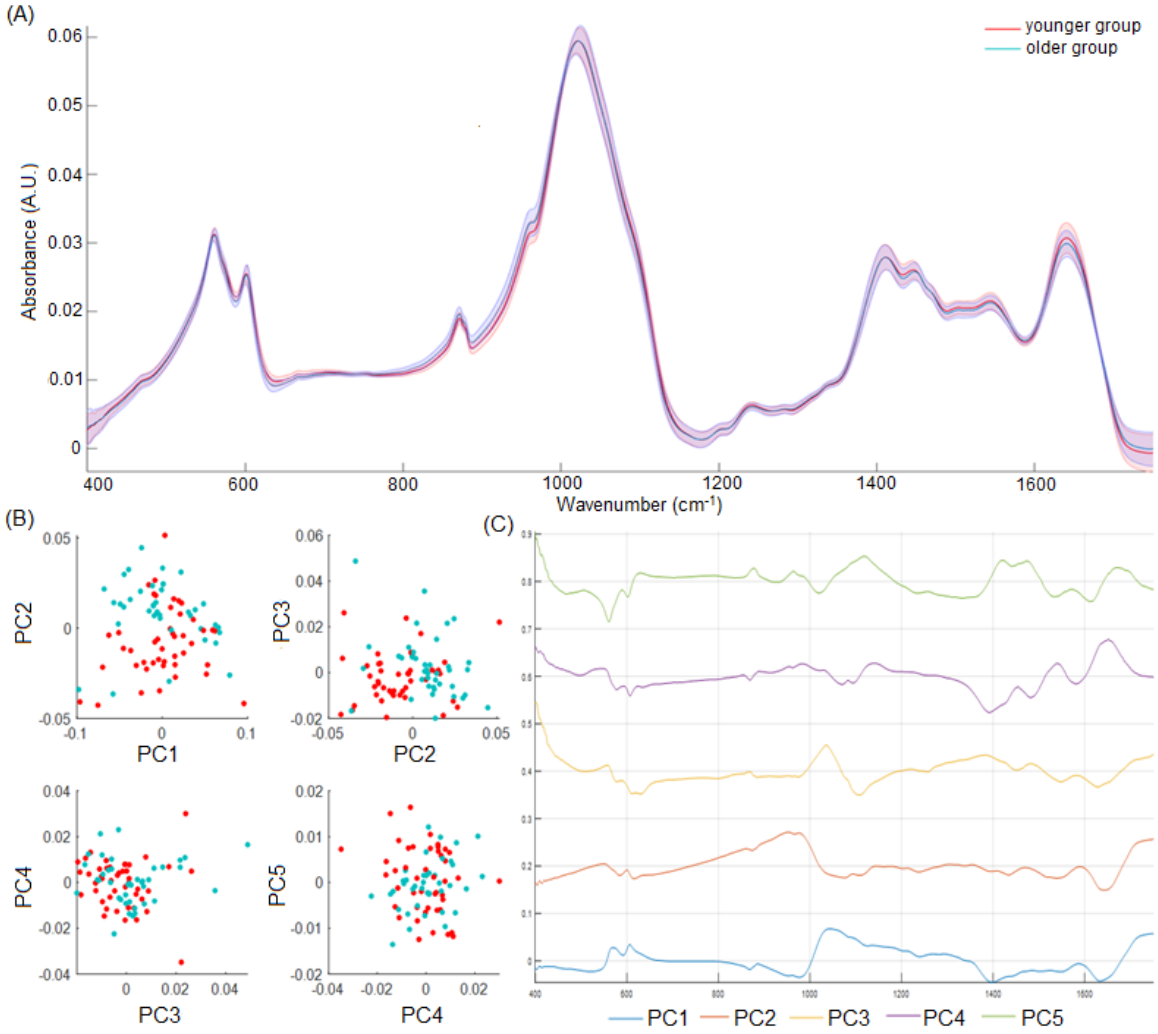

Figure 3.8. Representation of teeth with age groups below 40 years old – younger group – and over 60 years old – older group: (A) mean FTIR-ATR spectra of younger and older group; (B) PCA scores; (C) PCA loadings. PC1: 65.79%; PC2: 17.45%; PC3: 6.40%; PC4: 4.36%; PC5: 1.77%, exhibiting 95.76% of total variance.

Considering that the principal variation was observed in the $\nu_1,\nu_3(PO_4^{3-})$ domain, the analysis was thus restricted to the 430–1370 cm^{-1} range, since the information from the inorganic components seemed to be more relevant. In comparison to bone, a discriminating potential was observed for the organic part.

From Figure 3.9 it was possible to determine differences in PC3 scores, which revealed a notorious groups separation. Actually, the percentage of total variance along PC1 increased to 79.97%, indicating that this specific range contributed to the discrimination between age groups in teeth. PC2, PC3, PC4 and PC5 represented 9.42%, 4.45%, 2.25% and 1.79%, respectively, for a 97.79% total variance.

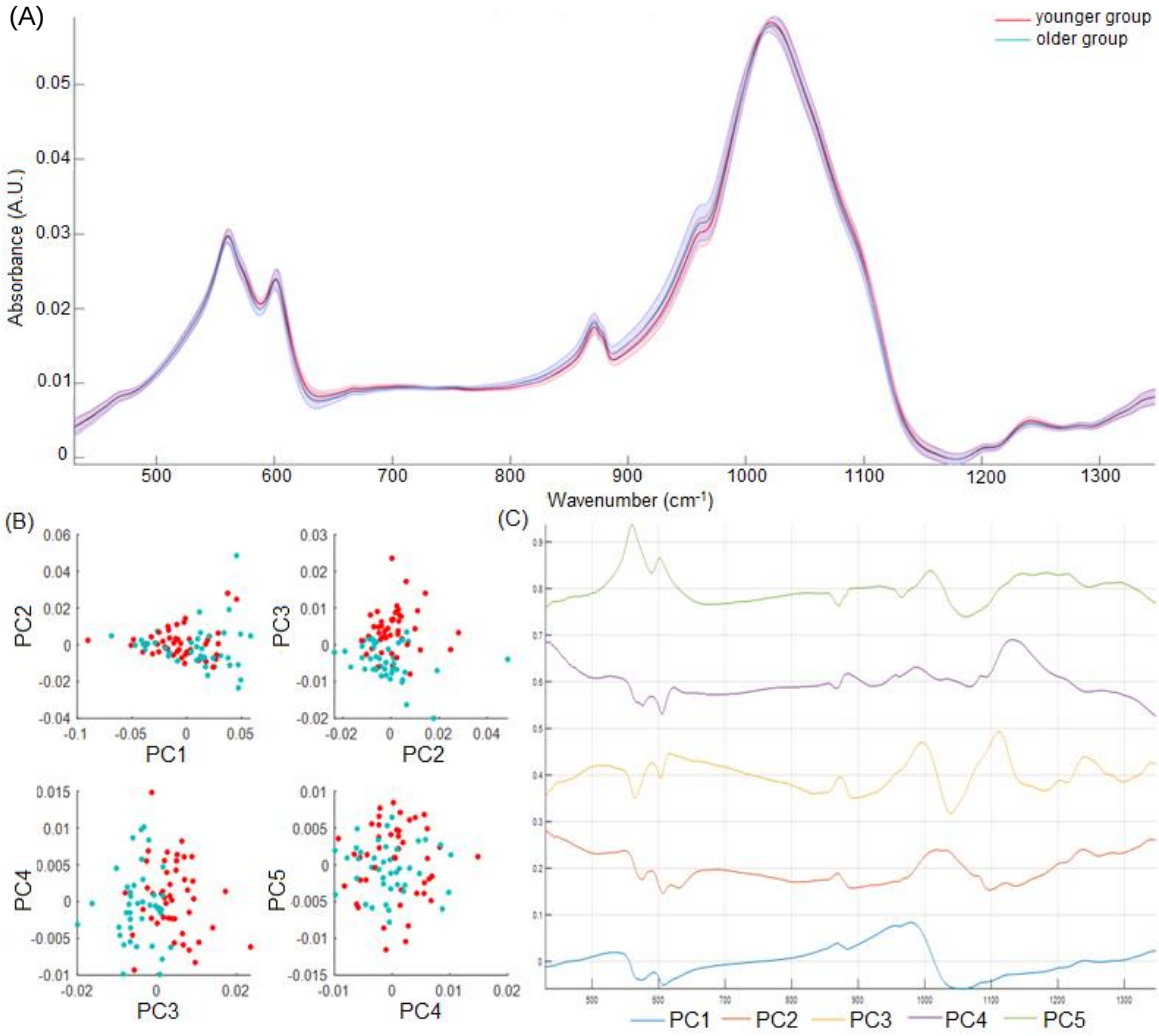

Figure 3.9. Representation of teeth correlation with age groups below 40 years old – younger group – and over 60 years old – older group – restricted to the 430–1370 cm^{-1} region: (A) mean FTIR-ATR spectra of younger and older group; (B) PCA scores; (C) PCA loadings. PC1: 79.87%; PC2: 9.42%; PC3: 4.45%; PC4: 2.25%; PC5: 1.79%, exhibiting 97.79% of total variance.

In order to better visualize the discriminating power, an analysis of the $\nu_1,\nu_3(PO_4^{3-})$ domain was performed, yielding an increased value of total variance of 89.29% for PC1. This means that the main spectral region contributing for an age group differentiation in teeth was in fact the $\nu_1,\nu_3(PO_4^{3-})$ domain, the main spectral variance occurring in the $\nu_1(PO_4^{3-})$ band, at 960 cm^{-1}, which seems to be directly related to the perfection of the atomic arrangement within mineral lattice [137].

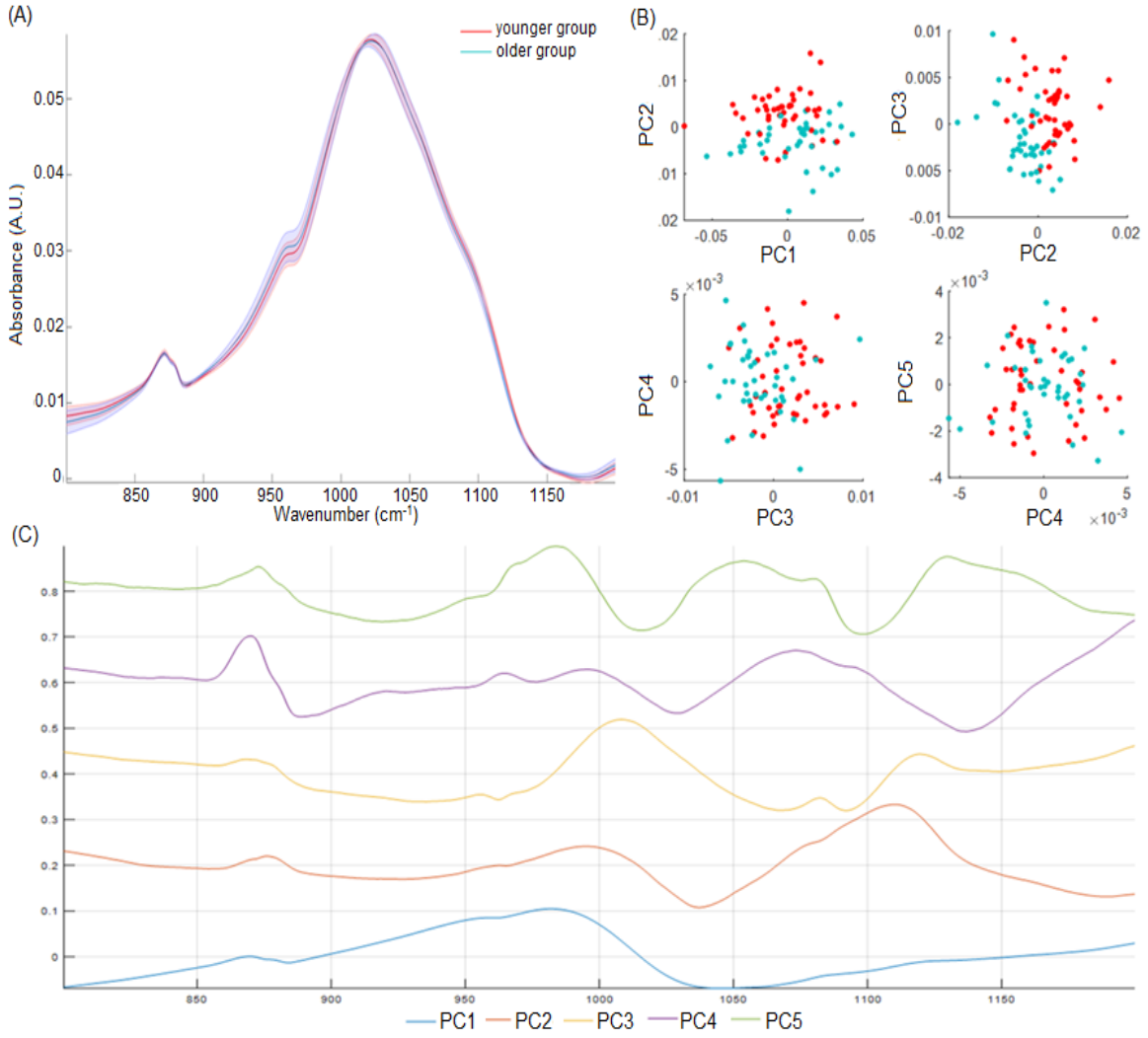

Figure 3.10. Representation of teeth correlation with age groups below 40 years old – younger group – and over 60 years old – older group – restricted to the $\nu_1,\nu_3(PO_4^{3-})$ domain: (A) mean FTIR-ATR spectra of younger and older group; (B) PCA scores; (C) PCA loadings. PC1: 89.29%; PC2: 6.07%; PC3: 2.62%; PC4: 0.86%; PC5: 0.46%, exhibiting 99.9% of total variance.

No visible differences were found between female and male samples, either considering the whole spectral range or solely either the inorganic or organic parts.

Teeth mostly comprise inorganic matter and a reduced organic fraction and adding to the fact of the minimal remodelling throughout life the result currently obtained is predictable. A significant spectral variation discriminating the younger – below 40 years old – and the oldest individuals – over 60 years old – occurs in the inorganic part, solely in the $\nu_1,\nu_3(PO_4^{3-})$ domain, indicating that the relative intensity and width of this peak vary with the mineral crystal lattice properties according to age. It should be pointed out that the thickness of cementum layer coating the teeth usually increases with age. Therefore, PCA analysis of this type of samples demonstrates a considerable capacity to discriminate variations across teeth idiosyncrasies.

In comparison to the results obtained for human bones, it is important to note that, in contrast to teeth, these underwent a variable burial period and suffered collagen degradation, resulting in predictable chemical alterations within their microstructure.

3.3. INFERENTIAL STATISTICAL ANALYSIS

In addition to PCA a statistical analysis taking into account spectral relationships was carried out. Possible association between age groups and age with calculated indices was therefore explored for bone types and teeth while the effect of sex was also tested.

3.3.1. BONES ANALYSIS

The mean and standard deviation was calculated for each mathematical relationship in order to obtain the coefficient of variation, expressing the variability of data. The coefficient presents the lowest variation in C/C, about 3.49%. For the crystallinity index 5.30% was obtained; 5.18% for C/P; 13.71% for API; 19.78% for BPI; 9.40% for ν_4PO_4/Amide I and 11.73% for ν_1PO_4/Amide I. In theoretical terms, a higher variation due to the extended age range was expectable.

Data was explored to recognize the presence of outliers and, consequently, they were removed. Since the data consisted in five different types of bone, parametric one-way ANOVA tests were applied to CI, C/P and C/C aiming to evaluate if statistically significant differences between them were present. For the same purpose, non-parametric Kruskal-Wallis tests were used regarding API, BPI, ν_4PO_4/Amide I and ν_1PO_4/Amide I. The descriptive statistics are given in Table 3.2. The effect size was calculated whenever significant results were obtained [153], in order to describe the relevance of the results.

The results of one-way ANOVA pointed to significant differences, with p-value inferior to .001, among bone types for the CI, C/P and C/C. After homogeneity of variance testing, the Tukey post-hoc test was used and significant differences were highlighted for the following pairwises: for the CI, femur *vs* rib ($p < .001$), femur *vs* parietal ($p < .01$), humerus *vs* rib ($p < .01$), and metatarsal *vs* rib ($p < .001$); for the C/P, rib *vs* metatarsal ($p < .001$); and for the C/C, rib *vs* femur ($p < .01$), metatarsal *vs* rib ($p < .001$) and rib *vs* parietal ($p < .01$). For all the remaining indices, the Kruskal-Wallis tests obtained significant values ($p < .01$).

The effect size presented small effect results for ν_1PO_4/Amide I (0.022), API (0.024), ν_4PO_4/Amide I (0.027), C/P (0.048) and C/C (0.051); intermediate effect to CI (0.074); and large effect to BPI (0.45).

Table 3.2. Descriptive statistics and results of one-way ANOVA tests for the CI, C/C and C/P indices and Kruskal-Wallis tests for the API, BPI, ν_4PO_4/Amide I and ν_1PO_4/Amide I indices, according to bone type.

VARIABLE	BONE TYPE	N	MEAN	STD. DEVIATION	MEDIAN	MINIMUM	MAXIMUM	RANGE	TEST	SIG.	EFFECT SIZE
CI	Femur	67	3.19	0.15	3.15	2.88	3.62	0.74	9.193	<.001*	0.074
	Humerus	65	3.23	0.17	3.18	2.91	3.68	0.77			
	Metatarsal	113	3.23	0.18	3.16	2.94	3.69	0.76			
	Rib	112	3.33	0.15	3.31	3.01	3.68	0.67			
	Parietal	106	3.30	0.17	3.27	2.96	3.68	0.72			
C/P	Femur	67	0.44	0.05	0.44	0.34	0.59	0.25	5.823	<.001*	0.048
	Humerus	65	0.44	0.05	0.45	0.31	0.52	0.22			
	Metatarsal	113	0.45	0.06	0.46	0.27	0.58	0.31			
	Rib	112	0.42	0.06	0.41	0.25	0.55	0.30			
	Parietal	106	0.44	0.05	0.44	0.33	0.56	0.24			
API	Femur	67	1.25	0.22	1.21	0.82	2.31	1.49	14.945	0.005*	0.024
	Humerus	65	1.23	0.19	1.20	0.92	2.28	1.36			
	Metatarsal	109	1.28	0.12	1.27	1.01	1.86	0.84			
	Rib	111	1.24	0.19	1.22	0.70	2.34	1.64			
	Parietal	104	1.27	0.14	1.24	1.04	2.15	1.11			
BPI	Femur	67	1.51	0.25	1.47	1.12	2.60	1.48	208.673	<.001*	0.45
	Humerus	65	1.48	0.24	1.47	0.98	2.50	1.52			
	Metatarsal	111	1.52	0.22	1.55	0.91	2.39	1.47			
	Rib	111	1.41	0.21	1.39	0.87	2.16	1.30			
	Parietal	106	1.07	0.14	1.08	0.81	1.73	0.91			
C/C	Femur	67	0.97	0.03	0.96	1.07	1.07	0.14	6.234	<.001*	0.051
	Humerus	65	0.97	0.03	0.96	0.91	1.07	0.16			
	Metatarsal	114	0.96	0.03	0.96	0.90	1.07	0.16			
	Rib	112	0.98	0.03	0.98	0.93	1.07	0.15			
	Parietal	106	0.97	0.03	0.96	0.90	1.04	0.14			

ν_4PO_4/Amide I	Femur	67	0.75	0.08	0.75	0.41	0.96	0.55	16.033	0.003*	0.027
	Humerus	65	0.76	0.07	0.76	0.46	0.89	0.43			
	Metatarsal	110	0.74	0.06	0.74	0.51	0.86	0.35			
	Rib	109	0.74	0.07	0.75	0.41	0.97	0.56			
	Parietal	106	0.75	0.07	0.76	0.45	0.89	0.45			
ν_1PO_4/Amide I	Femur	67	0.55	0.08	0.55	0.28	0.80	0.52	13.770	0.008*	0.022
	Humerus	65	0.56	0.07	0.56	0.29	0.71	0.42			
	Metatarsal	111	0.53	0.05	0.53	0.35	0.63	0.28			
	Rib	109	0.53	0.07	0.53	0.26	0.75	0.49			
	Parietal	106	0.54	0.06	0.55	0.27	0.64	0.37			

*statistically significant ate the 0.01 level.

Given the small differences among the humerus, the femur and the metatarsal, these were pooled into one large group of bones with diaphyses to allow an enlarged sample. The rib and the parietal were left as separate groups. The subsequent analysis was then made according to these three categories.

Regarding the discrimination obtained among bone types through PCA analysis, displayed from Figure 3.5 to 3.7, the main spectral variations occurred in the organic region – $\nu_3(CO_3^{2-})_B$, amide I and amide II – which differentiation is reflected exclusively throughout the respective bands intensities variations. In turn, the chemometric indices represents a relationship across the band intensities, reason why the discrimination does not appear in the same region of the spectrum. The differences were highlighted from CI, C/P and C/C, pointing that the ratios among the respective bands of phosphates and carbonates possess the potential to discriminate individualizing features of different bones. Although, discrimination does not occur in the same bone types, the spectroscopic indices found significant differences mainly in the rib, proving the heterogeneity of this bone – explained in section 3.1 – in comparison to the other ones.

To establish if sex differentiation was required to test the correlations between indices and age at death, parametric t-student tests were implemented for CI, C/P and C/C, while non-parametric Mann-Whitney tests were used to test API, BPI, ν_4PO_4/Amide I and ν_1PO_4/Amide I. The results for the testing of sex differentiation of each spectral relationship according to bone type are presented in Table 3.3. All p-values were higher than .01 thus not being statistically significant. Consequently, no significant sex differences were found allowing for the pooling of males and females thus avoiding the division of the data set into two smaller sets. As obtained for PCA analysis, no sex differentiation was detected, pointing that spectral variations between male and female do not occur.

To explore if any significant differences in chemometric indices were present among age groups, parametric one-way ANOVA tests were implemented for the CI and the C/P. However, no significant results were obtained thus demonstrating that these indices don't have any potential to discriminate among age groups – Table 3.4.

The remaining indices were tested through non-parametric Kruskal-Wallis tests. Only the C/C was significantly different among age groups, despite the small effect values (0.055 for long bones and 0.056 for ribs). So, Mann-Whitney tests were used for pairwise comparisons between age groups. Significant differences were detected for the following pairwises: 28 to 59 years old *vs* 80 to 89 years old (MW=539.000, $p < .001$); 28 to 59 years old *vs* 90 to 99 years old (MW=628.000, $p < .001$). The results can be deemed expectable since these groups are at opposite age ranges.

Table 3.3. Descriptive statistics according to each sex and results of t-student tests for the CI, C/C and C/P indices and Mann-Whitney tests for the API, BPI, ν_4PO_4/Amide I and ν_1PO_4/Amide I indices.

BONE TYPE	VARIABLE	SEX	N	MEAN	STD. DEVIATION	MEDIAN	MINIMUM	MAXIMUM	RANGE	TEST	SIG.
FEMUR, HUMERUS AND METATARSAL	CI	Female	132	3.22	0.15	3.17	2.94	3.70	0.76	-0.194	0.846
		Male	113	3.22	0.19	3.16	2.88	3.69	0.81		
	C/P	Female	132	0.44	0.05	0.45	0.27	0.58	0.31	0.200	0.841
		Male	113	0.44	0.06	0.45	0.29	0.59	0.29		
	API	Female	130	1.25	0.10	1.24	1.03	1.63	0.60	6789.0	0.430
		Male	111	1.26	0.23	1.23	0.82	2.31	1.49		
	BPI	Female	132	1.49	0.16	1.51	0.91	1.88	0.97	7299.0	0.961
		Male	111	1.52	0.29	1.50	0.98	2.60	1.62		
	C/C	Female	133	0.97	0.03	0.96	0.91	1.07	0.16	0.713	0.477
		Male	113	0.96	0.04	0.95	0.90	1.07	0.17		
	ν_4PO_4/Amide I	Female	131	0.75	0.05	0.75	0.58	0.88	0.30	6985.0	0.599
		Male	111	0.75	0.08	0.75	0.41	0.96	0.55		
	ν_1PO_4/Amide I	Female	132	0.54	0.05	0.54	0.37	0.66	0.29	6884.0	0.418
		Male	111	0.54	0.08	0.55	0.28	0.80	0.52		
RIB	CI	Female	59	3.34	0.13	3.35	3.11	3.60	0.49	0.754	0.452
		Male	53	3.31	0.17	3.28	3.01	3.69	0.67		
	C/P	Female	59	0.41	0.05	0.41	0.30	0.51	0.22	-1.320	0.189
		Male	53	0.42	0.06	0.43	0.25	0.55	0.30		
	API	Female	59	1.24	0.13	1.22	0.96	1.68	0.73	1515.0	0.911
		Male	52	1.24	0.24	1.23	0.70	2.34	1.64		
	BPI	Female	59	1.39	0.17	1.38	1.00	1.82	0.82	1361.0	0.307
		Male	52	1.44	0.24	1.40	0.87	2.16	1.30		
	C/C	Female	59	0.99	0.03	0.99	0.93	1.07	0.14	1.952	0.053
		Male	53	0.98	0.04	0.97	0.93	1.06	0.13		
	ν_4PO_4/Amide I	Female	58	0.74	0.06	0.75	0.59	0.88	0.28	1438.0	0.803
		Male	51	0.73	0.09	0.75	0.42	0.97	0.56		
	ν_1PO_4/Amide I	Female	58	0.53	0.05	0.53	0.39	0.66	0.26	1400.0	0.631
		Male	51	0.53	0.08	0.54	0.26	0.75	0.49		
PARIETAL	CI	Female	55	3.33	0.16	3.35	3.05	3.66	0.61	2.158	0.033
		Male	51	3.26	0.18	3.21	2.96	3.68	0.72		
	C/P	Female	55	0.43	0.05	0.44	0.35	0.53	0.18	-1.660	0.100

		Male	51	0.45	0.05	0.45	0.33	0.56	0.23		
	API	Female	54	1.27	0.12	1.25	1.04	1.60	0.56	1222.0	0.405
		Male	50	1.26	0.16	1.22	1.07	2.15	1.09		
	BPI	Female	55	1.05	1.25	1.06	0.83	1.30	0.47	1135.0	0.091
		Male	51	1.10	0.16	1.08	0.81	1.73	0.91		
	C/C	Female	55	0.97	0.03	0.97	0.91	1.04	0.13	2.228	0.025
		Male	51	0.96	0.03	0.95	0.90	1.04	0.14		
	ν_4PO_4/Amide I	Female	55	0.75	0.06	0.75	0.54	0.90	0.35	1181.0	0.161
		Male	51	0.76	0.07	0.76	0.45	0.86	0.41		
	ν_1PO_4/Amide I	Female	55	0.54	0.05	0.54	0.38	0.64	0.25	1114.0	0.068
		Male	51	0.55	0.06	0.56	0.27	0.62	0.35		

Table 3.4. Descriptive statistics according to each age group and results of one-way ANOVA tests for the CI and C/P indices and Mann-Whitney tests for the API, BPI, C/C, ν_4PO_4/Amide I and ν_1PO_4/Amide I indices.

BONE TYPE	VARIABLE	AGE GROUP	N	MEAN	STD. DEVIATION	MEDIAN	MINIMUM	MAXIMUM	RANGE	TEST	SIG.	EFFECT SIZE
FEMUR, HUMERUS AND METATARSAL	CI	0	45	3.23	0.19	3.17	2.91	3.68	0.77	1.976	0.099	---
		1	54	3.26	0.18	3.20	3.06	3.67	0.61			
		2	59	3.23	0.18	3.16	2.97	3.70	0.72			
		3	41	3.16	0.12	3.15	2.93	3.58	0.65			
		4	46	3.20	0.17	3.17	2.88	3.62	0.74			
	C/P	0	45	0.43	0.06	0.44	0.30	0.56	0.25	2.134	0.077	---
		1	54	0.43	0.06	0.44	0.27	0.56	0.29			
		2	59	0.44	0.06	0.46	0.29	0.55	0.25			
		3	41	0.46	0.05	0.46	0.37	0.58	0.21			
		4	46	0.45	0.06	0.46	0.33	0.59	0.26			
	API	0	44	1.25	0.17	1.26	0.82	1.63	0.80	2.705	0.608	---
		1	52	1.26	0.12	1.24	1.08	1.62	0.54			
		2	58	1.26	0.21	1.24	0.99	2.28	1.28			
		3	41	1.22	0.11	1.20	1.05	1.54	0.49			
		4	46	1.28	0.22	1.24	1.02	2.31	1.29			
	BPI	0	45	1.46	0.20	1.48	0.98	1.89	0.91	3.168	0.530	---

		1	53	1.47	0.18	1.51	0.91	1.94	1.03		
		2	58	1.52	0.27	1.54	1.05	2.53	1.48		
		3	41	1.52	1.63	1.52	1.24	1.96	0.72		
		4	46	1.56	0.30	1.53	1.09	2.60	1.51		
	C/C	0	45	0.98	0.03	0.97	0.94	1.07	0.14		
		1	54	0.97	0.03	0.96	0.92	1.04	0.11		
		2	59	0.96	0.03	0.95	0.91	1.07	0.16	16.250	0.003*	0.055
		3	42	0.96	0.03	0.95	0.92	1.07	0.14		
		4	46	0.96	0.03	0.95	0.90	1.05	0.14		
	ν_4PO_4/Amide I	0	45	0.76	0.08	0.75	0.58	0.96	0.38		
		1	52	0.74	0.05	0.74	0.60	0.84	0.24		
		2	58	0.74	0.07	0.74	0.46	0.88	0.42	4.452	0.348	---
		3	41	0.76	0.05	0.76	0.59	0.86	0.26		
		4	46	0.74	0.08	0.75	0.41	0.89	0.48		
	ν_1PO_4/Amide I	0	45	0.55	0.08	0.53	0.39	0.80	0.40		
		1	52	0.53	0.05	0.53	0.40	0.62	0.21		
		2	58	0.54	0.06	0.54	0.29	0.66	0.37	5.488	0.241	---
		3	42	0.55	0.05	0.56	0.37	0.64	0.27		
		4	46	0.54	0.07	0.55	0.28	0.66	0.38		
RIB	CI	0	15	3.36	0.20	3.36	3.01	3.68	0.67		
		1	26	3.33	0.14	3.33	3.08	3.65	0.58		
		2	29	3.36	0.12	3.36	3.18	3.63	0.44	1.408	0.236	---
		3	20	3.30	0.14	3.24	3.11	3.53	0.42		
		4	22	3.27	0.16	3.24	3.05	3.60	0.54		
	C/P	0	15	0.39	0.70	0.40	0.25	0.49	0.24		
		1	26	0.42	0.05	0.42	0.31	0.53	0.22		
		2	29	0.39	0.05	0.39	0.25	0.50	0.24	3.281	0.014	---
		3	20	0.44	0.05	0.45	0.35	0.53	0.18		
		4	22	0.43	0.06	0.44	0.33	0.55	0.21		
	API	0	15	1.23	0.17	1.27	0.72	1.45	0.73		
		1	26	1.29	0.18	1.26	0.95	1.68	0.73		
		2	29	1.21	0.26	1.18	0.70	2.33	1.64	4.759	0.313	---
		3	19	1.24	0.13	1.19	1.08	1.52	0.44		
		4	22	1.24	0.14	1.20	1.03	1.65	0.62		
	BPI	0	15	1.35	0.23	1.38	0.90	1.70	0.83	10.422	0.034	---

		1	26	1.42	0.18	1.40	1.04	1.80	0.76		
		2	28	1,32	0.16	1.33	0.87	1.68	0.81		
		3	20	1,49	0.20	1.49	1.21	2.16	0.95		
		4	22	1,48	0.25	1.46	1.12	2.12	0.99		
	C/C	0	15	1,00	0.04	1.00	0.94	1.07	0.13	13.670	0.008*	0.056
		1	26	0,99	0.03	0.99	0.94	1.06	0.12		
		2	29	0,99	0.03	0.99	0.94	1.05	0.10		
		3	20	0,97	0.03	0.96	0.93	1.05	0.12		
		4	22	0,97	0.03	0.95	0.93	1.03	0.11		
	ν_4PO_4/Amide I	0	14	0,74	0.03	0.75	0.66	0.78	0.12	4.508	0.342	---
		1	25	0,72	0.07	0.72	0.59	0.88	0.28			
		2	28	0,75	0.09	0.76	0.43	0.97	0.54			
		3	20	0,73	0.09	0.74	0.41	0.85	0.43			
		4	22	0,74	0.06	0.74	0.58	0.84	0.26			
	ν_1PO_4/Amide I	0	14	0,52	0.03	0.53	0.44	0.57	0.12	6.468	0.167	---
		1	25	0,52	0.06	0.51	0.39	0.66	0.26			
		2	28	0,55	0.08	0.55	0.26	0.75	0.49			
		3	20	0,53	0.08	0.55	0.27	0.64	0.37			
		4	22	0,54	0.06	0.55	0.38	0.64	0.25			
PARIETAL	CI	0	10	3,29	0.21	3.25	3.00	3.68	0.67	1.306	0.273	---
		1	25	3,35	0.17	3.29	3.12	3.66	0.54			
		2	30	3.30	0.16	3.30	3.04	3.61	0.58			
		3	20	3.23	0.16	3.16	3.06	3.62	0.56			
		4	21	3.28	0.19	3.27	2.96	3.64	0.68			
	C/P	0	10	0.44	006	0.45	0.36	0.53	0.17	1.159	0.334	---
		1	25	0.42	0.05	0.42	0.33	0.52	0.19			
		2	30	0.44	0.05	0.43	0.35	0.53	0.17			
		3	21	0.45	0.40	0.46	0.36	0.51	0.15			
		4	21	0.44	0.06	0.44	0.36	0.56	0.20			
	API	0	10	1.29	0.11	1.25	1.14	1.48	0.34	5.566	0.234	---
		1	25	1.26	0.12	1.25	1.05	1.51	0.46			
		2	29	1.27	0.10	1.25	1.10	1.53	0.43			
		3	19	1.22	0.13	1.19	1.04	1.60	0.56			
		4	21	1.29	0.22	1.25	1.11	2,15	1.05			
	BPI	0	10	1.07	0.14	1.09	0.86	1,30	0.44	3.152	0.533	---

	1	25	1.03	0.13	1.03	0.81	1.26	0.44			
	2	20	1.08	0.14	1.08	0.84	1.50	0.66			
	3	20	1.09	0.10	1.12	0.83	1.21	0.38			
	4	21	1.09	0.19	1.05	0.88	1.73	0.84			
	0	10	0.97	0.04	0.96	0.93	1.04	0.12			
	1	25	0.98	0.03	0.97	0.93	1.02	0.10			
C/C	2	30	0.97	0.03	0.96	0.91	1.04	0.12	6.460	0.167	---
	3	20	0.95	0.03	0.94	0.92	1.03	0.10			
	4	21	0.96	0.04	0.96	0.90	1.03	0.12			
	0	10	0.75	0.05	0.76	0.66	0.83	0.17			
	1	25	0.75	0.57	0.74	0.62	0.89	0.28			
ν_4PO_4/Amide I	2	30	0.74	0.07	0.76	0.45	0.82	0.37	5.921	0.205	---
	3	20	0.77	0,.07	0.80	0.54	0.83	0.29			
	4	21	0.74	0.08	0.76	0.47	0.85	0.38			
	0	10	0.53	0.05	0.54	0.46	0.61	0.16			
	1	25	0.54	0.04	0.53	0.43	0.60	0.17			
ν_1PO_4/Amide I	2	30	0.53	0.06	0.54	0.27	0.62	0.35	6.573	0.160	---
	3	21	0.56	0.06	0.58	0.38	0.64	0.25			
	4	21	0.54	0.07	0.55	0.30	0.62	0.32			

*statistically significant at the 0.01 level.

Given the significant association of the C/C with age groups, although partial, the potential of such association was investigated by building linear regression models based on this chemometric index to predict age group. The coefficients are reported in Table 3.5.

Table 3.5. Coefficients for the linear regression of age group from the C/C according to bone type.

BONE TYPE	CONSTANT	B	STD. ERROR	BETA	TEST	SIG.
FEMUR, HUMERUS AND METATARSAL	11.765	-10.148	2.620	-0.241	-3.873	<.001*
RIB	14.353	-12.479	3.519	-0.320	-3.546	0.001*
PARIETAL	8.396	-6.450	3.624	-0.172	-1.780	0.078

*statistically significant at 0.01 level.

Regression models for bones with diaphysis and for the ribs were statistically significant ($F=15.002$ and $p < .001$; $F=12.577$ and $p < .01$) and had small adjusted R^2 of 0.058 and 0.103, respectively. Table 3.6 presents the performance results of these two models when the coefficients were applied to the sample from which they have been calculated to assess how accurate would the prediction be. As can be observed, the root mean square error (RMSE) was quite high, being larger than one age group. The coefficient of variation (CV) for the absolute prediction error was also quite high demonstrating that the prediction error was quite uneven. This is supported by the mean absolute error (MAE) for each age group, which was very small for the intermediate group – 70 to 79 years old – but quite high for the other age groups, especially for the younger and older groups. This result indicates that the regression models presented a very varied performance according to each age group and were therefore quite unbalanced.

Table 3.6. Descriptives for the performance of regression models to age group according to bone types.

BONE TYPE	AGE GROUP	MAE	CV	RMSE
FEMUR, HUMERUS AND METATARSAL	0	1.84	63.51%	1.33
	1	0.92		
	2	0.25		
	3	0.94		
	4	1.94		
RIB	0	1.85	68.05%	1.25
	1	1.01		
	2	0.26		
	3	0.79		
	4	1.73		

3.3.1.1. PREDICTION OF CHRONOLOGICAL AGE THROUGH CHEMOMETRIC INDICES

Correlations between age and each chemometric index were also checked through Spearman tests for all indices – Table 3.7.

The C/C ratio presented statistically significant correlations with age for bones with diaphysis and the rib ($p < .001$ and $p = .001$, respectively). The C/P also presented significant results for bones with diaphysis ($p = .006$). To ensure that the referred indices actually predicts individual age, linear regression models were built, and coefficients are presented – in Table 3.8. The tolerance and VIF showed no problems of multicollinearity for multiple regression models. Regression models for bones with diaphysis were statistically significant ($F=8.180$ and $p < .001$) with an adjusted R^2 of 0.063 and only the C/C ratio had a significant contribution ($p < .01$) for the model comprising the femur, humerus and metatarsal. The performance results of the first model with the application of coefficients are displayed in Table 3.9.

Table 3.7. Descriptive statistics to Spearman correlation between age and indices, according to bone type models.

BONE TYPE	VARIABLE	N	MEAN	STD. DEVIATION	MINIMUM	MAXIMUM	RANGE	TEST	SIG.
FEMUR, HUMERUS AND METATARSAL	Age	246	71.91	16.56	28	96	68	---	---
	CI	245	3.22	0.17	2.88	3.70	0.82	-0.101	0.114
	C/P	245	0.44	0.58	0.27	0.59	0.32	0.176	0.006*
	API	241	1.26	0.18	0.82	2.31	1.49	-0.042	0.521
	BPI	243	1.51	0.23	0.91	2.60	1.69	0.124	0.054
	C/C	246	0.97	0.03	0.90	1.07	0.17	-0.254	<.001*
	ν_4PO_4/Amide I	242	0.75	0.07	0.41	0.96	0.55	0.027	0.673
	ν_1PO_4/Amide I	243	0.54	0.06	0.28	0.80	0.52	0.097	0.133
RIB	Age	112	73.37	15.52	28	96	68	---	---
	CI	112	3.33	0.15	0.13	3.68	0.67	-0.153	0.108
	C/P	112	0.42	0.06	0.25	0.55	0.30	0.172	0.070
	API	111	1.24	0.19	0.70	2.34	1.64	-0.082	0.393
	BPI	111	1.41	0.21	0.87	2.17	1.30	0.136	0.155
	C/C	112	0.98	0.03	0.93	1.07	0.15	-0.306	0.001*
	ν_4PO_4/Amide I	109	0.74	0.07	0.42	0.97	0.56	0.083	0.393
	ν_1PO_4/Amide I	109	0.53	0.07	0.26	0.7	0.49	0.183	0.057
PARIETAL	Age	106	74.44	14.81	28	96	68	---	---
	CI	106	3.30	0.17	2.96	3.68	0.72	-0.143	0.143
	C/P	106	0.44	0.05	0.33	0.56	0.23	0.111	0.259
	API	104	1.27	0.14	1.04	2.15	1.11	-0.085	0.393
	BPI	106	1.07	0.14	0.81	1.73	0.91	0.100	0.309
	C/C	106	0.97	0.03	0.90	1.04	0.14	-0.166	0.089
	ν_4PO_4/Amide I	106	0.75	0.07	0.44	0.89	0.45	0.062	0.528
	ν_1PO_4/Amide I	106	0.54	0.06	0.27	0.64	0.37	0.132	0.178

*statistically significant at the 0.01 level.

Table 3.8. Summary of results of linear regression of the variables C/C and C/P to predict the age at death, according to bone type.

BONE TYPE		CONSTANT	B	STD. ERROR	BETA	TEST	SIG.	TOLERANCE	VIF
FEMUR, HUMERUS AND METATARSAL	C/C	198.102	-130.268	49.309	-0.254	-2.642	0.009*	0.419	2.388
	C/P		-0.883	27.642	-0.003	-0.032	0.975		
RIB	C/C	195.823	-125.029	61.319	-0.273	-2.039	0.044	0.472	2.117
	C/P		1.428	35.689	0.005	0.040	0.968		
PARIETAL	C/C	243.014	-143.737	82.744	-0.326	-1.737	0.085	0.268	3.730
	C/P		-67.722	54.153	-0.234	-1.251	0.214		

*statistically significant at the 0.01 level.

The RMSE was extraordinarily high, indicating an error of 16 years for the model. The CV for the absolute prediction was also quite high demonstrating that the prediction error was quite uneven. This is supported by the MAE for each age category, which is high for the extremes – 28 to 59 years old and 90 to 99 years old –, and lower to the intermediate groups – from 60 to 89 years old. Again, this reflected the unbalanced performance of the model.

Table 3.9. Descriptives for the performance of regression models for individual age estimation, according to bones with diaphysis.

BONE TYPE	AGE	MAE	CV	RMSE
FEMUR, HUMERUS AND METATARSAL	28–59	25.86	78.50%	16.02
	60–69	7.25		
	70–79	4.45		
	80–89	9.40		
	90–99	19.17		

According to bone type models, the relationship among $\nu_3(CO_3^{2-})_{A+B}$ and $\nu_3(CO_3^{2-})_B$ intensities, reflected by the C/C ratio, encounters an association throughout age cohort and chronological age, despite the estimated error detected through the regression models. Even though, the band relative to A and B types of carbonate overlap with the deformation of methylene groups from lipids and protein, which indicates the possibility of an influence of the organic content of bone. And, as previously detected, the organic component shows potential to discriminate among types of bone.

Therefore, the carbonate content appears to be able to discriminate individuals of different ages.

3.3.1.2. THE EFFECT OF *POST-MORTEM* INTERVAL ON CHEMOMETRIC INDICES

To assess how reliable results were, it is important to understand if the *post-mortem* interval, PMI, has an effect on chemometric indices. For this purpose, Spearman correlations were used to test that hypothesis. Results are given in Table 3.10. Only the CI presented a significant result at the .01 level although with a small positive correlation. Indeed, Longato *et al.* [118] pointed a connection, indicating that short PMI reveals higher CI values when compared to specimens with a long PMI.

This means that the results obtained for the other indices, mainly the ones regarding the C/C, appear to have not been affected by PMI.

Table 3.10. Descriptive statistics to Spearman correlation between *post-mortem* interval and indices.

	CI	**C/P**	**API**	**BPI**	**C/C**	**ν_4PO_4/Amide I**	**ν_1PO_4/Amide I**
COEFFICIENT	0.141	-0.065	0.082	-0.111	0.036	-0.087	-0.048
SIG.	0.002*	0.161	0.080	0.017	0.444	0.063	0.306

*statistically significant at the 0.01 level.

Summarizing, no difference between humerus, femur and metatarsal have been previously found, so the long bones were grouped into the same group. Ribs and parietals present statistically significant differences when related to the other bones. The referred differentiation occurred through CI, C/P and C/C indices, indicating the potential of the relationship across the respective band intensities.

Age range differences were statistically significant in long bones and ribs regarding the C/C index; and in long bones to chronological age estimation to C/C index. Nevertheless, the regression model for age group and chronological age estimation demonstrates a high prediction error.

In summary, despite the significant p-values, regression models were not fit to predict the approximate age of an individual from its bones or teeth. The error is high and model performance is unbalanced according to each age range.

3.3.2. TEETH ANALYSIS

The coefficient of variation was calculated for the several relationships for teeth, obtaining the lowest variations for the C/C, about 1.91%, and 2.55% for the CI. The C/P obtained 15.01%, 18.76% for the API, 16.52% for the BPI, 16.52% for the ν_4PO_4/Amide and 11.44% for the ν_1PO_4/Amide I.

The data were explored, and after outliers have been removed, sex differences were analyzed through a parametric t-student test for all the indices – Table 3.11. The CI was the only ratio exhibiting a statistically significant result ($p < .01$). Nonetheless, considering the small contribution reflected by the effect size and the fact of being the only index contributing for sex differentiation, it was decided to pool men and women into the same variable. Furthermore, the effect size value presented an adverse effect (-0.624).

To explore if any significant differences in chemometric indices were present among age groups, non-parametric Kruskal-Wallis tests were employed – Table 3.12.

Statistically significant results ($p < .01$) were obtained for CI, C/C and ν_1PO_4/Amide I, thus non-parametric Mann-Whitney tests were applied for pairwise comparisons between age groups and significant differences for CI ($p < .001$) were observed for the extreme cohorts and, quite unexpectedly, between close age cohorts: 28 to 59 years old and 70 to 79 years old (MW=80.000); 28 to 59 years old and 80 to 89 years old (MW=70.000); 28 to 59 years old and 90 to 99 years old (MW=34.500); 60 to 69 years old and 70 to 79 years old (MW=44.000); 60 to 69 years old and 80 to 89 years old (MW=40.000) and 60 to 69 years old and 90 to 99 years old (MW=21.000) – Table 3.13. Hence, the crystallinity index appears to provide spectral information capable of discriminating age cohorts, which was verified through the large effect (0.453). For C/C and ν_1PO_4/Amide I the effect size was small (0.102 and 0.116, respectively).

Table 3.11. Descriptive statistics according to each sex and results of t-student tests for the CI, C/P, API, BPI, C/P, ν_4PO_4/Amide I and ν_1PO_4/Amide I indices.

VARIABLE	SEX	N	MEAN	STD. DEVIATION	MEDIAN	MINIMUM	MAXIMUM	RANGE	TEST	SIG.	EFFECT SIZE
CI	Female	47	2.97	0.07	2.90	2.84	3.11	0.27	-3.166	0.002*	-0.624
	Male	57	3.02	0.08	3.03	2.83	3.24	0.41			
C/P	Female	47	0.51	0.07	0.51	0.38	0.68	0.29	1.677	0.097	---
	Male	58	0.49	0.07	0.49	0.34	0.66	0.32			
API	Female	47	1.28	0.27	1.27	0.67	2.09	1.42	1.634	0.105	---
	Male	58	1.20	0.25	1.20	0.89	1.93	1.04			
BPI	Female	47	1.64	0.29	1.63	1.18	2.44	1.26	1.500	0.137	---
	Male	58	1.56	0.30	1.54	1.14	2.44	1.31			
CC	Female	47	0.94	0.02	0.94	0.90	0.97	0.07	1.772	0.079	---
	Male	58	0.93	0.02	0.93	0.87	0.98	0.10			
ν_4PO_4/Amide I	Female	45	0.78	0.13	0.77	0.57	1.07	0.50	-2.232	0.028	---
	Male	57	0.84	0.14	0.84	0.55	1.19	0.64			
ν_1PO_4/Amide I	Female	46	0.84	0.10	0.84	0.63	1.09	0.46	-2.183	0.031	---
	Male	56	0.88	0.92	0.90	0.67	1.05	0.38			

*statistically significant at the 0.01 level.

Table 3.12. Descriptive statistics to each age group results of Kruskal-Wallis tests for the CI, C/P, API, BPI, C/P, ν_4PO_4/Amide I and ν_1PO_4/Amide I indices.

VARIABLE	AGE GROUP	N	MEAN	STD. DEVIATION	MEDIAN	MINIMUM	MAXIMUM	RANGE	TEST.	SIG.	EFFECT SIZE
CI	0	29	2.937	0.06	2.95	2.83	3.06	0.23	46.841	<.001*	0.453
	1	16	2.95	0.04	2.94	2.89	3.03	0.14			
	2	19	3.03	0.07	3.32	2.90	3.24	0.34			
	3	20	3.04	0.07	3.05	2.90	3.16	0.25			
	4	20	3.04	0.05	3.04	2.97	3.19	0.22			
C/P	0	29	0.49	0.07	0.47	0.37	0.66	0.29	2.793	0.593	--
	1	16	0.52	0.07	0.05	0.40	0.68	0.27			
	2	20	0.48	0.08	0.47	0.34	0.63	0.27			
	3	20	0.49	0.08	0.50	0.38	0.63	0.25			
	4	20	0.50	0.68	0.50	0.37	0.66	0.28			

API	0	29	1.22	0.24	1.20	0.67	1.74	1.07	1.557	0.817	--
	1	16	1.31	0.30	1.31	0.92	2.09	1.17			
	2	20	1.24	0.31	1.18	0.89	1.78	0.90			
	3	20	1.20	0.22	1.20	0.89	1.55	0.66			
	4	20	1.23	0.26	1.22	0.88	1.93	1.05			
BPI	0	29	1.56	0.27	1.53	1.20	2.17	0.97	2.273	0.686	--
	1	16	1.68	0.30	1.64	1.25	2.44	1.19			
	2	20	1.60	0.36	1.55	1.13	2.24	1.10			
	3	20	1.57	0.29	1.56	1.18	2.05	0.87			
	4	20	1.60	0.28	1.59	1.17	2.44	1.27			
C/C	0	29	0.94	0.01	0.94	0.91	0.97	0.05	14.177	0.007*	0.102
	1	16	0.93	0.22	0.93	0.87	0.97	0.10			
	2	20	0.93	0.01	0.93	0.90	0.97	0.06			
	3	20	0.93	0.02	0.92	0.90	0.98	0.07			
	4	20	0.93	0.02	0.93	0.90	0.97	0.07			
ν_4PO_4/Amide I	0	28	0.80	0.11	0.83	0.59	1.01	0.42	1.613	0.807	--
	1	15	0.80	0.16	0.75	0.65	1.19	0.54			
	2	19	0.82	0.16	0.80	0.58	1.07	0.49			
	3	20	0.84	0.12	0.84	0.65	1.04	0.38			
	4	20	0.82	0.13	0.81	0.55	1.04	0.49			
ν_1PO_4/Amide I	0	28	0.82	0.09	0.80	0.65	0.96	0.31	15.249	0.004*	0.116
	1	15	0.80	0.11	0.78	0.62	0.97	0.35			
	2	19	0.87	0.10	0.88	0.67	1.09	0.42			
	3	20	0.90	0.07	0.90	0.72	1.05	0.32			
	4	20	0.90	0.10	0.92	0.65	1.04	0.39			

*statistically significant at the 0.01 level.

Table 3.13. Results of Mann-Whitney tests for pairwise comparison between age groups to CI index.

AGE GROUP	18–29	30–39	40–59	60–69	70–82
18-29	---	x	**	**	**
30-39	---	---	**	**	**
40-59	---	---	---	x	x
60-69	---	---	---	---	x
70-82	---	---	---	---	---

**: age cohorts' discrimination; x: absence of discrimination; --- nothing to state.

To ensure the potential of CI to predict age group, a linear regression model was created. The coefficients are displayed in Table 3.14, and the regression was statistically significant (F=55.110 and $p < 0.001$) with an adjusted R^2 of 0.351.

Table 3.14. Summary of linear regression of age groups correlation to CI.

VARIABLE	CONSTANT	B	STD. ERROR	BETA	TEST	SIG.
CI	-32.806	11.570	1.559	0.592	7.424	<.001*

*statistically significant at the 0.01 level.

To test the accuracy of the regression model, Table 3.15 presents the performance results when the coefficients were applied to the sample from which they were calculated. As can be noted, the RMSE was relatively high, being larger than one age group. The CV for the absolute prediction error was also quite high demonstrating that the prediction error was quite uneven. The MAE is similar for each age group, although somewhat higher, for the oldest group. The result indicates that the regression model presented an equal performance attending to each age group.

Table 3.15. Descriptives for the performance of regression models based on the CI for age groups.

AGE GROUP	MAE	CV	RMSE
0	0.93	72.89%	1.20
1	0.94		
2	0.95		
3	0.96		
4	1.06		

Similarly to the PCA teeth analysis, discrimination among age cohorts was also found to be better achieved through the inorganic component of teeth. However, for PCA analysis – Figure 3.9 and 3.10 –, observed main spectral variations occurred in the ν_1,ν_3(PO_4^{3-}) domain. The crystallinity index was slightly capable of discriminating among age classes, despite the large RMSE. Thus, results suggest that the dissimilarities among

the teeth age groups were partly reflected through the combination among the relative sizes of crystals and the atomic order within the lattice.

3.3.2.1. PREDICTION OF CHRONOLOGICAL AGE THROUGH CHEMOMETRIC INDICES

To investigate a possible correlation of individual age to each chemometric index, Spearman tests were applied – Table 3.16. Statistically significant correlations ($p < .001$) were found for the CI, C/C and ν_1PO_4/Amide I ratios.

Table 3.16. Descriptive statistics to Spearman correlation between age and indices.

VARIABLE	N	MEAN	STD. DEVIATION	MINIMUM	MAXIMUM	RANGE	TEST	SIG.
AGE	105	47.49	19.86	18	82	64	--	--
CI	104	2.99	0.08	2.83	3.24	0.41	0.60	<.001*
C/P	105	0.50	0.07	0.34	0.68	0.34	0.05	0.640
API	105	1.23	0.26	0.68	2.09	1.42	-0.05	0.592
BPI	105	1.60	0.30	1.14	2.44	1.31	0.02	0.856
C/C	105	0.93	0.02	0.87	0.98	0.10	-0.36	<.001*
ν_4PO_4/Amide I	102	0.82	0.13	0.55	1.19	0.64	0.09	0.358
ν_1PO_4/Amide I	102	0.86	0.10	0.63	1.09	0.43	0.34	<.001*

*statistically significant at the 0.01 level.

The regression model for individual age prediction is described in Table 3.17. It was statistically significant ($F=27.552$ and $p < .001$) and had an adjusted R^2 of 0.443. The results indicated that only CI and C/C possess a minor ability to predict individual age ($p < .001$). The tolerance and VIF values demonstrated no problems of multicollinearity.

Table 3.17. Summary of linear regression of age correlation with CI, C/C and ν_1PO_4/Amide I.

VARIABLE	CONSTANT	B	STD. ERROR	BETA	TEST	SIG.	TOLERANCE	VIF
CI	-93.826	174.787	25.166	0.640	6,945	<.001*	0.655	1.526
C/C		-386.704	91.854	-0.325	-4,210	<.001*	0.935	1.070
ν_1PO_4/Amide I		-24.351	19.297	-0.120	-1.262	0.210	0.621	1.611

*statistically significant at the 0.01 level.

Table 3.18 presents the performance results of coefficients application to assess how accurate the individual age based on CI and C/C values would be. The RMSE was extremely high, 26.72 years, which is considerably larger than one age group. However, the CV was very low. The MAE is similar and incredible high for each age group.

Table 3.18. Descriptives for the performance of regression models for chronological age.

AGE	MAE	CV	RMSE
18–29	24.45		
30–39	24.24		
40–59	23.98	57.28%	26.72
60–69	23.57		
70–82	24.22		

Nevertheless, Figure 3.11 displayed the linear regression of age correlation to CI. As noted above for the age cohorts, the CI also revealed some potential to predict chronological age in teeth.

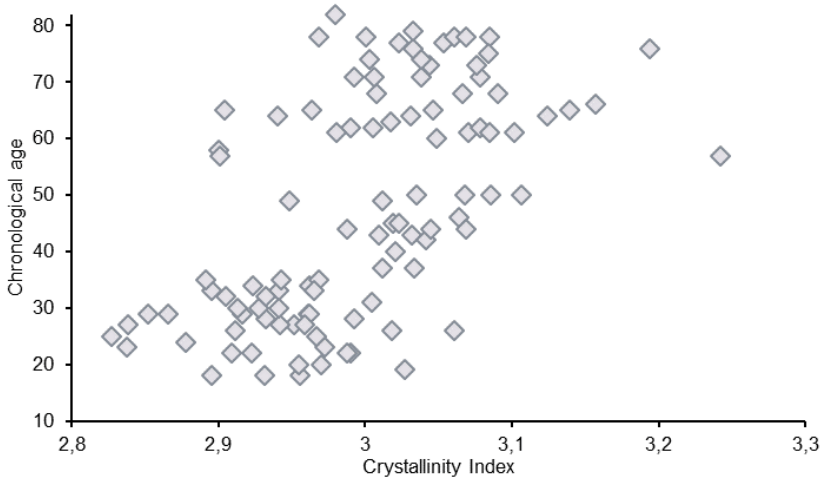

Figure 3.11. Graphic representation of chronological age correlation to crystallinity index.

Thus, an increasing of teeth individual age is accompanied with increasing crystallinity. However, besides the correlation observed for teeth, it was expectable that a correlation of bone age with CI was also observed, as has been reported previously [109, 122–124]. Possibly, the absence of correlation is linked to the several factors that influence the chemical characteristics and bone compositions both in *ante-* and *post-mortem* moments: metabolic processes of resorption and regeneration over life, pathologies, collagen degradation or post-burial alterations resulting in more ordered crystal lattices. Apart from the CI, the C/C ratio, showed statistically significant results in bones, in accordance with the described tendency of carbonate content increase with age [125, 126].

To accomplish the goal of predicting age, this study suggests that the CI and C/C ratios represent the most promising chemometric indices applicable to human bones and teeth.

Despite the expectable potential of the spectroscopic indices related to amide I, ν_4PO_4/Amide I and ν_1PO_4/Amide I, none demonstrated statistically significant results,

proving the incapacity of these spectral relationships to discriminate, either through age cohorts or chronological age, or to discriminate types of bone. In contrast to the demonstrated by Very *et al.* [127], which argued that positional and small intensity shifts in bands associated with amide I and amide II are consistent with the effect of aging; or the predictable spectral variations in amide I promoted by collagen degradation and the degree of bone remodelling rate according to the individual age.

The remaining indices, C/P, API and BPI did not provide any statistically significant regression model, suggesting that the ratios related to phosphates' and carbonates' content have no major contribution in this matter.

Despite the high prediction error estimated for the several regression models, spectral variations were found through chemometric indices which demonstrate an influence, even if minimal, of aging in bone and teeth chemical composition.

In order to improve the potential of this approach, additional considerations should be introduced for bone analysis: principally, a higher number of younger individuals, and the number of samples must be consistent to each age cohort. The present study mostly comprises older adults, and the lower correlations obtained were a reflection of that. Younger individuals possibly possess individualizing features capable of a clearer differentiation throughout spectral variation, taking into consideration the reduced susceptibility of youngers' bone to the age-related reduction of collagen, and the minimal variability of bone mineral density and remodelling rate [39, 70, 74–76]. This is less the case for elderly individuals who are more affected by deterioration of the bone microarchitecture, pathologies, and mainly, molecular changes in the inorganic and organic components of bone. Moreover, the bone mineral density factor should be incorporated as a variable in the analysis, possibly contributing to indicate the degree of chemical alterations affecting the bone: considering the reduction of BMD levels and consequential alterations, especially after menopause and during aging, when compared to the stable proportion for young adults [74].

Additionally, combining the age interval obtained through spectral variations using FTIR-ATR and the age interval from anthropological methods may help establishing a more precise prediction of the age at death estimation.

CHAPTER 4

CONCLUSION

4. CONCLUSION

When forensic scenarios comprise skeletonized remains, an attempt of estimating age at death is vital to achieve a biological profile which in turn may be paramount to obtain a positive identification. Whilst forensic anthropologist differentiates macroscopically the skeletal remains, in a chemical evaluation the sampling 'skeletal site' may influence the analysis, due to individual intrinsic characteristics and the intra-individual variability. In addition, post-burial conditions may differentially affect the skeleton.

Thus, the analysis of different bone types subjected to different parameters was imperative in this study, and FTIR-ATR spectral variations were evaluated through a multi-approach based on qualitative, exploratory and inferential statistical analyses. The main spectral variations observed occurred in $\nu_3(CO_3^{2-})_B$, amide II and amide I bands, and in chemometric indices concerning the CI, C/C and C/P ratios, which allowed a differentiation through ribs, parietal and long bones – femur, humerus and metatarsal.

As osteoporosis possesses a high incidence rate in women, when compared to men, it was expectable to observe a discrimination between sex. Nonetheless, no visible differences were found between male and female samples, either considering the whole spectral range or solely the inorganic or organic part for human bones and teeth.

Regarding bones analysis, non-significant discrimination among age cohorts was detected through the exploratory analysis, proposing that spectral variations according to age classes are marginal. In fact, although the C/C ratio showed a statistically significant difference among age cohorts in long bones and ribs and a significant correlation with chronological age in long bones, predictions presented somewhat high mean absolute errors. Although *post-mortem* taphonomy may have played a part in these results, that does not seem to have been too major. The C/C ratio appears to have not been significantly affected by *post-mortem* interval. Although, the extension of diagenetic changes is dependent on the amount of the inhumation period, on the type of soil in contact with the remains and on environmental factors, this study suggests that solely the crystallinity index varies according to *post-mortem* period: increased values were associated to the increment of PMI.

A significant spectral variation occurred for teeth, discriminating the younger and the older adults, by using the inorganic spectral signals assigned to the $\nu_1,\nu_3(PO_4^{3-})$ domain, which indicates that the relative intensity and width of the bands varies with mineral crystal lattice properties according to age. Relatively to the inferential statistical analysis, the CI proved more efficient in discriminating age cohorts. Therefore, the idiosyncrasies in teeth structure were reflected through the combination among the relative sizes of crystals and

the atomic order within the lattice. For the prediction of chronological age, the CI and C/C revealed some potential. Indeed, the linear regression indicated an adjusted R^2 of 0.443.

Overall, the CI and C/C ratios represent the most promising chemometric indices to attempt age at death estimation using human bones and teeth. Nevertheless, the regression models obtained for age cohort and chronological age estimation give rise to high prediction errors for human bones and teeth. A statistical limitation of this study is the small sample size for bones to young adults, so it is possible that enlarged samples with a better representation of younger individuals may allow for different results.

Anthropological macroscopic methods for age at death estimation of adults often lead to large estimation intervals. The chemometric approach here investigated does not appear to bring major improvements. However, a combination of other methods with the methodology here applied may possibly help establishing a more precise prediction of age at death estimation. Future work may focus on this research hypothesis.

One of the conclusions obtained in this study that the combination of the exploratory and inferential methods enables distinct information. Thus, the exploration of spectral variations occurred at the whole spectral range and the spectral relationships are complementary.

Furthermore, the clearly reflected variations across elemental structure of these skeletal elements fully justify the use of FTIR-ATR for human bones and teeth analysis in forensic laboratories. Adding to the fact that these facilities are often equipped with mid-FTIR apparatus, their application to skeletal remains bring numerous advantages: non-destructive analyses; quick data acquisition-time; reduced amount of sample required; hardly any sample preparation, the interferents are easily eliminated; and the collected results are extremely rich in information on both organic and inorganic components. Moreover, an additional study on the variations observed in samples from different operators led to the hypothesis that the sampling method influences the relative position of the bands in the spectrum. Thus, it is extremely important to develop a standard method for bone powder preparation to improve data accuracy, precision, comparability and reproducibility.

CHAPTER 5
REFERENCES

5. REFERENCES

1. Forensic Anthropology. In: Natl. Museum Nat. Hist. https://naturalhistory.si.edu/education/teaching-resources/social-studies/forensic-anthropology. Accessed 26 Jul 2019
2. Brough AL, Morgan B, Rutty GN (2015) The basics of disaster victim identification. J Forensic Radiol Imaging 3:29–37. doi: 10.1016/j.jofri.2015.01.002
3. Schmeling A, Geserick G, Reisinger W, Olze A (2007) Age estimation. Forensic Sci Int 165:178–181. doi: 10.1016/j.forsciint.2006.05.016
4. Blau S, Briggs CA (2011) The role of forensic anthropology in Disaster Victim Identification (DVI). Forensic Sci Int 205:29–35. doi: 10.1016/j.forsciint.2010.07.038
5. Cattaneo C (2007) Forensic anthropology: developments of a classical discipline in the new millennium. Forensic Sci Int 165:185–193. doi: 10.1016/j.forsciint.2006.05.018
6. Cógido Penal. In: Diário da República Eletrónico. https://dre.pt/web/guest/legislacao-consolidada/-/lc/107981223/201708230200/indice. Accessed 6 Jul 2019
7. Íşcan MY (2001) Global forensic anthropology in the 21st century. Forensic Sci Int 117:1–6 doi: 10.1016/S0379-0738(00)00433-3
8. Íşcan MY (2005) Forensic anthropology of sex and body size. Forensic Sci Int 147:107–112. doi: 10.1016/j.forsciint.2004.09.069
9. Franklin D (2010) Forensic age estimation in human skeletal remains: Current concepts and future directions. Leg Med 12:1–7. doi: 10.1016/j.legalmed.2009.09.001
10. White TD, Black MT, Folkens PA (2012) Assessment of age, sex, stature, ancestry, and identity of the individual. In: Human Osteology, Third Edit. Elsevier, pp 381–406
11. Cunha E, Baccino E, Martrille L, Ramsthaler F, Prieto J, Schuliar Y, Lynnerup N, Cattaneo C (2009) The problem of aging human remains and living individuals: A review. Forensic Sci Int 193:1–13. doi: 10.1016/j.forsciint.2009.09.008
12. Lovejoy C (1985) Dental wear in the Libben population. Its functional pattern and role in the determination of adult skeletal age at death. Am J Phys Anthropol 68:47–56. doi: 10.1002/ajpa.1330680105
13. Prince D, Kimmerle L, Konigsberg L (2008) A Bayesian approach to estimate skeletal age-at-death utilizing dental wear. J Forensic Sci 53:588–593. doi: 10.1111/j.1556-4029.2008.00714.x
14. Drusini A (1991) Age-related changes in root transparency of teeth in males and females. Am J Hum Biol 3:629–637. doi: 10.1002/ajhb.1310030613

15. Lamendin H, Baccino E, Humbert J, Tavernier JC, Nossintchouk RM, Zerilli A (1992) A simple technique for age estimation in adult corpus: the two criteria dental method. J Forensic Sci 37:1373–1379. doi: 10.1520/JFS13327J
16. Prince D, Ubelaker D (2002) Application of Lamendin's adult aging technique to a diverse skeletal sample. J Forensic Sci 47:107–16. doi: 10.1520/JFS15209J.
17. González-Colmenares G, Botella-López M, Moreno-Ruedo G, Fernández-Cardenete J (2007) Age estimation by a dental method: a comparison of Lamendin's and Prince & Ubelaker's technique. J Forensic Sci 52:1156–1160. doi: 10.1111/j.1556-4029.2007.00508.x.
18. Wittwer-Backofen U, Gampe J, Vaupel J (2004) Tooth cementum annulations for age estimation: results from a large known-age validation study. Am J Phys Anthropol 123:119–129. doi: 10.1002/ajpa.10303.
19. Czermak A, Czermak A, Ernst H, Grupe G (2006) A new method for the automated age-at-death evaluation by tooth-cementum annulation (TCA). Anthropol Anzeiger 64:25–40. doi: 10.2307/29542704
20. Ohtani S (1995) Studies on age estimation using racemization of aspartic acid in cementum. J Forensic Sci 40:805–807. doi: 10.1520/JFS15388J
21. Yekkala R, Meers C, Van Schepdael A, Hoogmartens J, Lambrichts I, Willems G (2006) Racemization of aspartic acid from human dentine in the estimation of chronological age. Forensic Sci Int 159:S89–S94. doi: 10.1016/j.forsciint.2006.02.022
22. Cameriere R, Ferrante L, Cingolani M (2004) Variations in pulp/tooth area ratios as an indicator of age: a preliminary study. J Forensic Sci 49:317–319. doi: 1520/JFS2003259
23. Cameriere S, Brogi C, Ferrante L, Mirtella D, Vultaggio C, Cingolani M, Fornaciari G (2006) Reliability in age determination by pulp/tooth ratio in upper canines in skeletal remains. J Forensic Sci 51:861–864. doi: 10.1111/j.1556-4019.2006.00159.x
24. Cameriere R, Cunha E, Sassaroli E, Nuzzolese E, Ferrante L (2009) Age estimation by pulp/tooth area ratio in canines: Study of a Portuguese sample to test Cameriere's method. Forensic Sci Int 193:128.e1-6. doi: 10.1016/j.forsciint.2009.09.011
25. Todd TW (1920) Age changes in the pubic bone. Am J Phys Anthropol 4:1–70. doi: 10.1002/ajpa.1330040102
26. Todd TW (1920) Age changes in the pubic bone: The white male pubis. Am J Phys Anthropol 3:285–334. doi: 10.1002/ajpa.1330030301
27. Brooks S, Suchey JM (1990) Skeletal age determination based on the os pubis: a comparison of the Acsádi-Nemeskéri and Suchey-Brooks methods. Hum Evol 5:227–238. doi: 10.1007/BF02437238

28. Lovejoy CO, Meindl RS, Pryzbeck TR, Mensforth RP (1985) Chronological metamorphosis of the auricular surface of the ilium: A new method for the determination of adult skeletal age at death. Am J Phys Anthropol 68:15-28. doi: 10.1002/ajpa.1330680103
29. Buckberry JL, Chamberlain AT (2002) Age estimation from the auricular surface of the ilium: A revised method. Am J Phys Anthropol 119:231–239. doi: 10.1002/ajpa.10130
30. Mulhern DM, Jones EB (2005) Test of revised method of age estimation from the auricular surface of the ilium. Am J Phys Anthropol 126:61–65. doi: 10.1002/ajpa.10410
31. Rougé-Maillart C, Vielle B, Jousset N, Chappard D, Telmon N, Cunha E (2009) Development of a method to estimate skeletal age at death in adults using the acetabulum and the auricular surface on a Portuguese population. Forensic Sci Int 188:91–95. doi: 10.1016/j.forsciint.2009.03.019
32. Íşcan MY, Loth SR (1986) Determination of age from the sternal rib in white females: a test of the phase method. J Forensic Sci 31:122–132. doi: 10.1520/JFS11107J
33. Íşcan MY, Loth SR (1986) Determination of age from the sternal rib in white males: a test of the phase method. J Forensic Sci 31: 122-132. doi: 10.1520/JFS11866J
34. İşcan MY, Loth SR, Wright RK (1987) Racial variation in the sternal extremety of the rib and its effect on age determination. J Forensic Sci 32:452-863. doi: 10.152/JFS11147J
35. İşcan MY, Loth SR, Wright RK (1984) Age estimation from the rib by phase analysis: white males. J Forensic Sci 29:1094-1104. doi: 10.1520/JFS11776J
36. İşcan MY, Loth SR, Wright RK (1984) Metamorphosis at the sternal rib end: A new method to estimate age at death in white males. Am J Phys Anthropol 65:147-156. doi: 10.1002/ajpa.1330650206
37. Wang XY, Zuo Y, Huang D, Hou XD, Li YB (2010) Comparative study on inorganic composition and crystallographic properties of cortical and cancellous bone. Biomed Environ Sci 23:473–480. doi: 10.1016/S0895-3988(11)60010-X
38. Clarke B (2008) Normal Bone Anatomy and Physiology. Clin J Am Soc Nephrol 3:S131–S139. doi: 10.2215/CJN.04151206
39. Boskey AL (2010) The Biochemistry of Bone: Composition and Organization. Osteoporisis in Men, Second Edi. Elsevier Inc., pp 3-13
40. Lee C, Einhom T (2001) The Bone Organ System, Form and Function. In: Marcus R, Feldman D KJ (ed) Osteoporosis, Second edi. Academic Press, pp 3–20
41. Kendall C, Eriksen AMH, Kontopoulos I, Collins MJ, Turner-Walker G (2018) Diagenesis of archaeological bone and tooth. Palaeogeogr Palaeoclimatol

Palaeoecol 491:21–37. doi: 10.1016/j.palaeo.2017.11.041

42. Boskey JA, Gokhale AL, Robey RP (2001) The Biochemistry of Bone. In: Marcus R, Feldman D, Kelsey J (eds) Osteoporosis, Second Edi. Academic Press, pp.107-188
43. Paschalis EP, Gamsjaeger S, Klaushofer K (2017) Vibrational spectroscopic techniques to assess bone quality. Osteoporos Int 28:2275–2291. doi: 10.1007/s00198-017-4019-y
44. Reidsma FH, van Hoesel A, van Os BJH, Megens L, Braddbaart F (2016) Charred bone: Physical and chemical changes during laboratory simulated heating under reducing conditions and its relevance for the study of fire use in archaeology. J Archaeol Sci Reports 10:282–292. doi: 10.1016/j.jasrep.2016.10.001
45. Boskey AL (2007) Mineralization of Bones and Teeth. Elements 3:385–392. doi: 10.2113/GELEMENTS.3.6.385
46. Sommerfeldt D, Rubin C (2001) Biology of bone and how it orchestrates the form and function of the skeleton. Eur Spine J 10:86–95. doi: 10.1007/s005860100283
47. Marques MPM, Gonçalves D, Amarante AIC, Makhoul CI, Parker SF, Batista de Carvalho LAE (2016) Osteometrics in burned human skeletal remains by neutron and optical vibrational spectroscopy. R Soc Chem 6:68638–68641. doi: 10.1039/c6ra13564a
48. LeGeros RZ, Trautz OR, Klein E, LeGeros JP (1969) Two types of carbonate substitution in the apatite structure. Experientia 25:5-7. doi: 10.1007/BF01903856
49. Mamede AP, Gonçalves D, Marques MPM, Batista de Carvalho LAE (2018) Burned bones tell their own stories: A review of methodological approaches to assess heat-induced diagenesis. Appl Spectrosc Rev 53:603–635. doi: 10.1080/05704928.2017.1400442
50. Lebon M, Reiche I, Bahain JJ, Chadefaux C, Moigne AM, Frohlich F, Sémah F, Schwarcz HP, Falguères C (2010) New parameters for the characterization of diagenetic alterations and heat-induced changes of fossil bone mineral using Fourier transform infrared spectrometry. J Archaeol Sci 37:2265–2276. doi: 10.1016/j.jas.2010.03.024
51. Snoeck C, Lee-Thorp JA, Schulting RJ (2014) From bone to ash: Compositional and structural changes in burned modern and archaeological bone. Palaeogeogr Palaeoclimatol Palaeoecol 416:55–68. doi: 10.1016/j.palaeo.2014.08.002
52. Astala R, Stott MJ (2005) First principles investigation of mineral component of bone: CO_3 substitutions in hydroxyapatite. Chem Mater 17:4125–4133. doi: 10.1021/cm050523b.
53. Wopenka B, Pasteris JD (2005) A mineralogical perspective on the apatite in bone. Mater Sci Eng C 25:131–143. doi: 10.1016/j.msec.2005.01.008

54. Ellingham STD, Thompson TJU, Islam M (2016) The effect of soft tissue on temperature estimation from burnt bone using Fourier transform infrared spectroscopy. J Forensic Sci 61:153–159. doi: 10.1111/1556-4029.12855
55. Carden A, Morris MD (2000) Application of vibrational spectroscopy to the study of mineralized tissues (review). J Biomed Opt 5:259. doi: 10.1117/1.429994
56. Farlay D, Panczer G, Rey C, et al (2010) Mineral maturity and crystallinity index are distinct characteristics of bone mineral. J Bone Miner Metab 28:433–445. doi: 10.1007/s00774-009-0146-7
57. Hollund HI, Ariese F, Fernandes R, Jans MME, Kars H (2013) Testing an alternative high-throughput tool for investigating bone diagenesis: FTIR in attenuated total reflection (ATR) mode. Archaeometry 55:507–532. doi: 10.1111/j.1475-4754.2012.00695.x
58. Bacon GE (1990) The dependence of human bone texture on life style. Proc R Soc B Biol Sci 240:363–370. doi: 10.1098/rspb.1990.0042
59. Boskey A (2003) Bone mineral crystal size. Osteoporos Int 14:16–21. doi: 10.1007/s00198-003-1468-2
60. Taylor MG, Parker SF, Simkiss K, Mitchell PCH (2001) Bone mineral: Evidence for hydroxy groups by inelastic neutron scattering. Phys Chem Chem Phys 3:1514–1517. doi: 10.1039/b005666i
61. Trueman CN, Privat K, Field J (2008) Why do crystallinity values fail to predict the extent of diagenetic alteration of bone mineral? Palaeogeogr Palaeoclimatol Palaeoecol 266:160–167. doi: 10.1016/j.palaeo.2008.03.038
62. Trueman CN, Palmer MR, Field J, Privat K, Ludgate N, Chavagnac V, Eberth D, Cifelli R, Rogers R (2008) Comparing rates of recrystallisation and the potential for preservation of biomolecules from the distribution of trace elements in fossil bones. Comptes Rendus Palevol 7:145–158. doi: 10.1016/j.crpv.2008.02.006
63. Jellinghaus K, Urban PK, Hachmann C, Bohnert M, Hotz G, Rosendahl W, Wittwer-Backofen U (2019) Collagen degradation as a possibility to determine the post-mortem interval (PMI) of human bones in a forensic context – A survey. Leg Med 36:96–102. doi: 10.1016/j.legalmed.2018.11.009
64. White TD, Black MT, Folkens PA (2012) Bone biology and variation. In: Human Osteology, Third Edit. Elsevier, pp 32–40
65. Lucas PW (2004) Dental Function Morphology: How teeth work. Cambridge University Press
66. Hillson S (2005) Teeth, Second Edi. Cambridge University Press
67. Hollund HI, Jans MME, Kars H (2014) How are teeth better than bone? An investigation of dental tissue diagenesis and state of preservation at a histological

scale (with photo catalogue). Internet Archaeol. doi: 10.11141/ia.36.7

68. Elliott JC (2002) Calcium Phosphate Biominerals. Rev Mineral Geochemistry 48:427–453. doi: 10.2138/rmg.2002.48.11
69. Gómez-Morales J, Iafisco M, Delgado-López JM, Sarda S, Drouet C (2013) Progress on the preparation of nanocrystalline apatites and surface characterization: Overview of fundamental and applied aspects. Prog Cryst Growth Charact Mater 59:1–46. doi: 10.1016/j.pcrysgrow.2012.11.001
70. McCreadie BR, Morris MD, Chen TC, Rao DS, Finney WF, Widjaja E, Goldstein SA (2006) Bone tissue compositional differences in women with and without osteoporotic fracture. Bone 39:1190–1195. doi: 10.1016/j.bone.2006.06.008
71. Cummaudo M, Cappella A, Biraghi M, Raffone C, Màrquez-Grant N, Cattaneo C (2018) Histomorphological analysis of the variability of the human skeleton: forensic implications. Int J Legal Med 132:1493–1503. doi: 10.1007/s00414-018-1781-0
72. Katsimbri P (2017) The biology of normal bone remodelling. Eur J Cancer Care (Engl) 26:1–5. doi: 10.1111/ecc.12740
73. Fahy GE, Deter C, Pitfield R, Miszkiewicz JJ, Mahoney P (2017) Bone deep: Variation in stable isotope ratios and histomorphometric measurements of bone remodelling within adult humans. J Archaeol Sci 87:10–16. doi: 10.1016/j.jas.2017.09.009
74. Szulc P (2018) Bone turnover: Biology and assessment tools. Best Pract Res Clin Endocrinol Metab 32:725–738. doi: 10.1016/j.beem.2018.05.003
75. Wang X, Shen X, Li X, Mauli Agrawal C (2002) Age-related changes in the collagen network and toughness of bone. Bone 31:1–7. doi: 10.1016/S8756-3282(01)00697-4
76. Burr DB (2002) The contribution of the organic matrix to bone's material properties. Bone 31:8–11. doi: 10.1016/s8756-3282(02)00815-3
77. Zioupos P, Currey JD, Hamer AJ (1999) The role of collagen in the declining mechanical properties of aging human cortical bone. J Biomed Mater Res 45:108-116. doi: 10.1002/(SICI)1097-4636(199905)45:<108::AID-JBM5>3.0.CO;2-A
78. Melton JL, Cooper C (2001) Magnitude and Impact of Osteoporosis and Fractures. In: R KM, Feldman D (eds) Osteoporosis, Second Edi. Academic Press, pp 557–565
79. Seeman E, Delmas PD (2006) Bone quality — The material and structural basis of bone strength and fragility. N Engl J Med 354:2250–2261. doi: 10.1056/nejmra053077
80. Cox G, Sealy J (2014) Investigating identity and life histories: Isotopic analysis and historical documentation of slave skeletons found on the Cape Town Foreshore, South Africa. Int J Hist Archaeol 1:207–224. doi: 10.1023/A:1027349115474

81. Parfitt A (2002) Misconceptions (2): Turnover is always higher in cancellous than in cortical bone. Bone 30:807–809. doi: 10.1016/S8756-3282(02)00735-4
82. Price TD, Burton JH, Bentley RA (2002) The characterization of biologically available strontium isotope ratios for the study of prehistoric migration. Archaeometry 44:117–135. doi: 10.1111/1475-4754.00047
83. Price TD, Manzanilla L, Middleton WD (2000) Immigration and the ancient city of Teotihuacan in Mexico: A study using strontium isotope ratios in human bone and teeth. J Archaeol Sci 27:903–913. doi: 10.1006/jasc.1999.0504
84. Hedges R (2007) Collagen Turnover in the Adult Femoral Mid-Shaft: Modeled From Anthropogenic Radiocarbon Tracer Masurements. Am J Phys Anthropol 133:808-816. doi: 10.1002/ajpa
85. Beasley MM, Bartelink EJ, Taylor L, Miller RM (2014) Comparison of transmission FTIR, ATR, and DRIFT spectra: Implications for assessment of bone bioapatite diagenesis. J Archaeol Sci 46:16–22. doi: 10.1016/j.jas.2014.03.008
86. Stathopoulou ET, Psycharis V, Chryssikos GD, Gionis V, Theodorou G (2008) Bone diagenesis: New data from infrared spectroscopy and X-ray diffraction. Palaeogeogr Palaeoclimatol Palaeoecol 266:168–174. doi: 10.1016/j.palaeo.2008.03.022
87. Berna F, Matthews A, Weiner S (2004) Solubilities of bone mineral from archaeological sites: The recrystallization window. J Archaeol Sci 31:867–882. doi: 10.1016/j.jas.2003.12.003
88. Trueman CNG, Behrensmeyer AK, Tuross N, Weiner S (2004) Mineralogical and compositional changes in bones exposed on soil surfaces in Amboseli National Park, Kenya: Diagenetic mechanisms and the role of sediment pore fluids. J Archaeol Sci 31:721–739. doi: 10.1016/j.jas.2003.11.003
89. Pestle WJ, Ahmad F, Vesper BJ, Cordell GA, Colvard MD (2014) Ancient bone collagen assessment by hand-held vibrational spectroscopy. J Archaeol Sci 42:381–389. doi: 10.1016/j.jas.2013.11.014
90. Rey C, Collins B, Goehl T, Dickson IR, Glimcher MJ (1989) The carbonate environment in bone mineral: A resolution-enhanced fourier transform infrared spectroscopy study. Calcif Tissue Int 45:157–164. doi: 10.1007/BF02556059
91. Miller LM, Vairavamurthy V, Chance MR, Mendelsohn R, Paschalis EP, Betts F, Boskey AL (2001) In situ analysis of mineral content and crystallinity in bone using infrared micro-spectroscopy of the v4 PO43- vibration. Biochim Biophys Acta 1527:11–19. doi: 10.1016/S0304-4165(01)00093-9
92. Thompson TJU, Islam M, Bonniere M (2013) A new statistical approach for determining the crystallinity of heat-altered bone mineral from FTIR spectra. J Archaeol Sci 40:416–422. doi: 10.1016/j.jas.2012.07.008

93. Thompson TJU, Islam M, Piduru K, Marcel A (2011) An investigation into the internal and external variables acting on crystallinity index using Fourier Transform Infrared Spectroscopy on unaltered and burned bone. Palaeogeogr Palaeoclimatol Palaeoecol 299:168–174. doi: 10.1016/j.palaeo.2010.10.044
94. Marques MPM, Mamede AP, Vassalo AR, Makhoul C, Cunha E, Gonçalves D, Parker SF, Batista de Carvalho LAE (2018) Heat-induced Bone Diagenesis Probed by Vibrational Spectroscopy. Sci Rep 8:1–13. doi: 10.1038/s41598-018-34376-w
95. Stuart B (2005) Infrared Spectroscopy. In: Kirk-Othmer Encycl. Chem. Technol. John Wiley & Sons, Inc., pp 1–20
96. Griffiths PR (2006) Introduction to Vibrational Spectroscopy. In: Handb. Biv. Spectrosc. John Wiley & Sons, Ltd, pp 33-43
97. Coates J (2004) Interpretation of Infrared Spectra, A Practical Approach. In: Meyers RA (ed) Encycl. Anal. Chem. John Wiley & Sons, Ltd, pp 1–23
98. Stuart B (1997) Biological Applications of Infrared Spectroscopy. John Wiley & Sons, Inc.
99. Nakamoto K (1963) Infrared Spectra of Inorganic and Coordination Compounds. John Wiley & Sons, Inc.
100. Shurvell HF (2006) Spectra− Structure Correlations in the Mid- and Far-Infrared. In: Chalmers JM (ed) Handb. Vib. Spectrosc. John Wiley & Sons, Ltd, pp 1783-1816
101. Khoshhesab ZM (2012) Reflectance IR Spectroscopy. In: Theophanides T (ed) Infrared Spectrosc. - Mater. Sci. Eng. Technol. InTech, pp 233-244
102. Thompson TJU, Gauthier M, Islam M (2009) The application of a new method of Fourier Transform Infrared Spectroscopy to the analysis of burned bone. J Archaeol Sci 36:910–914. doi: 10.1016/j.jas.2008.11.013
103. Surovell TA, Stiner MC (2001) Standardizing infra-red measures of bone mineral crystallinity: An experimental approach. J Archaeol Sci 28:633–642. doi: 10.1006/jasc.2000.0633
104. Grdadolnik J (2002) ATR-FTIR Spectroscopy: Its Advantages and Limitations. Acta Chim. Slov. 49:631–642.
105. Sponheimer M, Lee-Thorp JA (1999) Alteration of Enamel Carbonate Environments during Fossilization. J Archaeol Sci 26:143–150. doi: 10.1006/jasc.1998.0293
106. Patonai Z, Maasz G, Avar P, Schmidt J, Lorand T, Bajnoczky I, Mark L (2013) Novel dating method to distinguish between forensic and archeological human skeletal remains by bone mineralization indexes. Int J Legal Med 127:529–533. doi: 10.1007/s00414-012-0785-4
107. Wright LE, Schwarcz HP (1996) Infrared and isotopic evidence for diagenesis of bone apatite at Dos Pilas, Guatemala: Palaeodietary implications. J Archaeol Sci 23:933–

944. doi: 10.1006/jasc.1996.0087

108. Shemesh A (1990) Crystallinity and diagenesis of sedimentary apatites. Geochim Cosmochim Acta 54:2433–2438. doi: 10.1016/0016-7037(90)90230-I
109. Termine JD, Posner S (1966) Infrared analysis of rat bone: Age dependency of amorphous and crystalline mineral fractions. Science (80-) 153:1523–1525. doi: 10.1126/science.153.3743.1523
110. Rey C, Combes C, Drouet C, Glimcher MJ (2009) Bone mineral: update on chemical composition and structure. Osteoporos Int 20:2155–2155. doi: 10.1007/s00198-009-1063-2
111. Gonçalves D, Vassalo AR, Mamede AP, Makhoul C, Piga G, Cunha E, Marques MPM, Batista de Carvalho LAE (2018) Crystal clear: Vibrational spectroscopy reveals intrabone, intraskeleton, and interskeleton variation in human bones. Am J Phys Anthropol 00:1–17. doi: 10.1002/ajpa.23430
112. Weiner S, Bar-Yosef O (1990) States of preservation of bones from prehistoric sites in the Near East: A survey. J Archaeol Sci 17:187–196. doi: 10.1016/0305-4403(90)90058-D
113. Isaksson H, Turunen MJ, Rieppo L, Saarakkala S, Tamminen IS, Rieppo J, Kroger , Jurvelin JS (2010) Infrared spectroscopy indicates altered bone turnover and remodeling activity in renal osteodystrophy. J Bone Miner Res 25:1360–1366. doi: 10.1002/jbmr.10
114. France CAM, Thomas DB, Doney CR, Madden O (2014) FT-Raman spectroscopy as a method for screening collagen diagenesis in bone. J Archaeol Sci 42:346–355. doi:10.1016/j.jas.2013.11.020
115. Barth A, Zscherp C (2002) What vibrations tell us about proteins. Q Rev Biophys 35:369–430. doi: 10.1017/S0033583502003815
116. Mamede AP, Vassalo AR, Piga G, Cunha E, Parker SF, Marques MPM, Batista de Carvalho LAE, Gonçalves D (2018) The potential of bioapatite hydroxyls for research on archeological burned bone. Anal Chem 90:11556–11563. doi: 10.1021/acs.analchem.8b02868
117. Howes JM, Stuart BH, Thomas PS, Raja S, O'Brien C (2012) An investigation of model forensic bone in Soil environments studied using Infrared Spectroscopy. J Forensic Sci 57:1161–1167. doi: 10.1111/j.1556-4029.2012.02236.x
118. Longato S, Wöss C, Hatzer-Grubwieser P, Bauer C, Parson W, Unterberger SH, Kuhn V, Pemberger N, Pallua AK, Recheis W, Lackner R, Stalder R, Pallua JD (2015) Post-mortem interval estimation of human skeletal remains by micro-computed tomography, mid-infrared microscopic imaging and energy dispersive X-ray mapping. Anal Methods 7:2917–2927. doi: 10.1039/c4ay02943g

119. Woess C, Unterberger SH, Roider C, Ritsch-Marte M, Pemberger N, Cemper-Kiesslich J, Hatzer-Grubwieser P, Parson W, Pallua JD (2017) Assessing various Infrared (IR) microscopic imaging techniques for post-mortem interval evaluation of human skeletal remains. PLOS One 12:1–16. doi: 10.1371/journal.pone.0174552
120. Wang Q, Zhang Y, Lin H, Zha S, Fang R, Wei X, Fan S, Wang Z (2017) Estimation of the late postmortem interval using FTIR spectroscopy and chemometrics in human skeletal remains. Forensic Sci Int 281:113–120. doi: 10.1016/j.forsciint.2017.10.033
121. Nakano T, Umakoshi Y, Tokumura A (2002) Variation in crystallinity of hydroxyapatite and the related calcium phosphates by mechanical grinding and subsequent heat treatment. Metall Mater Trans A 33:521–528. doi: 10.1007/s11661-002-0114-5
122. Bartsiokas A, Middleton AP (1992) Characterization and dating of recent and fossil bone by X-ray diffraction. J Archaeol Sci 19:63–72. doi: 10.1016/0305-4403(92)90007-P
123. Paschalis EP, Betts F, DiCarlo E, et al (1997) FTIR microspectroscopic analysis of normal human cortical and trabecular bone. Calcif Tissue Int 61:480–486. doi: 10.1007/s002239900371
124. Matsushima N, Hikichi K (1989) Age changes in the crystallinity of bone mineral and in the disorder of its crystal. Biochim Biophys Acta 992:155–159. doi: 10.1016/0304-4165(89)90004-4
125. Rey C, Renugopalakrishnan V, Collins B, Glimcher MJ (1991) Fourier Transform Infrared Spectroscopic Study of the Carbonate Ions in Bone Mineral During Aging. Calcif Tissue Int 49:251–258. doi: 10.1007/BF02556214
126. Ou-Yang H, Paschalis EP, Mayo WE, Boskey AL, Mendelsohn R (2001) Infrared Microscopic Imaging of Bone: Spatial Distribution of CO32-. J Bone Miner Res 16:893–900. doi: 10.1359/jbmr.2001.16.5.893
127. Very JM, Gibert R, Guilhot B, Debout M, Alexandre C (1997) Effect of aging on the amide group of bone matrix, measured by FTIR spectrophotometry, in adult subjects deceased as a result of violent death. Calcif Tissue Int 60:271–275. doi: 10.1007/s002239900228
128. Akkus O, Adar F, Schaffler MB (2004) Age-related changes in physicochemical properties of mineral crystals are related to impaired mechanical function of cortical bone. Bone 34:443–453. doi: 10.1016/j.bone.2003.11.003
129. Person A, Bocherens H, Mariotti H, Renard M (1996) Diagenetic evolution and expermental heating of bone phosphate. Palaeogeogr Palaeoclimatol Palaeoecol 126:135–149. doi: 101016/S0031-0182(97)88906-7
130. Schwarz C, Debruyne R, Kuch M, McNally E, Schwarcz H, Aubrey AD, Bada J, poinar H (2009) New insights from old bone: DNA preservation and degradation in

permafrost preserved mammoth remains. Nucleic Acid Res 37:3215–3229. doi: 10.1093/nar/gkp159

131. Ferreira MT, Vicente R, Navega D, Gonçalves D, Curate F, Cunha E (2014) A new forensic collection housed at the University of Coimbra, Portugal: The 21st century identified skeletal collection. Forensic Sci Int 245:202.e1-e5. doi: 10.1016/j.forsciint.2014.09.021
132. Oliveira-Santos I, Gouveia M, Cunha E, Gonçalves D (2017) The circles of life: age at death estimation in burnt teeth through tooth cementum annulations. Int J Legal Med. 131:527-536. doi: 10.1007/s00414-016-1432-2
133. Gouveia MF, Oliveira Santos I, Santos AL, Gonçalves D (2017) Sample-specific odontometric sex estimation: A method with potential application to burned remains. Sci Justice 57:262–269. doi: 10.1016/j.scijus.2017.03.001
134. Nagy G, Lorand T, Patonai Z, Montsko G, Bajnoczky I, Marcsik A, Mark L (2008) Analysis of pathological and non-pathological human skeletal remains by FT-IR spectroscopy. Forensic Sci Int 175:55–60. doi: 10.1016/j.forsciint.2007.05.008
135. Bonnier F, Byrne HJ (2012) Understanding the molecular information contained in principal component analysis of vibrational spectra of biological systems. Analyst 137:322–332. doi: 10.1039/c1an15821j
136. Morgan GA, Leech NL, Gloeckmer GW, Barrett KC (2004) SPSS for Introductory Statistics, Second Edi. Lawrence Erlbaum Associates, Inc.
137. Gadaleta SJ, Paschalis EP, Betts F, Mendelsohn R, Boskey AL (1996) Fourier Transform Infrared Spectroscopy of the Solution-Mediated Conversion of Amorphous Calciu Phosphate to Hydrocyapatite: New Correlations between X-Ray Diffraction and Infrared Data. Calcif Tissue Int 58:9–16. doi: 10.1007/BF02509540
138. Paschalis EP, DiCarlo E, Betts F, Sherman P, Mendelsohn R, Boskey AL (1996) FTIR microspectroscopic analysis of human osteonal bone. Calcif Tissue Int 59:480–487. doi: 10.1007/BF00369214
139. Rey C, Shimizu M, Collins B, Glimcher M (1991) Resolution-enhanced fourier transform infrared spectroscopy study of the environment of phosphate ion in the early deposits of a solid phase of calcium phosphate in bone and enamel and their evolution with age: 2. Investigations in the v_3PO_4 domain. Calcif Tissue Int 383–388. doi: 10.1007/BF02555847
140. Skedros JG, Knight AN, Clark GC, Crowder CM, Dominguez VM, Qiu S, Muhlem DM, Donahue SW, Busse B, Hulsey BI, Zedda M, Sorenson SM (2013) Scaling of Haversian canal surface area to secondary osteon bone volume in ribs and limb bones. Am J Phys Anthropol 151:230–244. https://doi.org/10.1002/ajpa.22270
141. Zapata J, Pérez-Sirvent C, Martínez-Sánchez MJ, Tovar P (2006) Diagenesis, not

biogenesis: Two late Roman skeletal examples. Sci Total Environ 369:357–368. doi: 10.1016/j.scitotenv.2006.05.021

142. King CL, Tayles N, Gordon KC (2011) Re-examining the chemical evaluation of diagenesis in human bone apatite. J Archaeol Sci 38:2222–2230. doi: 10.1016/j.jas.2011.03.023
143. Paschalis EP, Verdelis K, Doty SB, Boskey AL, Mendelsohn R, Yamauchi M (2001) Spectroscopic characterization of collagen cross-links in bone. J Bone Miner Res 16:1821–1828. doi: 10.1359/jbmr.2001.16.10.1821
144. Nielsen-Marsh CM, Hedges REM (1999) Bone porosity and the use of mercury intrusion porosimetry in bone diagenesis studies. Archaeometry 41:165–174. doi: 10.1111/j.1475-4754.1999.tb00858.x
145. Nielsen-Marsh CM, Hedges REM (2000) Patterns of diagenesis in bone II: Effects of acetic acid treatment and the removal of diagenetic CO_3^{2-}. J Archaeol Sci 27:1151–1159. doi: 10.1006/jasc.1999.0538
146. Lanfranco AM, Schofield PF, Murphy PJ, Honson ME, Mosselmans JFW, Valsami-Jones E (2003) Characterization and identification of mixed-metal phosphates in soils: the application of Raman spectroscopy. Mineral Mag 67:1299–1316. doi: 10.1180/0026461036760166
147. Thomas DB, Fordyce RE, Frew RD, Gordon KC (2007) A rapid, non-destructive method of detecting diagenetic alteration in fossil bone using Raman spectroscopy. J Raman Spectrosc 38:1533–1537. doi: 10.1002/jrs.1851
148. Udvardi B, Kovács IJ, Fancsik T, Kónya P, Bátori M, Stercel F, Falus G, Szalai Z (2017) Effects of Particle Size on the Attenuated Total Reflection Spectrum of Minerals. Appl Spectrosc 71:1157–1168. doi: 10.1177/0003702816670914
149. Regev L, Poduska KM, Addadi L, Weiner S, Boaretto E (2010) Distinguishing between calcites formed by different mechanisms using infrared spectrometry: Archaeological applications. J Archaeol Sci 37:3022–3029. doi: 10.1016/j.jas.2010.06.027
150. Poduska KM, Regev L, Boaretto E, Addadi L, Weiner S, Kronik L, Curtarolo S (2011) Decoupling local disorder and optical effects in infrared spectra: Differentiating between calcites with different origins. Adv Mater 23:550–554. doi: 10.1002/adma.201003890
151. Kontopoulos I, Presslee S, Penkman K, Collins MJ (2018) Preparation of bone powder for FTIR-ATR analysis: The particle size effect. Vib Spectrosc 99:167–177. doi: 10.1016/j.vibspec.2018.09.004
152. Kristova P, Hopkinson LJ, Rutt KJ (2015) The effect of the particle size on the fundamental vibrations of the [CO32-] Anion in Calcite. J Phys Chem A 119:4891–

4897. doi: 10.1021/acs.jpca.5b02942

153. Lenhard W, Lenhard A (2016) Calculation of Effect Sizes. In: Psychometria. https://www.psychometrica.de/effect_size.html. Accessed 20 Jul 2019

APPENDIX

Figure A1. Representation of teeth with age groups below 50 years old – younger group – and over 50 years old – older group: (A) mean FTIR-ATR spectra of younger and older group; (B) PCA scores; (C) PCA loadings. PC1: 65.98%; PC2: 16.61%; PC3: 6.83%; PC4: 4.35%; PC5: 1.73%, exhibiting 95.50% of total variance.

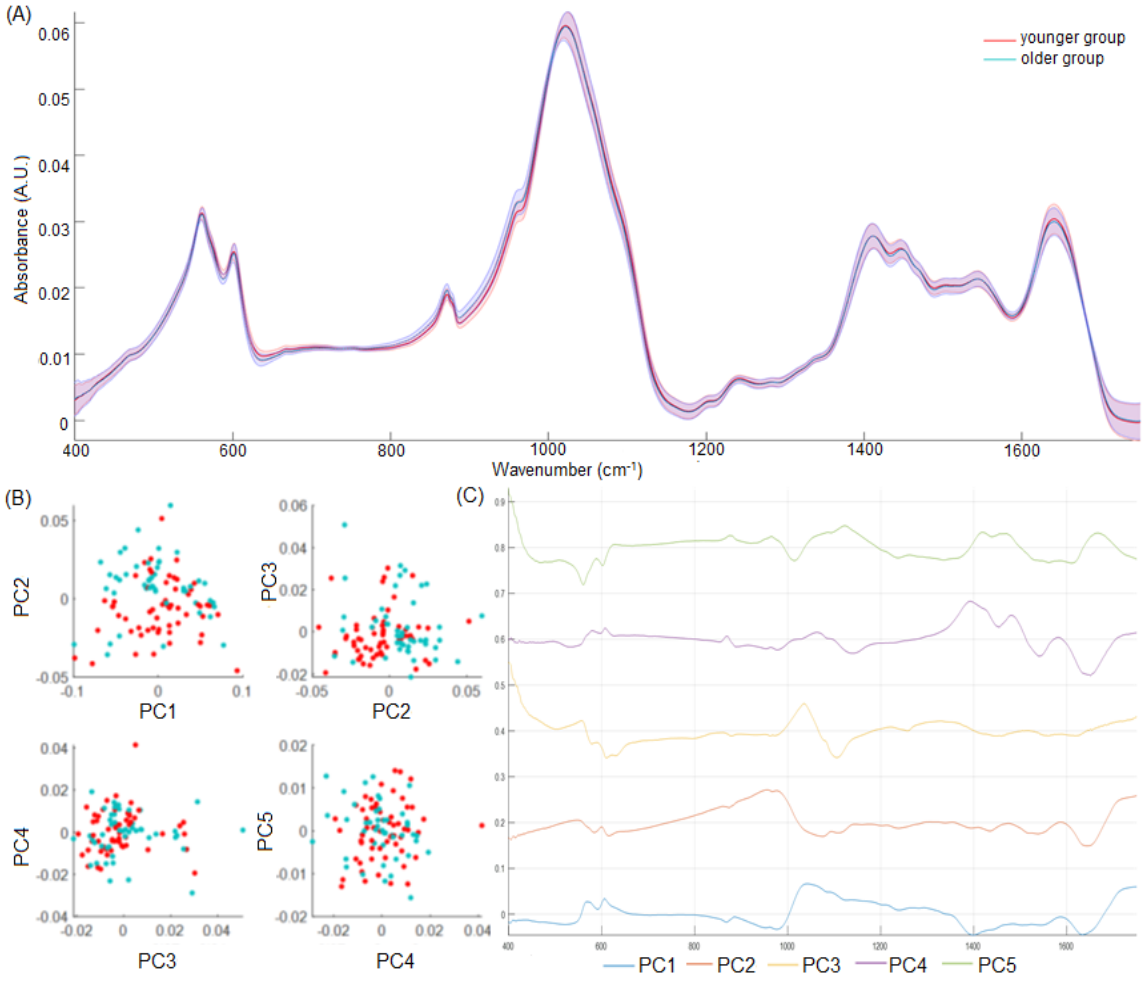

Figure A2. Representation of teeth with age groups below 40 years old – younger group – and over 40 years old – older group: (A) mean FTIR-ATR spectra of younger and older group; (B) PCA scores; (C) PCA loadings. PC1: 65.98%; PC2: 16.61%; PC3: 6.83%; PC4: 4.35%; PC5: 1.73%, exhibiting 95.50% of total variance.